Strength Characterization of Open-Graded Aggregates for Structural Backfills

PUBLICATION NO. FHWA-HRT-15-034

JUNE 2015

U.S. Department of Transportation
Federal Highway Administration

Research, Development, and Technology
Turner-Fairbank Highway Research Center
6300 Georgetown Pike
McLean, VA 22101-2296

FOREWORD

State and local transportation agencies frequently use crushed, manufactured open-graded aggregates (OGA) as structural backfill material for retaining walls, bridge foundations, and other ground improvement applications, yet their strength characteristics are not fully understood or applied. The friction angle is required to efficiently design for lateral earth pressures and bearing capacity, but because of the large size of the standard American Association of State Highway and Transportation Officials (AASHTO) OGAs, this parameter cannot be measured with standard testing equipment. Instead, current practice is to select a low, default friction angle, which can lead to over-conservative, less cost-effective designs. To address this gap, research was initiated by the Federal Highway Administration's Turner-Fairbank Highway Research Center (TFHRC) to establish a knowledge base on the most commonly used AASHTO OGAs. The study included a systematic approach to fully characterize the strength parameters utilizing the large scale direct shear and triaxial devices in the TFHRC geotechnical laboratory. Relationships between other important soil parameters on the friction angle, as well as the impact of different automated testing devices and data interpretation methods, were also investigated. This report presents the results of this research and will assist State and local transportation agencies, researchers, and design consultants in gaining confidence on the use of higher friction angles for structural backfills to optimize the design of geotechnical features.

Jorge E. Pagán-Ortiz
Director, Office of Infrastructure
Research and Development

TECHNICAL REPORT DOCUMENTATION PAGE

1. Report No. FHWA-HRT-15-034	2. Government Accession No.	3. Recipient's Catalog No.
4. Title and Subtitle Strength Characterization of Open-Graded Aggregates for Structural Backfills		5. Report Date June 2015
		6. Performing Organization Code: HRDI-40
7. Author(s) Nicks, J.E., Gebrenegus, T., Adams, M.T.		8. Performing Organization Report No.
9. Performing Organization Name and Address Turner-Fairbank Highway Research Center 6300 Georgetown Pike McLean, VA 22101		10. Work Unit No.
		11. Contract or Grant No. N/A
12. Sponsoring Agency Name and Address Office of Infrastructure R&D FHWA Research, Development and Technology 6300 Georgetown Pike McLean, VA 22101		13. Type of Report and Period Covered Technical
		14. Sponsoring Agency Code
15. Supplementary Notes None.		

16. Abstract

Open-graded aggregates are common in road and bridge construction because they are easy to place, and they have the advantages of very low fine content, free-draining characteristics, low frost heave potential, and simple quality assurance testing. They are a suitable alternative to well-graded aggregate blends in many applications. Another key benefit is their strength, but this attribute it is often not accounted for in design. This report presents strength characteristics of 16 open-graded aggregates commonly selected as structural backfills and discusses the impact of different test and data interpretation methods. Results of large-scale direct shear and large diameter triaxial tests indicate higher strengths for these materials than typical default values typically assumed in design. It was also observed that the mean grain size, sphericity, angularity, and void ratio play a role in the measured friction angles. This information will help designers better understand these backfills and aid in the cost-effective design of retaining walls and bridge foundations.

17. Key Words	18. Distribution Statement
Friction angle, strength, open-graded aggregate, structural backfill, retaining wall, bridge foundation	No restrictions. The report will be available to the public at FHWA: www.fhwa.dot.gov/research or NTIS: www.ntis.gov.

19. Security Classif. (of this report)	20. Security Classif. (of this page)	21. No. of Pages	22. Price
Unclassified	Unclassified	149	N/A

Form DOT F 1700.7 (8-72) **Reproduction of completed page authorized**

SI* (MODERN METRIC) CONVERSION FACTORS

APPROXIMATE CONVERSIONS TO SI UNITS

Symbol	When You Know	Multiply By	To Find	Symbol
		LENGTH		
in	inches	25.4	millimeters	mm
ft	feet	0.305	meters	m
yd	yards	0.914	meters	m
mi	miles	1.61	kilometers	km
		AREA		
in^2	square inches	645.2	square millimeters	mm^2
ft^2	square feet	0.093	square meters	m^2
yd^2	square yard	0.836	square meters	m^2
ac	acres	0.405	hectares	ha
mi^2	square miles	2.59	square kilometers	km^2
		VOLUME		
fl oz	fluid ounces	29.57	milliliters	mL
gal	gallons	3.785	liters	L
ft^3	cubic feet	0.028	cubic meters	m^3
yd^3	cubic yards	0.765	cubic meters	m^3
		NOTE: volumes greater than 1000 L shall be shown in m^3		
		MASS		
oz	ounces	28.35	grams	g
lb	pounds	0.454	kilograms	kg
T	short tons (2000 lb)	0.907	megagrams (or "metric ton")	Mg (or "t")
		TEMPERATURE (exact degrees)		
^oF	Fahrenheit	5 (F-32)/9 or (F-32)/1.8	Celsius	^oC
		ILLUMINATION		
fc	foot-candles	10.76	lux	lx
fl	foot-Lamberts	3.426	$candela/m^2$	cd/m^2
		FORCE and PRESSURE or STRESS		
lbf	poundforce	4.45	newtons	N
lbf/in^2	poundforce per square inch	6.89	kilopascals	kPa

APPROXIMATE CONVERSIONS FROM SI UNITS

Symbol	When You Know	Multiply By	To Find	Symbol
		LENGTH		
mm	millimeters	0.039	inches	in
m	meters	3.28	feet	ft
m	meters	1.09	yards	yd
km	kilometers	0.621	miles	mi
		AREA		
mm^2	square millimeters	0.0016	square inches	in^2
m^2	square meters	10.764	square feet	ft^2
m^2	square meters	1.195	square yards	yd^2
ha	hectares	2.47	acres	ac
km^2	square kilometers	0.386	square miles	mi^2
		VOLUME		
mL	milliliters	0.034	fluid ounces	fl oz
L	liters	0.264	gallons	gal
m^3	cubic meters	35.314	cubic feet	ft^3
m^3	cubic meters	1.307	cubic yards	yd^3
		MASS		
g	grams	0.035	ounces	oz
kg	kilograms	2.202	pounds	lb
Mg (or "t")	megagrams (or "metric ton")	1.103	short tons (2000 lb)	T
		TEMPERATURE (exact degrees)		
^oC	Celsius	1.8C+32	Fahrenheit	^oF
		ILLUMINATION		
lx	lux	0.0929	foot-candles	fc
cd/m^2	$candela/m^2$	0.2919	foot-Lamberts	fl
		FORCE and PRESSURE or STRESS		
N	newtons	0.225	poundforce	lbf
kPa	kilopascals	0.145	poundforce per square inch	lbf/in^2

*SI is the symbol for the International System of Units. Appropriate rounding should be made to comply with Section 4 of ASTM E380.
(Revised March 2003)

TABLE OF CONTENTS

LIST OF FIGURES

LIST OF TABLES

LIST OF ABBREVIATIONS

AASHTO	American Association of State Highway and Transportation Officials
AIMS	Aggregate imaging measurement system
AIMS2	Second generation aggregate imaging measurement system
CC	Consolidation curve
COV	Coefficient of variation
CV	Constant volume
DS	Direct shear
FHWA	Federal Highway Administration
FM	Fineness modulus
LDTX	Large diameter triaxial
LSDS	Large-scale direct shear
LVDT	Linear variable differential transformer
MC	Mohr-Coulomb
MSE	Mechanically stabilized earth
NAVFAC	Naval Facilities Engineering Command
OG	Open-graded
OGA	Open-graded aggregate
PS	Plane strain
SDS	Standard direct shear
TFHRC	Turner-Fairbank Highway Research Center
TX	Triaxial
ZDA	Zero dilation angle

LIST OF SYMBOLS

α	Angle of the modified (stress-path) failure envelope
$\Delta(\sigma'_1-\sigma'_3)$	Change in effective deviator stress due to the membrane correction
Δh	Change in horizontal displacement
Δv	Change in vertical displacement
ε_1	Axial strain
ε_V	Volumetric strain
σ'_1	Effective major principal stress
σ'_3	Effective minor principal stress
σ'_c	Effective confining stress
$\sigma'_{c,1}$	Low-range effective confining stress
$\sigma'_{c,2}$	Mid-range effective confining stress
$\sigma'_{c,3}$	High-range effective confining stress
σ'_d	Deviator stress
σ'_n	Effective normal stress
τ	Shear strength
τ_f	Shear stress at failure
ϕ	Friction angle
ϕ_{DS}	Friction angle measured from direct shear testing
ϕ_{TX}	Friction angle measured from triaxial testing
ϕ'	Effective friction angle
ϕ'_μ	True friction angle
ϕ'_{cv}	Constant volume effective friction angle
$\phi'_{cv,dry}$	Constant volume effective friction angle under dry conditions
$\phi'_{cv,LDTX}$	Constant volume effective friction angle from LDTX testing
$\phi'_{cv,LSDS,dry}$	Constant volume effective friction angle from LSDS testing under dry conditions

$\phi'_{cv,sat}$	Constant volume effective friction angle under saturated conditions
$\phi'_{cv,SDS}$	Constant volume effective friction angle from SDS testing
ϕ'_{Dense}	Friction angle for aggregates tested at a dense state
ϕ'_{f}	Dilation corrected friction angle
ϕ'_{Loose}	Friction angle for aggregates tested at a loose state
ϕ'_{Medium}	Friction angle for aggregates tested at a medium dense state
ϕ'_{s}	Secant, or peak effective friction angle
$\phi'_{s,LDTX}$	Effective secant friction angle from LDTX testing
$\phi'_{s,LSDS,sat}$	Effective secant friction angle from LDTX testing
$\phi'_{t,LDTX}$	Effective tangent friction angle from LDTX testing
$\phi'_{t,LSDS,dry}$	Effective tangent friction angle from LSDS testing under dry conditions
$\phi'_{t,LSDS,sat}$	Effective tangent friction angle from LSDS testing under saturated conditions
$\phi'_{t,SDS}$	Effective tangent friction angle from SDS testing
ϕ'_{t}	Tangent effective friction angle
ψ	Dilation angle
ψ_{max}	Maximum dilation angle
A	Nonlinear material constant (Charles and Watts 1980)
A_c	Corrected area
A_o	Original sample area
a	Experimental constant
b	Nonlinear material constant (Charles and Watts 1980)
c	Cohesion
c′	Effective cohesion determined from the Mohr-Coulomb approach
c'_{SDS}	Effective cohesion from standard direct shear testing
Cc	Coefficient of curvature
Cu	Coefficient of uniformity

d_{10}	Particle diameter at which 10 percent of the sample is finer, by mass
d_{30}	Particle diameter at which 30 percent of the sample is finer, by mass
d_{50}	Median grain size; particle diameter at which 60 percent of the sample is finer, by mass
d_{60}	Particle diameter at which 60 percent of the sample is finer, by mass
d_{85}	Particle diameter at which 85 percent of the sample is finer, by mass
$d\varepsilon_1$	Incremental axial strain
$d\varepsilon_3$	Incremental lateral strain
d_{max}	Maximum diameter of the aggregate sample
D	Sample diameter
D_c	Specimen diameter at the end of the consolidation phase
E_m	Young's modulus for the membrane material
F	Area correction actor
h	horizontal displacement
K_a	Active earth pressure coefficient
L	Distance from intersection of bisector line and consolidation curve for the membrane penetration correction
n	Porosity
N_γ	Bearing capacity factor
N_c	Bearing capacity factor
N_q	Bearing capacity factor
p'	Effective mean stress path
q	Shear stress path
t_{90}	Time needed to achieve 90 percent of the total consolidation
t_m	Thickness of the membrane

CHAPTER 1. INTRODUCTION

1.1 PROBLEM STATEMENT

Open-graded aggregates (OGA), or poorly graded aggregates, are defined by their gradation, with most particles being uniform in size. They can be rounded or angular and classified as either sand or gravel. OGAs are used in concrete and asphalt mixes as well as for transportation structures, where requirements often specify the use of angular open-graded (OG) gravels. The primary advantages of using this type of material are ease of constructability, very low fine content, free-draining characteristics, low frost heave potential, and simple quality assurance testing, with a method specification for compaction. Angular OGAs also have the added benefit of increased strength compared with rounded aggregates. Because of these qualities, State and local transportation agencies are more routinely specifying crushed, manufactured OGAs for wall, roadway, and bridge construction. The American Association of State Highway and Transportation Officials (AASHTO) classifies manufactured OGAs according to the M43 gradation based on standard sizes for processed aggregates; the equivalent ASTM standard is D448.[(1,2)]

In the design of retaining walls and foundation systems, the friction angle and cohesion are important parameters to define the strength of the backfill, commonly described by the Mohr-Coulomb (MC) failure envelope. The AASHTO OGAs are cohesionless, and the friction angle can be measured using laboratory testing devices, including plane strain (PS), direct shear (DS), and triaxial (TX) devices, although DS and TX are the most common. Oftentimes, however, designers will either have scalped samples tested or simply use a default friction angle of 34 degrees in lieu of testing. These measures are considered conservative; however, the actual strength properties of OGAs have not been systematically measured nor have the influences of various testing devices on the results been studied.

1.2 OBJECTIVES

The Federal Highway Administration (FHWA) initiated a research program to conduct laboratory testing of common AASHTO OGAs. The primary objectives of this program are to quantify the strength parameters, determine the influence of various factors on strength, and evaluate different testing devices. As a starting point, testing commenced using a large-scale direct shear (LSDS) device to measure the friction angle of uncompacted, common AASHTO OG aggregates.[(3)] In addition, standard DS and large-diameter triaxial (LDTX) devices were used in this study. The study also looked at whether strength (i.e., friction angle) could be correlated to other properties of the backfill.

1.3 REPORT OUTLINE

This research report will detail the results of the testing program and is organized as follows:

- Chapter 2 provides background information on the use and design of OGAs in the transportation sector, the various testing and data interpretation methods available, and the associated implications.

- Chapter 3 details the laboratory testing program and presents the results. Beyond strength, the gradation, density, repose angle, angularity, and texture were measured using appropriate devices and standards.

- Chapter 4 describes the data analysis for different testing devices and data reduction methods. In addition, correlations between various soil properties and strength parameters were examined.

- Chapter 5 presents a summary of the testing and provides conclusions that transportation agencies can consider when designing with AASHTO OGAs. Additional research gaps and future research plans within FHWA are also discussed.

CHAPTER 2. BACKGROUND

2.1 USE OF OGAs

Manufactured OGAs are used in a variety of transportation applications, including retaining wall backfill, concrete, asphalt, pavement structures, and foundation support. These materials are selected primarily because of their strength, excellent drainage properties, and speed of placement in the field. The first known attempt by AASHTO to standardize gradations for processed aggregates was in 1988, which followed ASTM standard D448 (published in 1986). The standard included 19 gradations, ranging from 4 inches minus material to 0.375 inch minus material. While six additional versions have since come out, the same gradations and nomenclature is used; the biggest difference is the elimination of metric units.

For some projects, contractors and designers have the flexibility to select backfills that meet certain requirements; in other projects, the backfill type is specified by the owner. Many State transportation departments and other transportation agencies have specifications related to the use of AASHTO M 43, but these guidelines are primarily focused on concrete and pavement design requirements.(See references 4 through 7.) For structural backfills, the specifications are typically more open where OG or well-graded aggregates meeting the broad gradation and durability requirements can be used.

2.2 STRENGTH PROPERTIES OF GRANULAR MATERIALS

The shear strength (τ) of granular materials is the measure of their resistance to mass deformation developed from a combination of particle rolling, sliding, and crushing.[8] The interparticle attraction or cohesion (c) and the angle of internal friction (ϕ) are the two commonly used parameters employed to quantify the shear strength. The values of these strength parameters are not constant, varying as a function of the loading condition, stress history, compaction, relative density, confining pressure, grain shape, hardness, and mineralogy, among other factors.

The peak friction angle at a given applied confinement is one of the measured parameters during shear testing that is widely adopted to characterize the shear strength of granular materials. Rowe (1962) proposed that the mobilized peak friction angle can be represented as the sum of the resistance to the interparticle sliding, or true friction angle (ϕ'_u), the resistance to crushing and rearrangement, and resistance due to dilation of the material (figure 1).[9] It should be noted that figure 1 displays a general trend, and the magnitude and exact shape of the components within the sketch could change slightly at extreme levels of confining stress or for samples with heterogeneous mineral composition and shape.

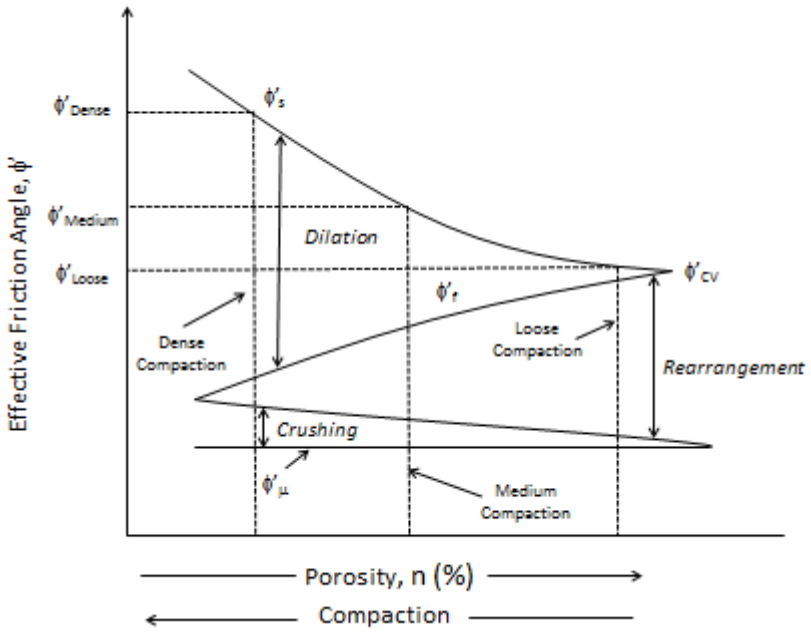

Figure 1. Chart. Effect of porosity and compaction on the shear strength of granular materials (modified from Rowe, 1962).[9]

As shown in figure 1, the rate of dilation is higher under denser states. The reason is that in a dense medium, rearrangement is limited, forcing particles to climb over each other during shearing and resulting in volume expansion and higher measured friction angles. With the increase in void ratio, the contribution from the dilation component diminishes gradually, and the particles shear primarily by rearrangement of adjacent particles, which results in more contraction and less dilation of the granular material during shear.[10] The general observation is that there is a net increase of the mobilized friction angle with the decrease in initial porosity because the rate of increase of the dilatancy component is higher than the rate of decrease of the rearrangement. The critical state is defined at the density state where the granular materials shear at a constant volume and stress state. At this state, the dilatancy rate diminishes and approaches zero; hence, the friction angle at this critical state is termed the constant volume (CV) friction angle (ϕ'_{cv}).

Visualizing the shear strength as a function of varying confining stress for a given density state, similar components comprise the mobilized peak friction angle (figure 2). At high effective confining stresses, the relative movement of the particles via dilation will reduce significantly. In addition, a high breakage rate through crushing will result in contraction, shifting the phase from the initially achieved true friction angle to a new phase of non-constant volume.[11]

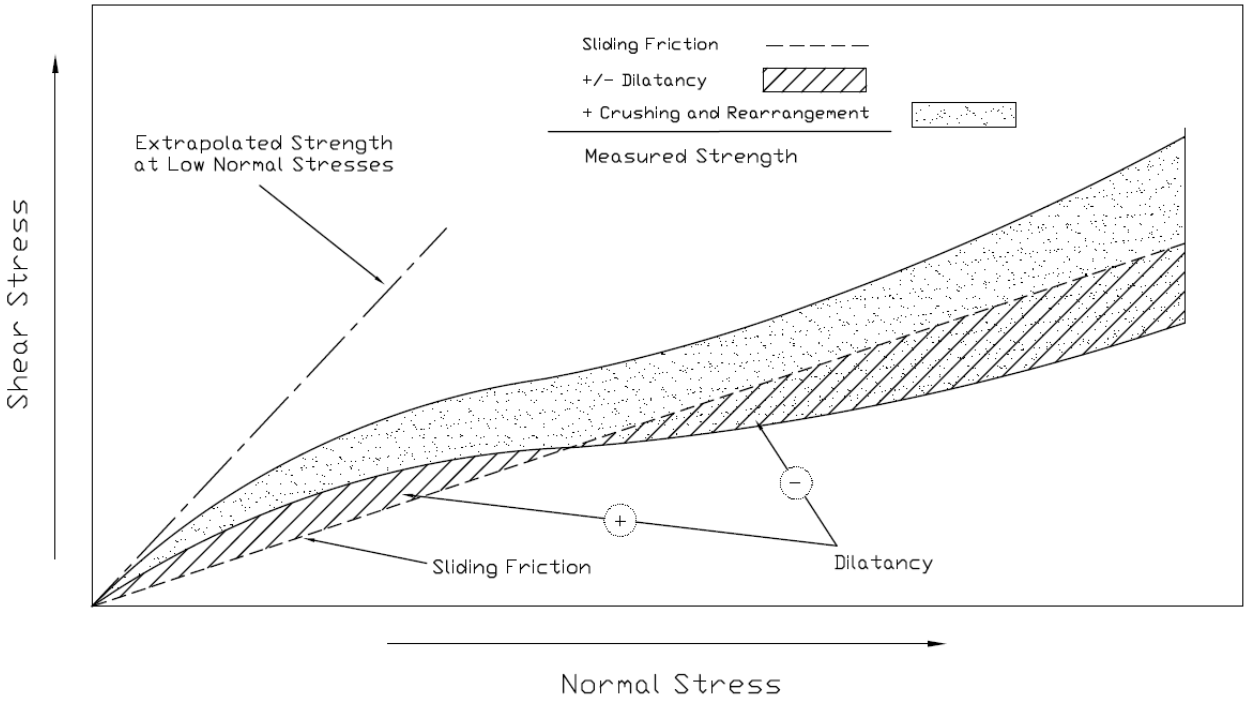

Figure 2. Chart. The theoretical determination of the drained shear strength for sands based on the three components that comprise the mobilized friction angle (after Lee and Seed, 1967).[(11)]

Knowledge about the contributing factors and the various laboratory shear strength tests, data interpretation, and the application of the strength parameters for designing geotechnical applications with OGAs is therefore important. In-situ tests are available to quantify or correlate with in-place shear strength; however, this study focuses on the laboratory analysis.

Laboratory Testing

The state of in-situ shearing deformations—which can eventually lead to failure—is oftentimes best approximated as a PS problem. For instance, the failures in several geotechnical applications such as landslide problems, retaining walls, earth dams, long foundations, culverts, pipe lines, tunnels, and beam foundations, for the most part, are all cases of PS; however, there is considerable difficulty in designing and conducting PS shear tests. Such tests require the fabrication of a special fixture, membrane, accessories, and preparation of a prismatic soil specimen.[(12)] The complexity of the PS shear test leads geotechnical engineering researchers and practitioners to the simpler DS or TX tests to characterize the shear strength of geomaterials.

Both DS and TX methods have been widely accepted for design and research to determine shear strength. The wide popularity of TX compression tests is partially because of the numerous structures designed and constructed based on the strength data from TX that perform well after many years, the ability of TX tests to combine simplicity with versatility, the ability to allow drainage control, the reproduction of the effects of most common field loading conditions, and the application of the desired major and minor principal stresses.[(13)] The wide application of DS tests in characterizing the strength parameters of granular materials is attributed to their

simplicity, requirement of shorter experimental run times, and ability to predetermine the orientation of the failure surface as desired and allow determination of the residual strength.[14] However, the inability to control the drainage and the non-uniformity of stress and strain in DS tests relative to PS and TX tests inhibits the suitability of DS apparatuses in studies that involve the stress-strain behavior of granular materials.

Note that there are several drawbacks associated with TX and DS tests relative to tests using a PS apparatus. One of the major differences between TX and PS is that in TX-based tests, the applied stresses are axisymmetric, leading to the absence of intermediate principle stresses. The DS tests are closer to the PS condition, but the geometry and boundary conditions of the DS test predetermine the localized region of high strains through which failure is forced to happen; failure is not allowed to occur along its natural plane.[15] The PS tests are better suited to help us understand the in-situ strain localization problems and shear band formations.[16] Several studies have reported the formation of shear bands along a well-defined shear failure plane in PS compression tests, whereas samples sheared in a TX apparatus rarely developed a distinct shear plane.[17,18,19] Instead, some microscale observations using advanced imaging techniques proved the prevalence of complex fan-shaped patterns in samples subjected to TX-based compression tests.[20,21]

The other difference among the different laboratory shear tests is the imposed lateral boundary conditions.[22] Both PS and DS tests have a rigid boundary condition that significantly reduces the grain movements during shearing. The flexible membrane boundary in TX tests allows lateral movement of the particles, which inhibits mobilization of the friction angles. The other marked difference of the testing methods is their effect on post peak strain behavior. For sand, Sterpi (2000) indicated that TX-based tests suggest a perfectly plastic behavior, whereas the PS results showed marked strain softening effects, in particular for the denser samples or for high values of confining stress levels.[23] In general, the measured shear strength from PS testing is greater than that measured from DS testing, which is greater than that measured from TX testing.

Regardless of test device, the determination of strength and deformation parameters for granular materials that contain particles of larger sizes such as rockfill materials and OGAs requires equipment of unconventional dimensions.[24] To be characterized by the conventional DS and TX apparatuses, which require smaller-sized specimens, the sizes of particles are reduced based on various modeling techniques. As cited by Honkanadavar and Sharma (2013), four modeling techniques are used to reduce the size of the prototype material: the scalping technique, the parallel gradation technique, the generation of a quadratic grain size distribution curve, and the replacement technique. (See references 25 through 29.) Following the findings of Ramamurthy and Gupta, which indicated that the parallel gradation was the best method, several other researchers have conducted shear tests on modeled materials based on the parallel gradation technique. (See references 30, 29, 24, and 31.) The results from these modeled materials could potentially lead to inaccurate deformation behavior and failure modes because of the inevitable size-dependent dilation and different mechanisms of particle crushing.[32] Therefore, the use of large-scale triaxial and direct shear apparatus is imperative for a realistic depiction of the strength and deformation characteristics of aggregates with large-size grains such OGAs.

Data Interpretation

The shear strength of granular materials is usually characterized by the angle of internal friction (ϕ) and cohesion (c). Because of the high drainage rate in OGAs, shear studies for OGAs should be conducted under drained condition, and for this reason, the stresses and strength parameters will be presented in their effective stress forms (e.g., ϕ', c', σ'_1, σ'_3). There are three concepts of presenting the values of friction angles for any shear test. First, a secant or peak friction angle (ϕ'_s) can be determined for a given test subjected to a specific effective consolidation stress and assuming a zero c-value due to the absence of cohesion in OGAs (figure 3). Secondly, a combined or tangent friction angle (ϕ'_t) can also computed for the same aggregate type (examined as the best-fit across a series of stress levels) to form the MC failure envelope (figure 3). Lastly, a CV friction angle can be computed as the friction angle in which there is zero dilation, termed the zero dilation angle (ZDA) approach.[3]

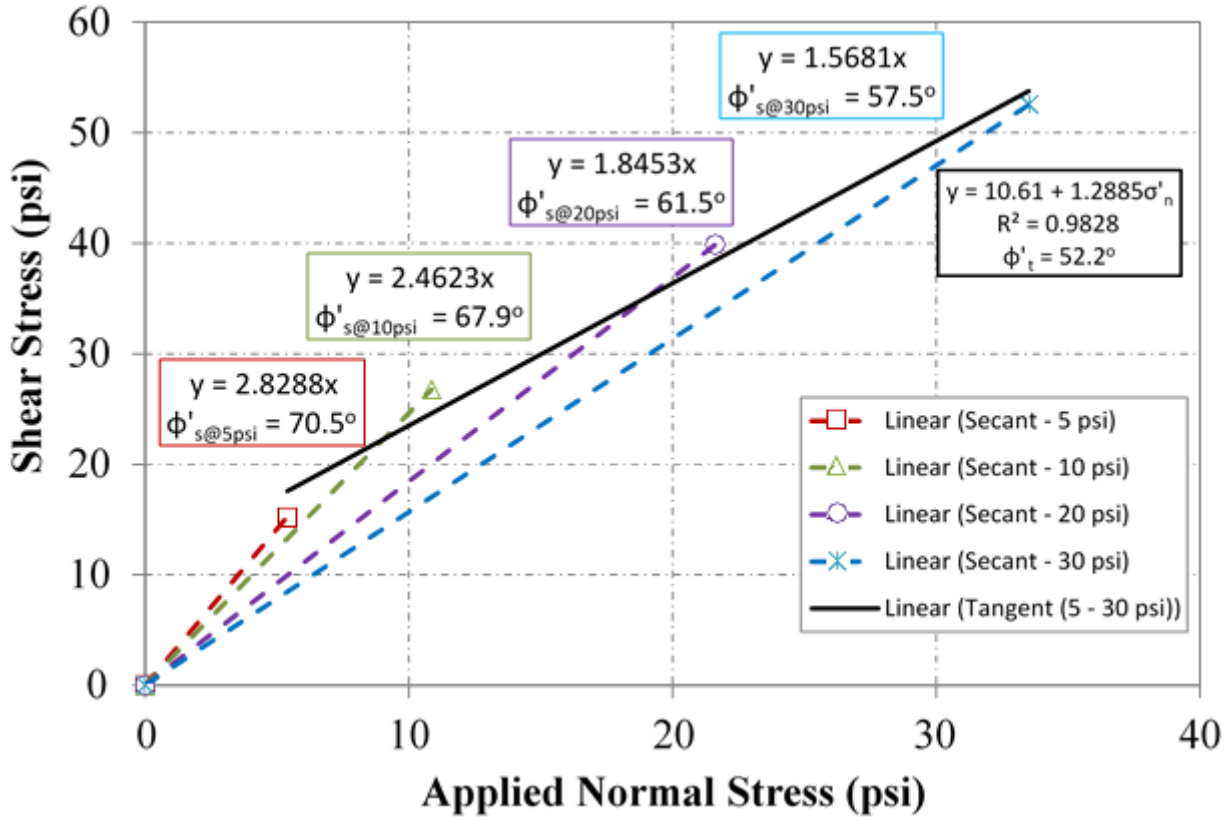

Figure 3. Chart. Secant (ϕ'_s) and tangent (ϕ'_t) friction angle illustration for DS testing.

The MC failure criterion is the most commonly adopted approach to determine ϕ'_t (equation 1).

$$\tau_f = c' + \sigma_n^{'} \tan \phi' \quad (1)$$

Where:

τ_f = Shear stress at failure.
$c^{'}$ = Effective cohesion.
$\sigma^{'}_n$ = Effective normal stress.
$\phi^{'}$ = Effective angle of internal friction.

For OGAs that are cohesionless, the cohesive term is zero. This approach assumes that shear failure starts at a point in a mass of soil when, on some surface passing through the point, a critical combination of shearing and normal stresses is reached.[10] The TX and DS equipment are developed to determine and investigate these critical combinations; the results are then used to compute the strength parameters.

In TX compression tests, it is assumed that only principal stresses are applied to the boundaries of the specimen, with the strength parameters extracted from the measured major (σ'_1) and minor ($\sigma^{'}_3$) principal stresses at failure. The shear stress path (q) and mean stress path ($p^{'}$) representations are computed for a series of tests according to equation 2 and equation 3, respectively.[33]

$$q = \frac{\sigma_1^{'} - \sigma_3^{'}}{2} \quad (2)$$

$$p' = \frac{\sigma_1^{'} + \sigma_3^{'}}{2} \quad (3)$$

When looking at stress paths, a modified failure envelope based on the p and q values was developed, commonly called the K_f line.[34] The envelope is defined by equation 4.

$$q = p^{'} \times \tan \alpha \quad (4)$$

Where:

α = Angle that the modified (stress-path) failure envelope makes with the horizontal.

The relationship between the tangent effective friction angle ($\phi^{'}_t$) and α is shown in equation 5.

$$\phi_t^{'} = \sin^{-1}(\tan \alpha) \quad (5)$$

For TX tests, the value of the secant or peak friction angle ($\phi^{'}_s$) for each specific test is computed using equation 6, which is developed from Mohr's circles by applying trigonometric relationships.[34]

$$\phi_s' = \sin^{-1}\left(\frac{\sigma_1' - \sigma_3'}{\sigma_1' + \sigma_3'}\right) \quad (6)$$

Unlike in TX tests, the major and minor principal stresses in DS tests are not measured. Hence, the applied normal stress and measured shear stress at failure are used to compute these strength parameters. Similar to TX test, the individual pairs of τ_f and σ'_n from a series of tests of the same aggregate type as a function of various confining stress are plotted, and the MC linear failure envelope is developed as the best fit line of the peak shear and normal stress values at these different stress points (figure 3). The value of ϕ'_t is then computed as the arctangent of the slope of the linear fit. The ϕ'_s value for each specific shear test is determined according to equation 7.

$$\phi_s' = \tan\left(\frac{\tau_f}{\sigma_n'}\right) \quad (7)$$

The linear MC failure criterion is the linear representation of the otherwise nonlinear failure envelope of the strength behavior. Several approaches have been developed to describe this nonlinear increase in peak shear strength of granular materials as a function of the increasing confining stress. The power strength function (equation 8) that was developed by Charles and Watts has been also adopted by other several other researchers with some modifications to the original equation. (See references 35 through 38.)

$$\tau = A\sigma_n^b \quad (8)$$

Where:

A and *b* = nonlinear material constants that are determined by curve fitting of the experimental data. This power curve strength model can be used to interpret data from both TX and DS tests.

Other models, such as the Hoek-Brown model, have been established to characterize strength of rock materials in terms of major and minor principal stresses. Therefore, they are more valid to TX data.[39,40,41] This model also has material constants that need to be estimated from the geological data and additional tests like uniaxial compressive strength. Nicks and Adams (2013) employed a ZDA that is based on the linear relationship between the friction angles and the dilation angles as a function of varying consolidation stresses for the same aggregate.[3] According to Bolton (1986), the y-intercept of the best-fit linear envelope in this approach corresponds to the constant volume or critical state friction angle (ϕ'_{cv}).[42] The advantage of this technique is that the effect of dilation is negated and a conservative shear strength value results without relying on an apparent cohesion value as in the linear MC approach.

This study focuses on the simple approaches that are used to determine common shear strength parameters (e.g. ϕ'_s, ϕ'_t,and ϕ'_{cv}) applicable for both TX and DS tests to have an unbiased comparison and an approach that does not require any additional strength tests. The MC linear relationship is widely used and accepted because of its reasonable tolerance for the majority of geotechnical applications.[36] This approach also does not require any other strength test or geological data and can be used to extract ϕ'_s and ϕ'_t for both TX and DS tests. The ZDA is another simple method to compute ϕ'_{cv}. Therefore, these two approaches are adopted and

compared in this study to characterize the strength parameters of the OGAs based on the TX and DS apparatuses.

Design Practices

The design practices in problems involving the application of stresses to soils may be divided into (a) deformation-controlled design (e.g., settlement), and (b) failure-controlled design (e.g., bearing resistance).[43] In other terms, the service and strength limit states must be satisfied in design. For applications involving relatively rigid structures such as bridge foundations and retaining walls, where deformations are expected to be low, the strength limit of the backfill or underlying soil is especially important. The shear strength of the backfill is therefore a key parameter in design.

Failure-controlled design for geotechnical applications involves the determination of the internal angle of friction (ϕ), which is one of the fundamental engineering parameters. The friction angle is critical because it is used to compute lateral pressures and bearing resistance. For transportation applications, the AASHTO Load and Resistance Factor Design Bridge Design and Constructions Specifications are primarily employed.[44,45,46] For mechanically stabilized earth (MSE) walls, the design specifications note that a value of 34 degrees may be assumed for the friction angle, with a limit of 40 degrees if tested. The construction specifications require verification of the design assumption that the material exhibits a friction angle of at least 34 degrees on the portion passing the No. 10 (0.08-inch) sieve, as determined by the standard direct shear (SDS) test.[45] No testing is required for backfills where 80 percent of the sizes are greater than 0.75 inch. While the AASHTO specifications do not prohibit the use of OGAs, FHWA guidelines for MSE walls, which are adopted by many transportation agencies, recommend the use of well-graded materials.[47,48] For geosynthetic reinforced soil walls and abutments, both OGAs and well-graded aggregates meeting a minimum friction angle of 38 degrees can be used in construction. No maximum limitation is imposed if appropriately tested in the laboratory.

Based on a survey of State transportation departments, approximately 74 percent responded that they use assumed strength parameters for backfills in retaining wall design, with 65 percent of the respondents assuming a friction angles of 34 degrees or less.[49] When testing is performed, 60 percent and 70 percent stated that they use direct shear and triaxial devices, respectively. A review of the literature found reported friction angles for poorly graded granular materials tested using DS and TX devices (table 1). Despite the availability of vast strength data that demonstrate friction angles higher than the default of 34 degrees for various granular materials conducted using all kinds of shearing tests devices, there is very limited data on large-sized aggregates with a narrow gradation, such as the AASHTO M43 aggregates (e.g., OGAs). Three studies were found that examined materials close to the No. 7, No. 56, and No. 57 aggregates.[50,51,52]

For the approximate No. 7 aggregate, the difference between standard DS and TX tests was about 7 degrees; the TX results were 15 percent less than the DS results (table 1). For the approximate No. 56 aggregate, the difference was significantly larger between the two types of tests, with the TX 25 degrees, or 33 percent, lower than the DS. The researcher acknowledged that in most reported works in literature, the difference in friction angles are much lower, but the researcher concluded that such reports are not valid for the tested Bremanger sandstone.[51]

Two researchers reported friction angles for the No. 57 aggregate; however, both focused on either TX or DS testing, with no comparison.

Limited studies do show the comparison of ϕ' values from both TX and DS tests for OGAs. From table 1, the maximum reported is 33 percent, with TX values being lower than DS; while high, this finding is consistent with other research findings showing that TX friction angles are lower than DS, which are lower than PS. (See references 53 through 56.) Based on a compilation of various studies on sand, Kulhawy and Mayne (1990) presented the relationship for DS and TX compression testing, also as a function of the CV friction angle (equation 9).[57]

$$\phi_{DS} = \tan^{-1}\{\tan(1.12\phi_{TX})\cos(\phi_{cv})\} \quad (9)$$

This relationship is based on sands and standard testing devices. Because of the lack of a sufficient database of the strength and stress-strain properties of the AASHTO M 43 designated aggregates, there is an absence of any established relationships of strength data between PS condition (as well as DS test) and the axisymmetric loading condition of TX tests. Therefore, the scarcity of such data is one of the major motivations of this work.

Table 1. Reported friction angles from DS and TX testing.

Sample No.	Backfill Soil Description	d_{max} (inches)	Test Method	ϕ' (degrees)[1]	Reference
1	Uniform subrounded fine to medium sand	0.187	DS	43	58
2	Uniformly graded fine to medium sand	0.630	DS	41	
3	Clean uniform-size washed sand with some gravel	0.315	DS	46–53	
4	Poorly graded sand with gravel	—	TX	38	59
5	Non-plastic poorly graded sand	—	TX	38	
6	Poorly graded sand	—	DS	36.4	48
7	Poorly graded sand	—	DS	38.5	
8	Poorly graded sand	—	DS	39.2	
9	Poorly graded sand	—	DS	40.9	
10	Poorly graded sand	—	DS	41.5	
11	Poorly graded sand	—	DS	42.4	
12	Durable sandstone	12.00	DS (square, 5 ft)	43 (32 psi confinement)	60
		0.75	DS (circular, 0.5 ft)	52.5 (32 psi confinement)	
	Non-durable silty shale rock	12.00	DS (square, 5 ft)	44 (32 psi confinement)	
		0.75	DS (circular, 0.5 ft)	52.2 (39 psi confinement)	
13	Manufactured granular material	0.787	DS	44–45 (e_o = 0.68–0.69)	61
				36–38 (e_o = 0.8–0.83)	
			TX	42–45 (e_o = 0.68–0.69)	
	Rockfill material	1.969	DS	51–55 (e_o = 0.37)	
				37–38 (e_o = 0.56)	
			TX	52–55 (e_o = 0.37)	

Sample No.	Backfill Soil Description	d_{max} (inches)	Test Method	ϕ' (degrees)[1]	Reference
				48–49 (e_o = 0.42)	
	Rockfill material	3.937	DS	50–54 (e_o = 0.42)	
				38–39 (e_o = 0.56)	
14	Dacite rock material (close to a No. 7)	1.476	TX	41	50
			DS	48.3	
	Crushed stone and crushed sandstone	1.476	TX	50.1	
			DS	56	
15	Andesite rockfill material	1.969	TX	39.9–57.8	24
16	Poorly graded sandstone rockfill (close to a No. 56)	—	TX DS	49.9 74.9	51
17	No. 57 (Limestone)—Low density	—	TX	53.5 (σ'_3 = 4 psi) 42.8 (σ'_3 = 30.3 psi)	52
	No. 57 (Limestone)—High density			53.1 (σ'_3 = 3.7 psi) 44.1 (σ'_3 = 30 psi)	
	No. 57 (Phyllite)—Low density	—	TX	54.6 (σ'_3 = 3.9 psi) 51 (σ'_3 = 9.7 psi)	
	No. 57 (Phyllite)—High density			56.1 (σ'_3 = 4 psi) 52.8 (σ'_3 = 9.8 psi)	
18	Densified No. 57 crushed stone	—	DS	49	62

[1]Unless specified for a single confining pressure, ϕ' refers to the tangent friction angle obtained from the Mohr-Coulomb failure envelope.
DS = Direct shear.
TX = Triaxial.
— = Information not provided

2.3 DESIGN IMPLICATIONS

As previously discussed, the strength of these materials is an important design consideration. For OGAs, the strength is primarily defined by the internal friction angle (ϕ). The selection of friction angle, therefore, has significant impacts on the design of geotechnical features. It plays a role in the earth pressure coefficients, used in the determination of lateral earth pressures. In retaining wall design, the active earth pressure coefficient (K_a) is often used for failure conditions (equation 10). The higher the friction angle, the lower the coefficient, and thus the lower the lateral pressures that need to be resisted in design.

$$K_a = \tan^2\left(45^o - \frac{\phi}{2}\right) \quad (10)$$

The internal friction angle is also important in determining bearing capacity factors (table 2) used in the conventional equation to estimate nominal bearing resistance, described by Munfakh et al. (2001).[44,45] As the bearing factors increase in value, the bearing resistance also increases, thus reducing the required size of the foundation. Table 3 illustrates the impact of using higher friction angles on K_a and the bearing capacity factors, N_c, N_q, and N_γ. The difference in K_a between 34 degrees and 45 degrees is a factor of 1.6; the differences in bearing resistance are even higher. By utilizing the actual strength properties of OGAs rather than defaulting to 34 degrees, more cost-effective designs can be realized.

Table 2. Bearing capacity factors.[44]

ϕ	N_c	N_q	N_γ	ϕ	N_c	N_q	N_γ
0	5.14	1.0	0.0	23	18.1	8.7	8.2
1	5.4	1.1	0.1	24	19.3	9.6	9.4
2	5.6	1.2	0.2	25	20.7	10.7	10.9
3	5.9	1.3	0.2	26	22.3	11.9	12.5
4	6.2	1.4	0.3	27	23.9	13.2	14.5
5	6.5	1.6	0.5	28	25.8	14.7	16.7
6	6.8	1.7	0.6	29	27.9	16.4	19.3
7	7.2	1.9	0.7	30	30.1	18.4	22.4
8	7.5	2.1	0.9	31	32.7	20.6	26.0
9	7.9	2.3	1.0	32	35.5	23.2	30.2
10	8.4	2.5	1.2	33	38.6	26.1	35.2
11	8.8	2.7	1.4	34	42.2	29.4	41.1
12	9.3	3.0	1.7	35	46.1	33.3	48.0
13	9.8	3.3	2.0	36	50.6	37.8	56.3
14	10.4	3.6	2.3	37	55.6	42.9	66.2
15	11.0	3.9	2.7	38	61.4	48.9	78.0
16	11.6	4.3	3.1	39	67.9	56.0	92.3
17	12.3	4.8	3.5	40	75.3	64.2	109.4
18	13.1	5.3	4.1	41	83.9	73.9	130.2
19	13.9	5.8	4.7	42	93.7	85.4	155.6
20	14.8	6.4	5.4	43	105.1	99.0	186.5
21	15.8	7.1	6.2	44	118.4	115.3	224.6
22	16.9	7.8	7.1	45	133.9	134.9	271.8

Table 3. Impact of friction angle on geotechnical constants in design.

ϕ	K_a	N_c	N_q	N_γ
34	0.282	42.2	29.4	41.1
40	0.217	75.3	64.2	109.4
45	0.171	133.9	134.9	271.8

CHAPTER 3. TEST PROGRAM AND RESULTS

3.1 MATERIALS

In this study, 12 of the 19 AASHTO M43 gradations are tested and selected because of their common use in geotechnical applications as well as the limitations of the testing equipment available (table 4). The 12 unique samples ranged from an AASHTO No. 10 to an AASHTO No. 5. For the No. 8 aggregate, five different samples were tested to investigate the effect of source; four were from various quarries around the Commonwealth of Virginia, and one was from Defiance County, OH. In total, 16 aggregates were tested in this study.

Table 4. Selected AASHTO M43-05 (ASTM D448) aggregate designations.

	Percent Passing Through Sieve											
Sieve No.	**No. 5**	**No. 56**	**No. 57**	**No. 6**	**No. 67**	**No. 68**	**No. 7**	**No. 78**	**No. 8**	**No. 89**	**No. 9**	**No. 10**
1.5 inches	100	100	100									
1 inch	90–100	90–100	95–100	100	100	100						
0.75 inches	20–55	40–85		90–100	90–100	90–100	100	100				
0.50 inches	0–10	10–40	25–60	20–55			90–100	90–100	100	100		
0.375 inches	0–5	0–15		0–15	20–55	30–65	40–70	40–75	85–100	90–100	100	100
4		0–5	0–10	0–5	0–10	5–25	0–15	5–25	10–30	20–55	85–100	85–100
8			0–5		0–5	0–10	0–5	0–10	0–10	5–30	10–40	
16						0–5		0–5	0–5	0–10	0–10	
50										0–5	0–5	
100												10–30

There are two geologic materials for the series of aggregates tested in this study: diabase and limestone (table 5). All of the aggregates tested are diabase except for the No. 89 and various No. 8 samples, which are limestone (Nos. 8A, 8B, 8C, and 8D). Diabase is an igneous rock, whereas limestone is a sedimentary rock. Typically, igneous rocks will be harder/stronger than sedimentary rocks. The limestone in Defiance County, OH, is from the Devonian period, while the limestone found in Virginia is from the Triassic period.[63, 64] Pictures of each sample tested are shown in appendix A.

Table 5. OGAs tested.

AASHTO Gradation	Rock Source	Location
No. 5	Diabase	Ashburn, VA
No. 56	Diabase	Ashburn, VA
No. 57	Diabase	Sterling, VA
No. 6	Diabase	Ashburn, VA
No. 67	Diabase	Ashburn, VA
No. 68	Diabase	Sterling, VA
No. 7	Diabase	Ashburn, VA
No. 78	Diabase	Sterling, VA
No. 8A	Limestone (Devonian)	Defiance County, OH
No. 8B	Limestone (Triassic)	Staunton, VA
No. 8C	Limestone (Triassic)	Harrisonburg, VA
No. 8D	Limestone (Triassic)	Stafford, VA
No. 8E	Diabase	Ashburn, VA
No. 89	Limestone (Devonian)	Defiance County, OH
No. 9	Diabase	Sterling, VA
No. 10	Diabase	Ashburn, VA

3.2 LABORATORY TESTING AND RESULTS

Because the AASHTO manufactured OG aggregates had not been fully characterized, a suite of tests was conducted, including gradation, minimum and maximum density, repose angle, angularity, texture, and strength.

Gradation

The first step with each aggregate was to perform a sieve analysis on oven-dried samples to ensure that the gradation of the sample met the appropriate AASHTO M43 specifications (figure 4). The sieve analysis was conducted according to the AASHTO T27 test method.[65] Particle sizes of interest, the coefficient of uniformity (C_u) and coefficient of curvature (C_c), and the Unified Soil Classification System classification are presented in table 6. The fine content for the aggregates (percent passing the No. 200 sieve) is less than 3 percent, except for the No. 10 aggregate, which has about 11 percent (appendix A). Aggregates larger than a No. 9 are classified as poorly graded gravels; No. 9 and No. 10 are both poorly graded sands.

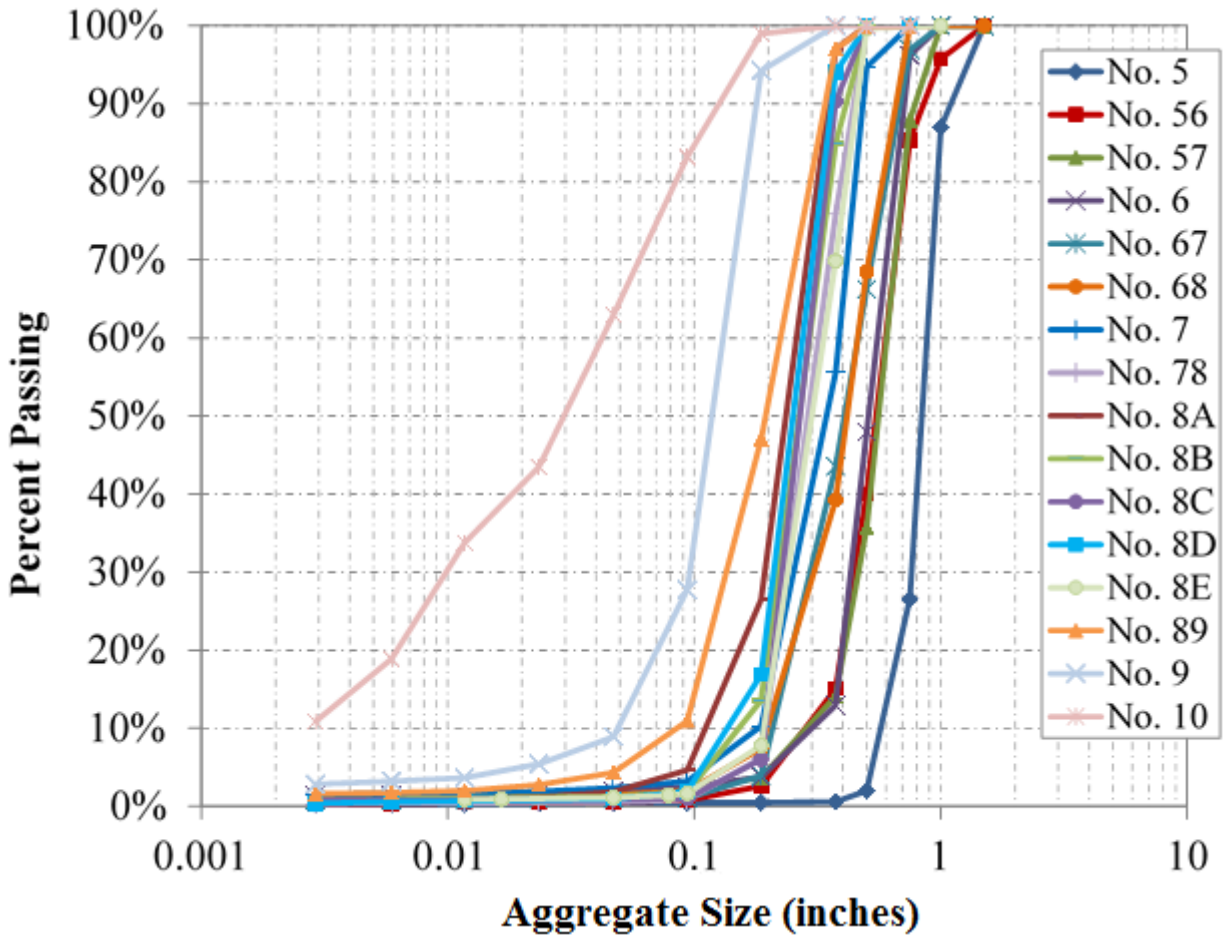

Figure 4. Graph. Sieve analysis results of tested aggregates.

In addition, the fineness modulus (FM) was estimated for each aggregate. The FM is typically used in pavement and concrete materials. According to the manual for concrete practice, the FM is a factor obtained by adding the total percentages by weight of an aggregate sample retained on each of a specified series of sieves and dividing the sum by 100; in the United States, the standard sieve sizes are No. 100, No. 50, No. 30, No. 16, No.8, No.4, 0.375 inches, 0.75 inches, and 1.5 inches.[66] The FM was shown analytically to be proportional to the average of the logarithmic particle size distribution (the higher the value, the more coarse the aggregate). In the standard specification for concrete aggregates (ASTM C33), the FM for fine aggregate must be between 2.3 and 3.1.[67]

Density

The minimum and maximum dry unit weight for the aggregates were determined using the funnel (Method A of ASTM D4254) and vibratory table (Method 1A of ASTM D4253) methods, respectively.[68,69] This information is useful in calculating the weight of the material for geotechnical applications and in determining relative compaction and relative density for laboratory testing requirements. In the field, compaction control for OGAs is typically a method-based specification, such as compact to non-movement or no appreciable displacement and

assess with visual inspection.[70] Other methods of compaction control have included the use of a nuclear density gauge and soil stiffness gauge.[71]

Table 6. Aggregate gradation and classification.

Sample	d_{max} (inches)	d_{85} (inches)	d_{60} (inches)	d_{50} (inches)	d_{30} (inches)	d_{10} (inches)	C_u	C_c	FM	USCS
No. 5	1.5	0.992	0.888	0.847	0.764	0.582	1.53	1.13	7.71	GP
No. 56	1.5	0.748	0.61	0.555	0.45	0.299	2.04	1.11	6.95	GP
No. 57	1	0.736	0.616	0.569	0.467	0.301	2.05	1.18	6.88	GP
No. 6	1	0.692	0.563	0.511	0.436	0.315	1.79	1.07	6.78	GP
No. 67	1	0.653	0.466	0.41	0.311	0.216	2.16	0.96	6.51	GP
No. 68	0.75	0.631	0.434	0.421	0.32	0.202	2.15	1.17	6.46	GP
No. 7	0.75	0.469	0.389	0.352	0.269	0.184	2.11	1.01	6.23	GP
No. 78	0.75	0.423	0.332	0.305	0.251	0.197	1.69	0.96	6.15	GP
No. 8A	0.5	0.343	0.276	0.250	0.196	0.117	2.36	1.19	5.68	GP
No. 8B	0.5	0.38	0.31	0.283	0.23	0.16	1.78	1.18	5.96	GP
No. 8C	0.5	0.36	0.31	0.29	0.24	0.20	1.57	0.96	5.99	GP
No. 8D	0.5	0.35	0.29	0.268	0.22	0.14	1.86	1.24	5.85	GP
No. 8E	0.5	0.438	0.345	0.315	0.254	0.194	1.78	0.96	6.19	GP
No. 89	0.5	0.33	0.236	0.198	0.143	0.087	2.71	1.00	6.35	GP
No. 9	0.375	0.174	0.139	0.125	0.097	0.05	2.78	1.35	4.64	SP
No. 10	0.375	0.1045	0.0433	0.031	0.0102	0.0029	14.93	0.83	2.98	SP

FM = Fineness modulus.
GP = Poorly graded gravel.
SP = Poorly graded sand.
USCS = Unified Soil Classification System.

Because of the wide range of aggregate sizes tested, two cylindrical molds were used: a 0.1-ft^3 mold for aggregates with a maximum diameter less than or equal to 0.75 inches, and a 0.5-ft^3 mold for aggregates larger than 0.75 inch (figure 5). For the minimum density test, a scoop was used to place all aggregates, except the No. 9 and No. 10 aggregates, for which a pouring device with a 1-inch diameter spout was used for placement. Three sets of tests were performed for each aggregate, and the average minimum index density is reported in table 7.

For the maximum density tests, double amplitude of vertical vibration of 0.013 inch at 60 Hz was set. A digital linear variable differential transformer (LVDT) was used to measure the sample displacement during vibratory testing (figure 6). Two tests were performed on each aggregate, and the average maximum index density was reported (table 7). The No. 10 aggregate was the heaviest, weighing as much as a conventional well-graded aggregate, but it also has the highest coefficient of uniformity (C_u).

Figure 5. Photo. Mold (0.1 ft^3) for funnel and vibratory table tests.

Table 7. Unit weight of aggregates.

Sample	Minimum (pcf)	Maximum (pcf)
No. 5	94.9	109.6
No. 56	100.6	103.8
No. 57	95.4	108.7
No. 6	101.0	110.3
No. 67	106.2	124.10
No. 68	96.9	115.9
No. 7	103.3	120.9
No. 78	92.3	109.6
No. 8A	85.7	101.3
No. 8B	—	—
No. 8C	—	—
No. 8D	—	—
No. 8E	97.9	112.8
No. 89	88.4	108.2
No. 9	92.3	110.7
No. 10	115.8	146.3

— = Not measured.

Figure 6. Photo. LVDT and mold set-up for vibratory table tests.

Repose Angle

The angle of repose is the maximum angle relative to the horizontal direction that a material can naturally sustain. Various methods are available to measure the repose angle; the one adopted by the authors consists of scooping the aggregate into a 6-inch diameter hollow cylinder resting vertically on a level platform and then slowly raising the cylinder to allow the aggregate to naturally fall into a conical pile (figure 7 and figure 8). The repose angle was then measured using an average of two methods: (1) protractor device tilted to match the slope of the pile in five locations, and (2) string method whereby the circumference of the stockpile was measured three times and compared with the volume of the aggregate to determine the height and corresponding angle (table 8).

The full set of results is provided in appendix A. Because the No. 8 aggregate study was started after initiation of the strength characterization, the repose angle was not tested for the various source locations because the results indicated no correlation. In any case, a general trend is found where the repose angle increases with increasing mean grain size, as expected (figure 9).[(72)]

Figure 7. Photo. Repose angle cylinder test.

Figure 8. Photo. Aggregate pile to determine repose angle.

Table 8. Repose angle of aggregates.

Sample	Repose Angle		
	Angle Finder	String Method	Average
No. 5	30.1	31.5	30.8
No. 56	31.4	29.6	30.5
No. 57	29.7	30.8	30.2
No. 6	31.2	29.7	30.4
No. 67	27.6	28.4	28.0
No. 68	32.3	29.5	30.4
No. 7	29.3	27.9	28.6
No. 78	33.6	32.6	33.1
No. 8A	31.1	30.8	31.0
No. 8B	—	—	—
No. 8C	—	—	—
No. 8D	—	—	—
No. 8E	—	—	—
No. 89	29.9	31.6	30.7
No. 9	26.8	27.8	27.3
No. 10	27.4	25.3	26.4

— = Not measured.

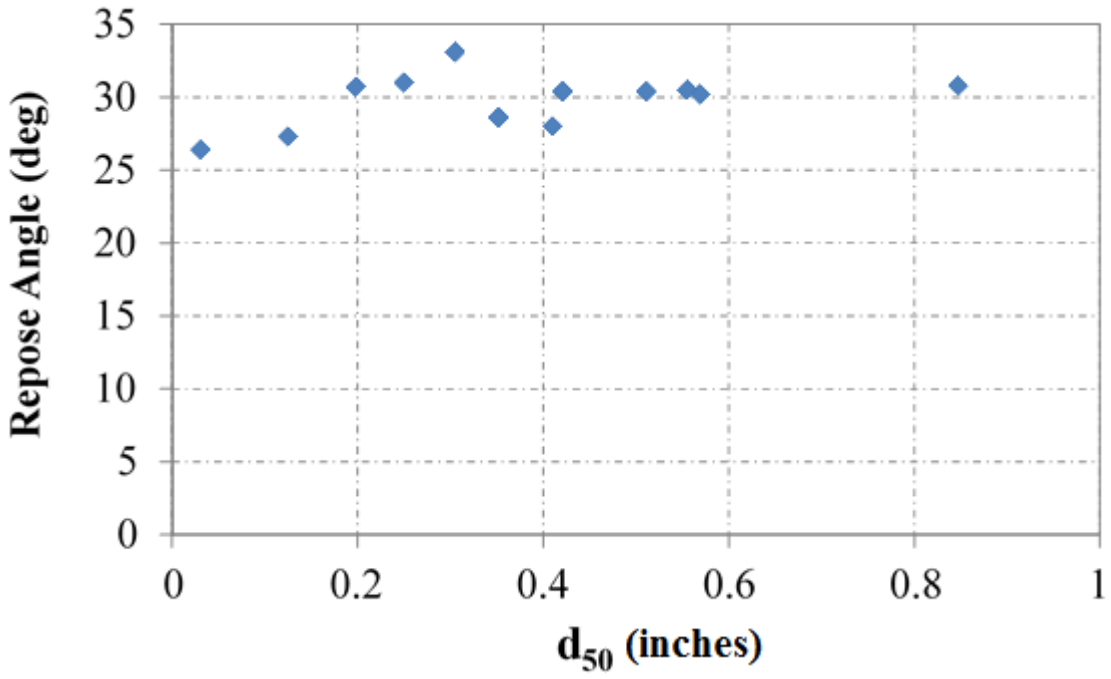

Figure 9. Chart. Relationship between repose angle and mean aggregate size.

Angularity, Texture, and Sphericity

The aggregate imaging measurement system (AIMS) is a device that combines hardware that can capture real-time digital images of fine and course aggregates with software that can process those images and analyze the distribution of particle angularity, texture, and sphericity for the sample.[73] The second-generation AIMS device (AIMS2) is primarily used in the pavement industry for asphalt and concrete design; however, its applicability for structural backfill was investigated in this study. The procedure involves placing aggregates within an indented slot on a circular tray; the plate is then rotated slowly with a backlight, illuminating it as a digital camera takes images of the aggregates. Algorithms within the companion software convert the images to a graphical output describing the aggregates' angularity, texture, sphericity, and other parameters.

Angularity describes variations at the edges of the aggregates; in AIMS, it was defined as an index in terms of rounded, sub-rounded, sub-angular, or angular (figure 10), but in AIMS2, this index was changed to low, moderate, high, and extreme, although the relative range of the categories did not change.[74,73] To better relate angularity (as well as texture and sphericity) for geotechnical applications, the initial AIMS classifications are used herein. The surface texture of aggregates is also important; the index is defined in terms of polished or smooth, or low, moderate and high roughness (figure 11). Sphericity describes the degree of cubicalness of an aggregate; it is defined in terms of high sphericity (e.g., the aggregate is roughly the same dimension in all axes), moderate sphericity (i.e., semi-circular), low sphericity (i.e., semi-elongated), and flat/elongated (figure 12).

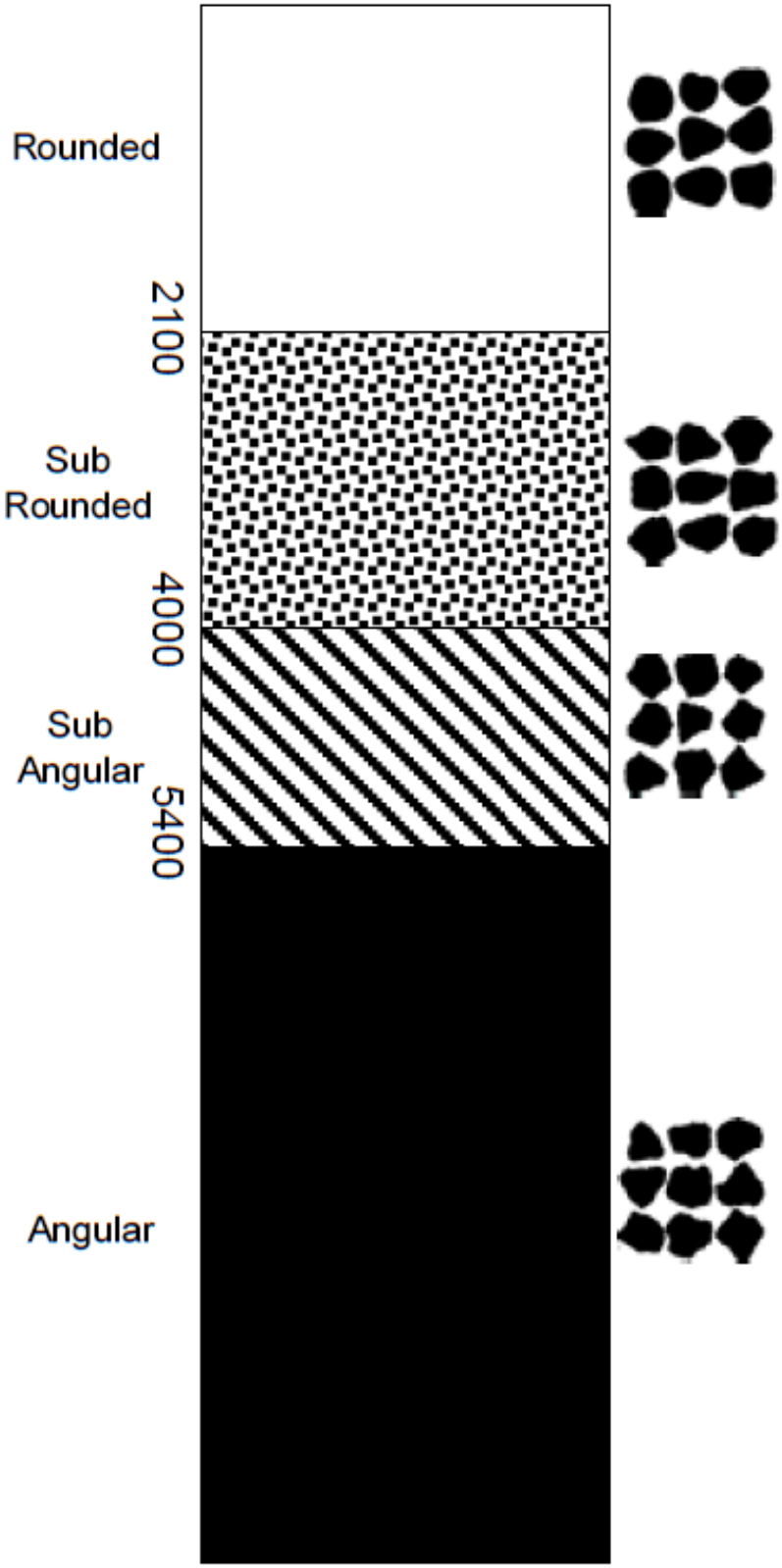

Figure 10. Diagram. AIMS angularity index classification ranges.[74]

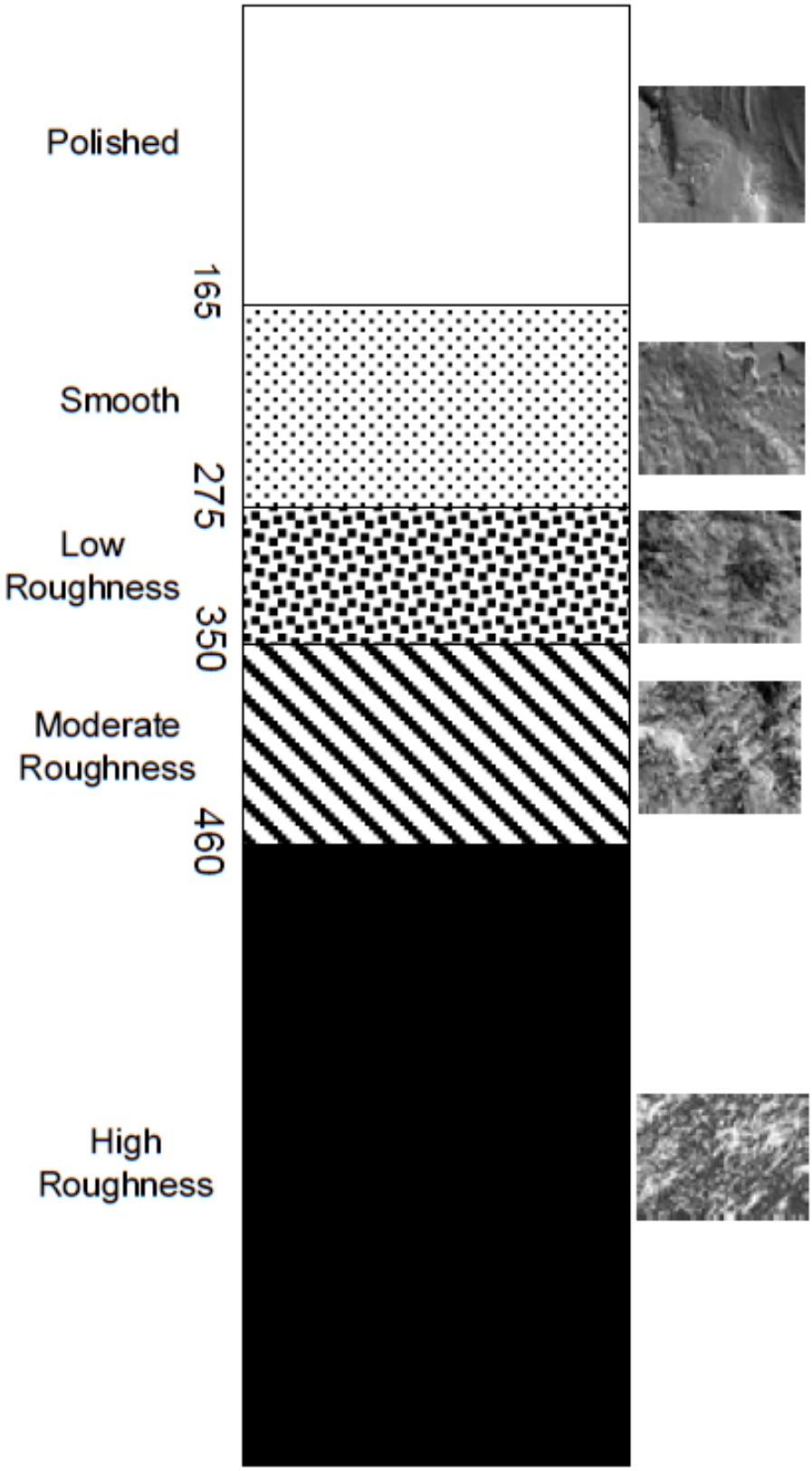

Figure 11. Diagram. AIMS texture classification ranges.[74]

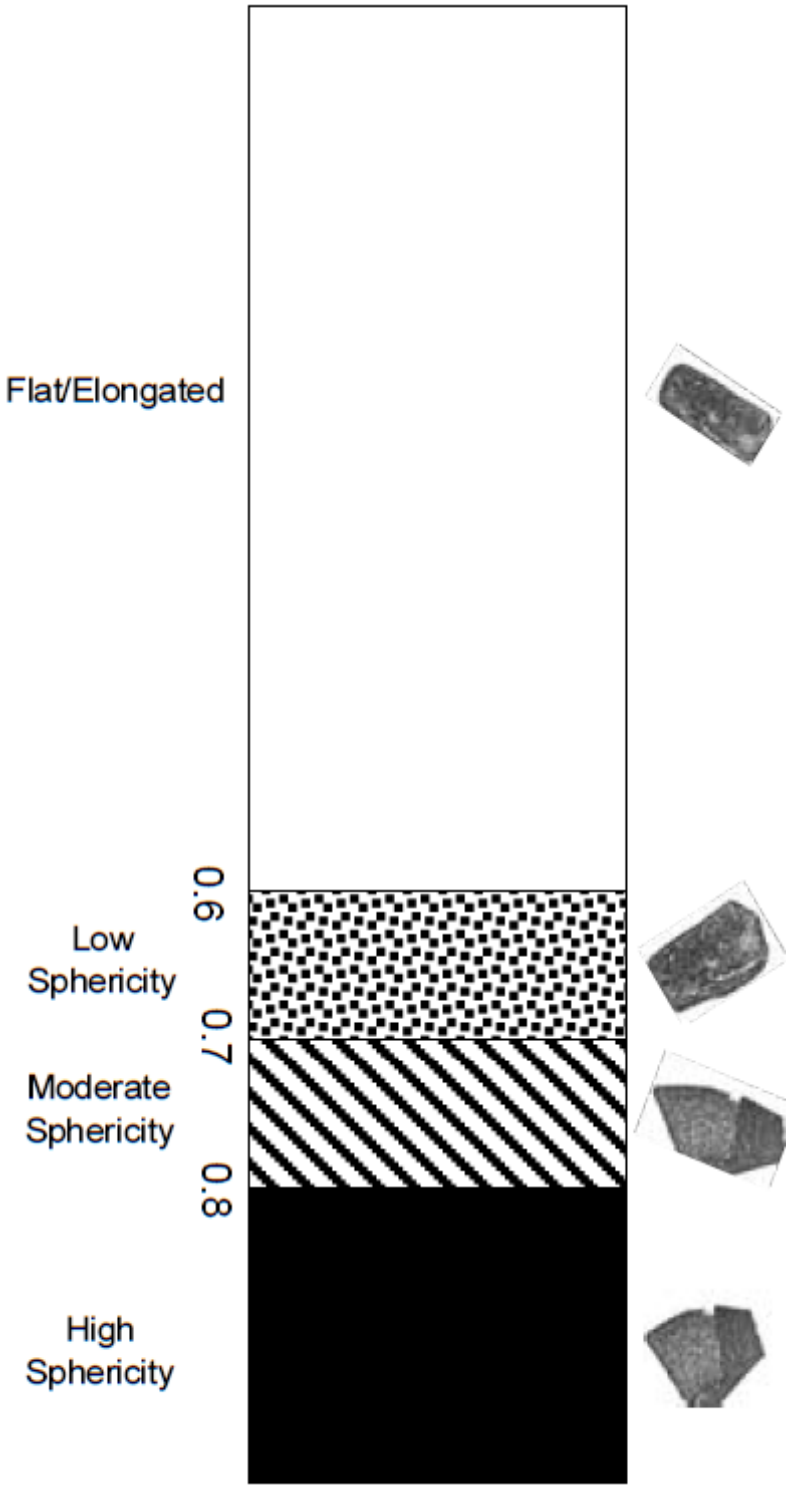

Figure 12. Diagram. AIMS sphericity index classification ranges.[74]

AIMS2 measures angularity by the gradient method, texture by wavelet analysis, and sphericity by three-dimensional measurements taken from the microscope (for depth) and the image from the camera (using eigenvector analysis).[73] After performing the analysis, the cumulative

distribution of angularity, texture, and sphericity indexes for all particles making up the aggregate sample tested was then plotted (figure 13, figure 14, and figure 15, respectively). The averages for each aggregate are presented in table 9.

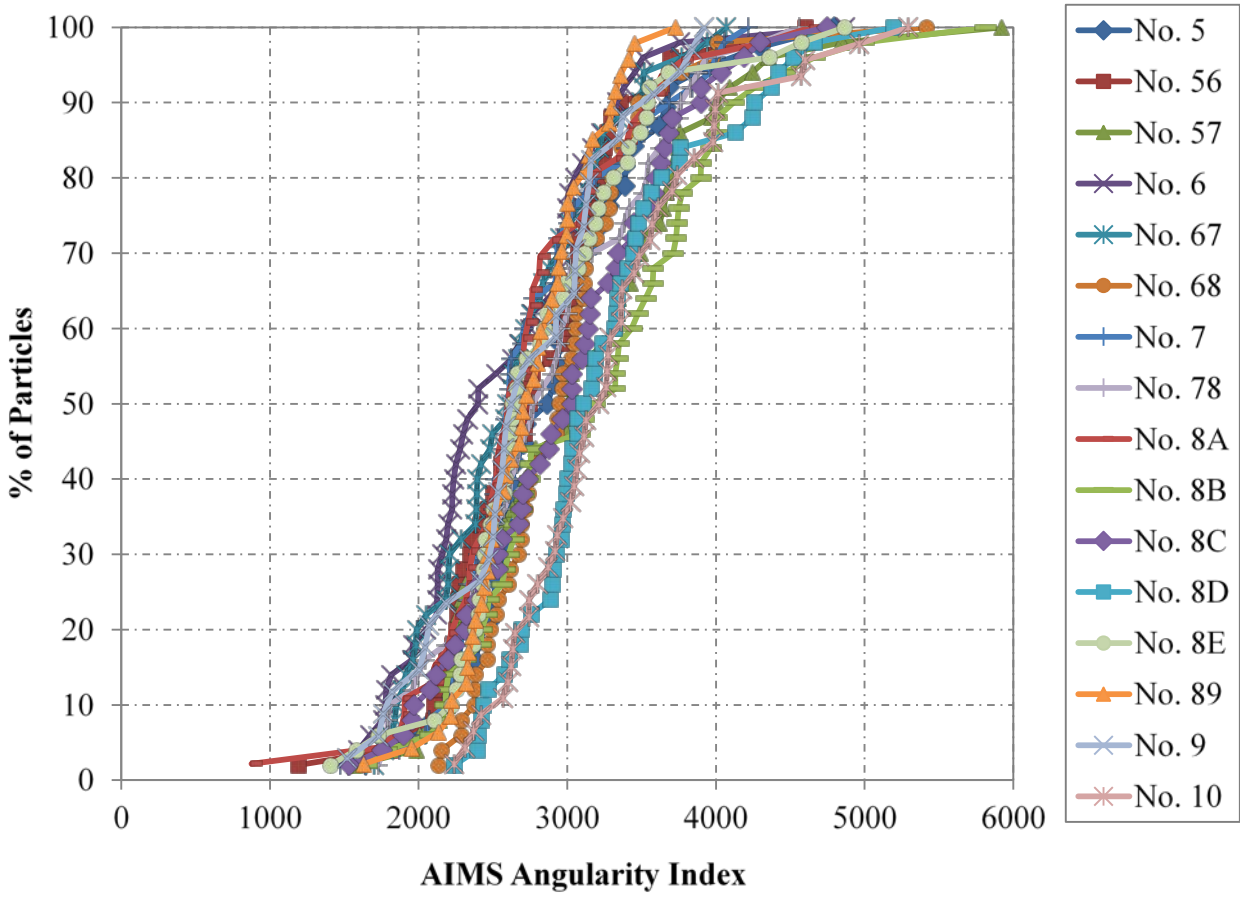

Figure 13. Chart. Angularity results from AIMS2.

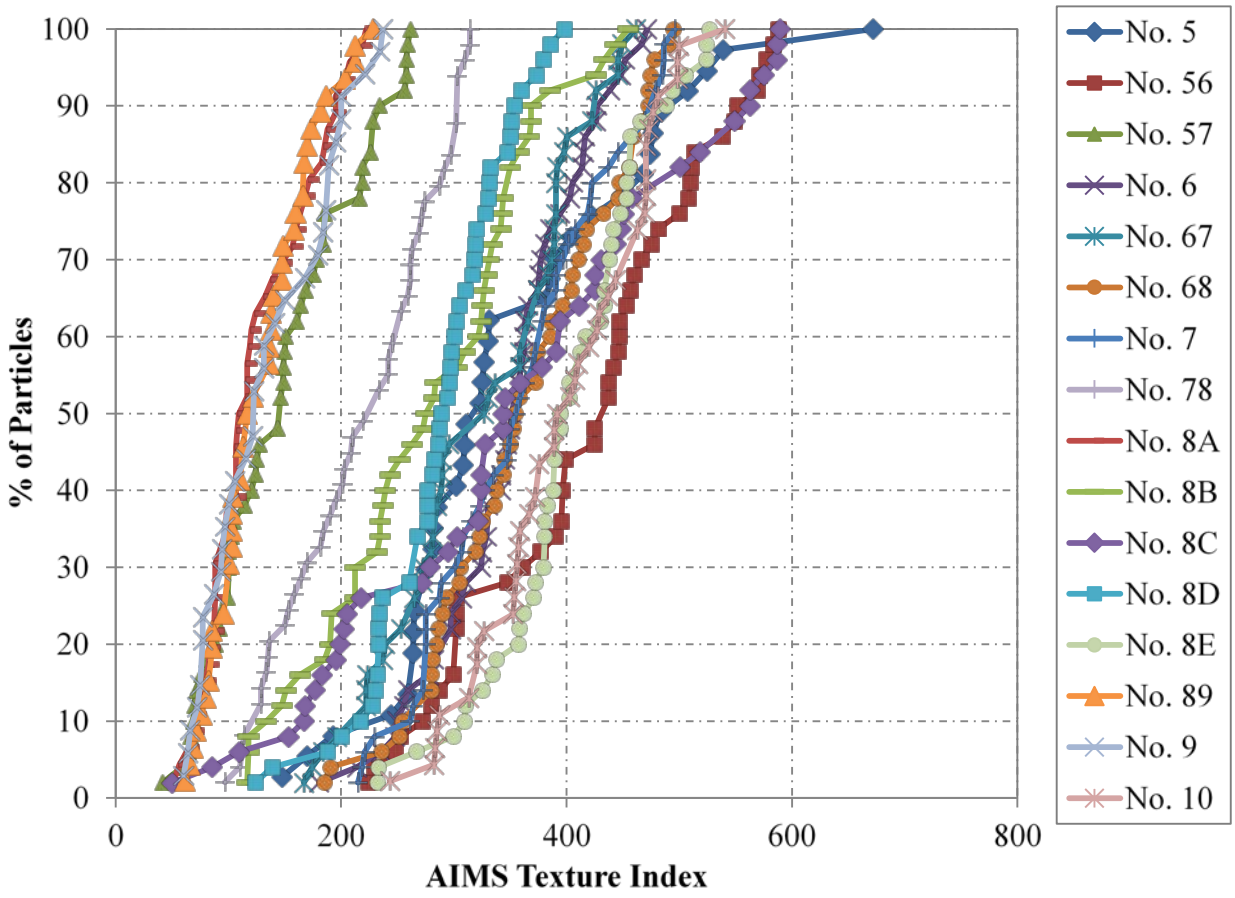

Figure 14. Chart. Texture results from AIMS2.

Although visual analysis suggests the aggregates are angular, the average of the measured distributions using AIMS2 is between 2,100 and 4,000, indicating that the aggregates are sub-rounded based on the AIMS classification (table 9). The texture and sphericity of the aggregates were slightly more scattered. Characterizing the aggregates based on AIMS results in six sample groups: (1) No. 5, No. 56, No. 68, No. 8C, and No. 8E all have sub-rounded angularity, moderate roughness, and low sphericity; (2) No. 57, No. 8A, No. 89, and No. 9 all have sub-rounded angularity, polished texture, and low sphericity; (3) No. 6, No. 67, and No. 7 all have sub-rounded angularity, moderate roughness, and moderate sphericity; (4) No. 8B and No. 8D both have sub-rounded angularity, low roughness, and flat/elongated particles; (5) No. 10 is similar to Nos. 8B and 8D, except it has flat/elongated particles; and (6) No. 78 is the only aggregate with a smooth texture and low sphericity. Note that these properties are specific to the aggregates tested in this study, as evidenced by the various No. 8 aggregates. The use of AIMS in the classification of aggregates for structural backfill will be further investigated.

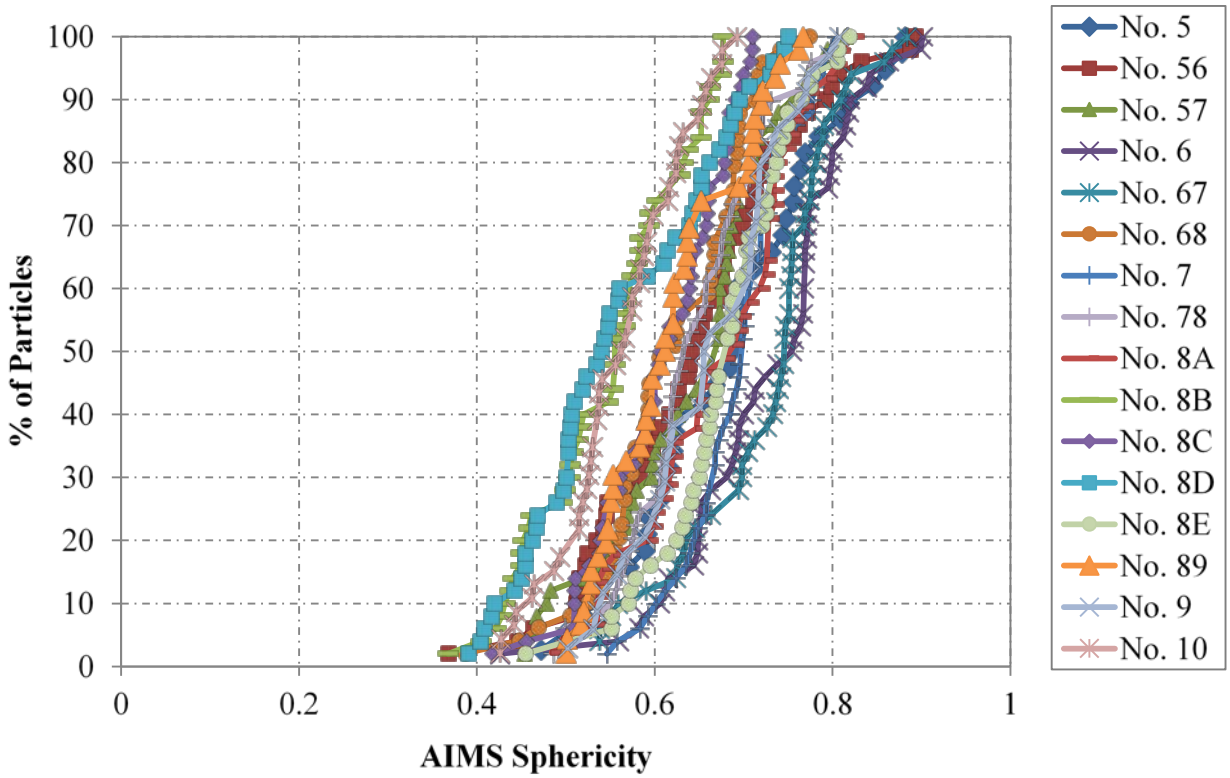

Figure 15. Chart. Sphericity results from AIMS2.

Table 9. Summary of AIMS2 average results for angularity, texture, and sphericity.

Sample	Angularity		Texture		Sphericity	
	Average Index	Classification	Average Index	Classification	Average Index	Classification
No. 5	2915.2	Sub-Rounded	375.6	Moderate Roughness	0.688	Low
No. 56	2774.7	Sub-Rounded	447.4	Moderate Roughness	0.644	Low
No. 57	3083.1	Sub-Rounded	161.2	Polished	0.662	Low
No. 6	2577.2	Sub-Rounded	360.1	Moderate Roughness	0.74	Moderate
No. 67	2643.1	Sub-Rounded	361.1	Moderate Roughness	0.741	Moderate
No. 68	2985.8	Sub-Rounded	373.5	Moderate Roughness	0.64	Low
No. 7	2770.5	Sub-Rounded	370.2	Moderate Roughness	0.714	Moderate
No. 78	2869.6	Sub-Rounded	232.5	Smooth	0.654	Low
No. 8A	2714.6	Sub-Rounded	154.2	Polished	0.682	Low
No. 8B	3202.1	Sub-Rounded	295.9	Low Roughness	0.565	Flat/Elongated
No. 8C	2984.3	Sub-Rounded	379.3	Moderate Roughness	0.629	Low
No. 8D	3269.3	Sub-Rounded	298.1	Low Roughness	0.567	Flat/Elongated
No. 8E	2834.2	Sub-Rounded	419.8	Moderate Roughness	0.699	Low
No. 89	2742.1	Sub-Rounded	152.1	Polished	0.641	Low
No. 9	2726.2	Sub-Rounded	149.8	Polished	0.675	Low
No. 10	3295.5	Sub-Rounded	418.4	Moderate Roughness	0.581	Flat/Elongated

Strength

The strength of the aggregates was determined using three different devices: SDS, LSDS, and LDTX. In each test, samples were placed in the devices uncompacted with a relative density around 30 percent based on the vibratory table tests (table 7).

Standard Direct Shear Tests

Oftentimes, soil samples will be sent for DS testing to determine the strength parameters (friction angle and cohesion) of the material. The most common DS devices are either 2.5 inches in diameter or 4 inches square. According to ASTM D3080, the maximum particle size of the sample tested must be less than $1/10^{th}$ the width or diameter of the device; for a 2.5-inch diameter device, the maximum particle size is limited to 0.25 inch, and for the 4-inch square device, the maximum particle size is limited to 0.4 inch.[(75)] For this reason, samples are often scalped, which neglects the effect the larger aggregate particles may have on strength.

From table 6, only two of the smaller AASHTO M43 aggregates could be tested in a standard 4-inch DS device: the No. 9 and No. 10. For most geotechnical applications utilizing OGAs, where a minimum of 0.5-inch maximum particle size is typically specified, standard DS testing cannot be performed. This limitation requires either (a) scalping the sample, whereby material greater than that which can be tested according to ASTM is removed; (b) generating a parallel gradation with the material, whereby the maximum gradation is $1/10^{th}$ the DS device size with the remaining gradation curve parallel to that of the actual sample; or (c) testing in a larger DS device, whereby nothing special needs to be done to the sample.

Test Setup: To evaluate the impact of scalping the sample, SDS tests were performed according to ASTM D3080 using a 2.5-inch circular device in the geotechnical laboratory at FHWA's Turner-Fairbank Highway Research Center (TFHRC) (figure 16); material larger than the No. 4 sieve (opening size of 0.187 inches) was removed prior to testing. The shear rate was set at 0.002 inches/min based on the maximum measured time for 90 percent consolidation (t_{90}) using the square root of time method (Taylor's method); the gap size was 0.025 inches.[(75)]

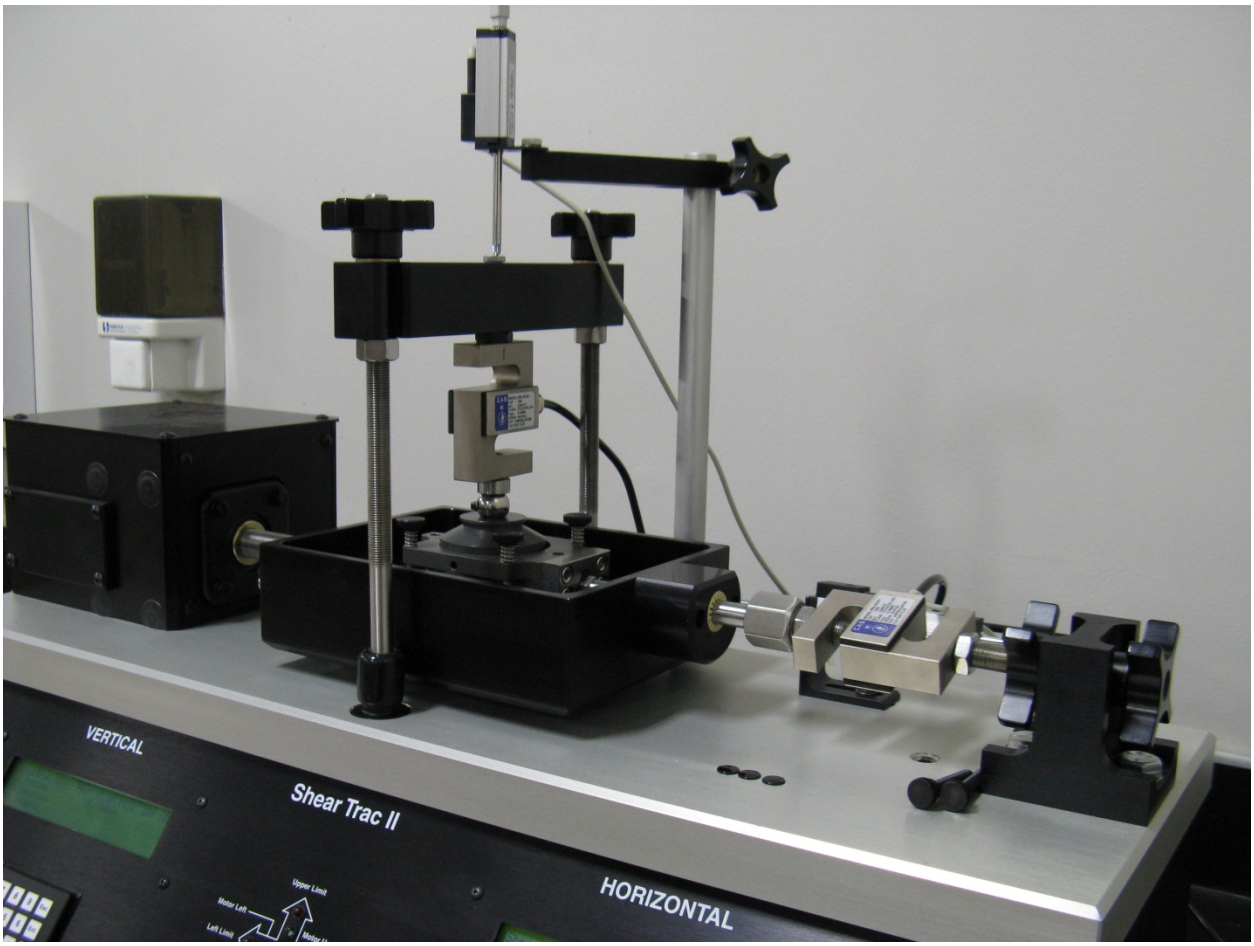

Figure 16. Photo. SDS test device at TFHRC.

Prior to testing the aggregates, three sets of tests were performed using Ottawa 20/30 sand to ensure appropriate and repeatable results with the SDS device. The resulting measured peak friction angles for each test (dry and uncompacted), using the conventional MC criteria, are

shown in table 10. The values are all less than 3 percent of the average, or 33 degrees for the tangent friction angle, which is consistent for Ottawa sand and demonstrates the repeatability of the test method.[76,77]

Table 10. Ottawa test results using SDS device and MC approach.

Test	Tangent Friction Angle (degree)	Secant Friction Angle at 5 psi (degree)
1	34	34
2	32	31
3	33	32

After verification of the test apparatus and procedures using Ottawa sand, four tests were performed for each AASTHO aggregate tested, at different applied normal stresses: 5, 10, 20, and 30 psi. This range of stresses was selected based on typical loads a retaining wall or foundation utilizing these aggregates may experience, with 30 psi equivalent to most in-service, bridge-bearing pressures. The samples were tested in a dry condition.

For each initial applied normal stress, the shear stress and horizontal displacement were measured during shear using a load cell and LVDT, respectively. An example for the No. 57 aggregate is shown in figure 17.

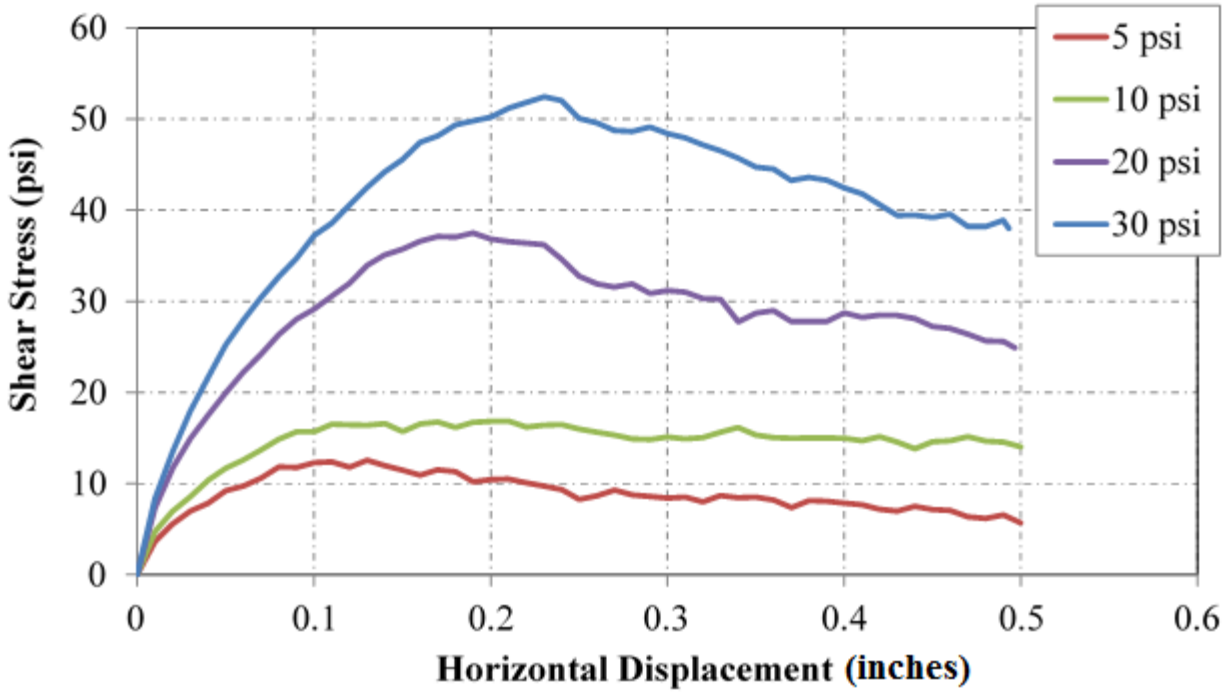

Figure 17. Chart. Shear stress versus horizontal displacement for No. 57 from SDS tests.

The peak shear stress (τ_f) is equal to the maximum measured during testing. In some cases, the peak shear stress was not always reached. (See figure 18 as an example.) The peak was therefore determined to equal the shear stress measured at a lateral strain of 20 percent (or 0.5 inches for a 2.5-inch device).[75]

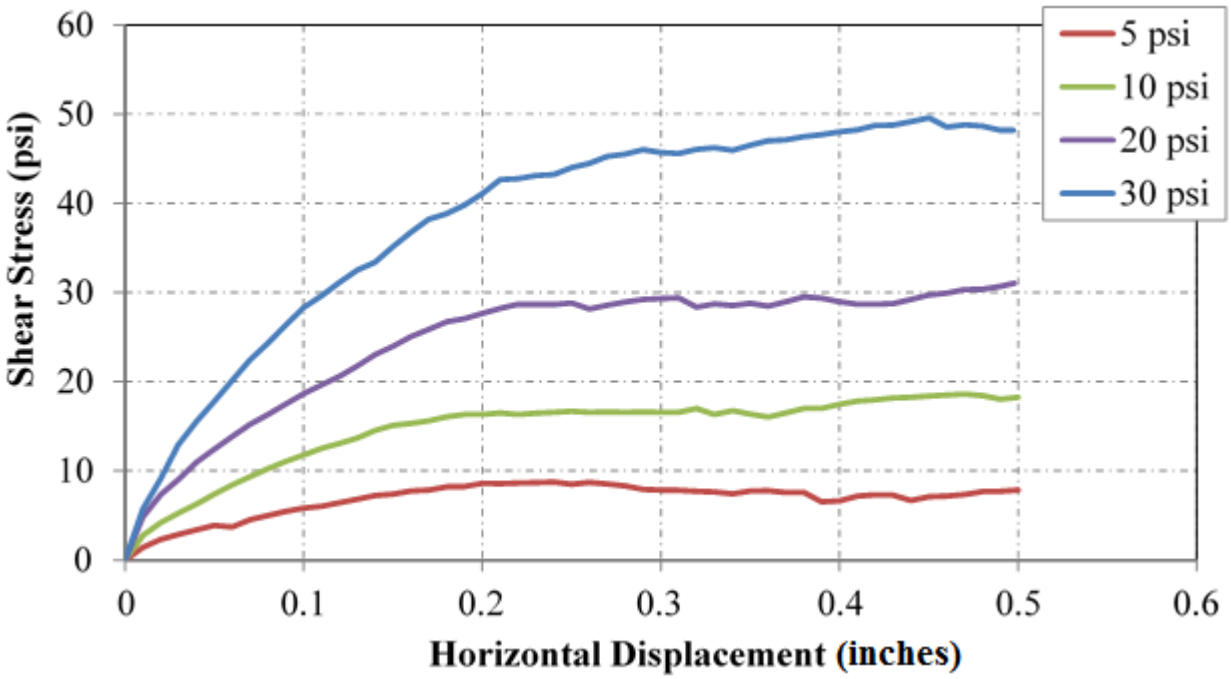

Figure 18. Chart. Shear stress versus horizontal displacement for No. 5 from SDS tests.

MC Approach: Using the MC approach, the peak shear stress is then compared with the corresponding applied normal stress. Note that the applied normal stress must be corrected during the shear phase because the contact area is constantly changing. For a circular sample, the area correction factor (*F*) is found using equation 11.

$$F = \frac{2}{\pi}\left\{\cos^{-1}\left(\frac{h}{D}\right) - \frac{\Delta h}{D}\left(1 - \left[\frac{h}{D}\right]^{2}\right)\right\} \quad (11)$$

Where:

h = Horizontal displacement.
D = Sample diameter.

The correction factor is then applied to the original sample area (A_o) to determine the corrected area (A_c); see equation 12.

$$A_c = FA_o \quad (12)$$

This post-processing procedure was performed on each set of results to determine the normal pressure at the point of peak shear stress. No correction is needed for the recorded shear stress.

The peak, or secant, friction angle (ϕ'_s) at each corresponding applied normal stress (σ'_n) is calculated according to equation 13.

$$\phi'_s = \tan^{-1}\left(\frac{\tau_f}{\sigma'_n}\right) \quad (13)$$

If a known applied load is given, then the corresponding peak friction angle can be directly selected (termed the secant angle of friction); however, oftentimes the stresses will be variable so a tangent internal angle of friction (ϕ'_t) is determined over a range of stresses. The best-fit linear regression through the four points represents the MC failure envelope. (See figure 19 as an example.) The tangent of the slope is equal to the internal friction angle, and the shear stress intercept is equal to the (apparent) cohesion.

The results of standard DS testing using the linear MC approach for all of the aggregates are presented in table 11. Note that aggregates 8B, 8C, 8D, and 8E were not scalped and tested using the standard DS device. Appendix A provides the standard DS test results (peak shear and corresponding normal stress) leading to the resulting friction angle and measured cohesion in table 11.

The measured friction angles range between 43 and 57 degrees, with an average of 52 degrees. The results are generally within 10 percent of the average. The scalped samples indicate high strength, but the accuracy is unknown because the majority of the particles were removed. Eight of the samples removed about 90 percent of the sample or more during scalping, but two of the samples (No. 9 and No. 10) did not need much scalping, so their results may be more reliable. Comparison to large-scale testing will help in the analysis.

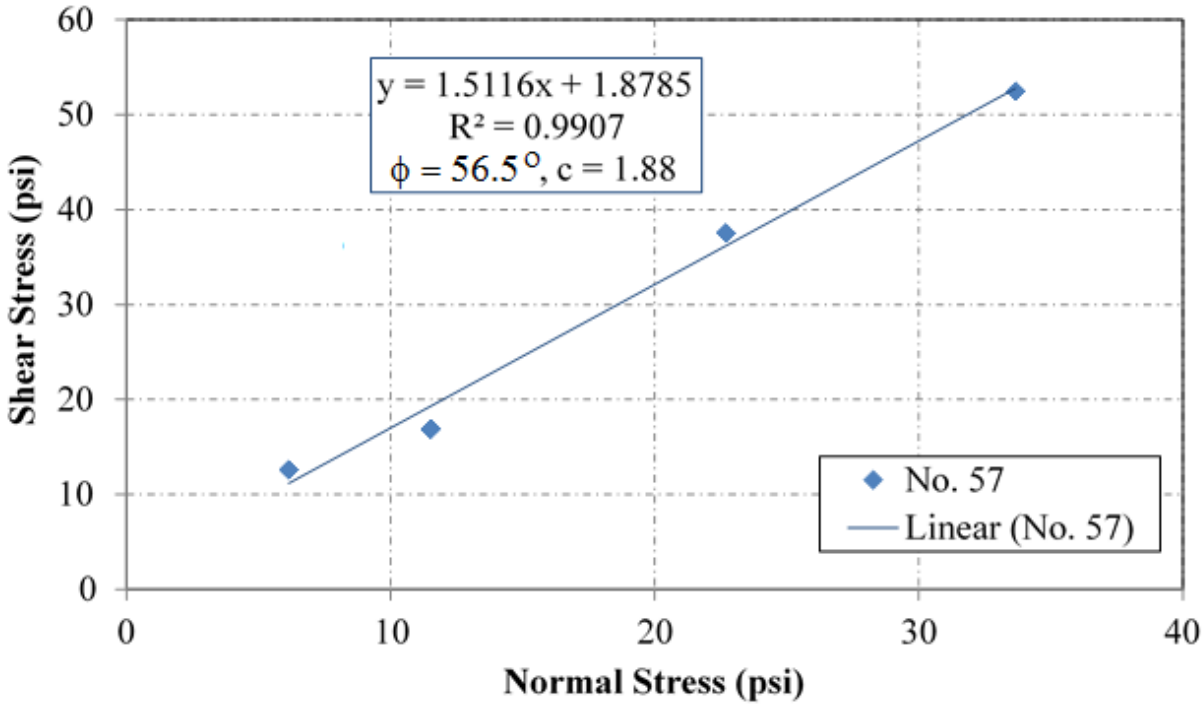

Figure 19. Chart. Shear versus normal stress for No. 57 using SDS.

Table 11. SDS test results using MC approach.

Sample	Percent Passing No. 4 Sieve (figure 4)	$\phi'_{t,SDS}$ (degree)	c'_{SDS} (psi)
No. 5	0.46	50.1	1.7
No. 56	2.58	51.7	6.5
No. 57	3.67	56.5	1.9
No. 6	3.72	51.7	4.2
No. 67	3.96	57.3	7.1
No. 68	7.40	42.8	9.5
No. 7	10.26	54.6	7.8
No. 78	6.18	51.3	9.7
No. 8A	26.50	53.0	5.2
No. 8B	—	—	—
No. 8C	—	—	—
No. 8D	—	—	—
No. 8E	—	—	—
No. 89	47.01	54.0	6.1
No. 9	94.22	50.2	3.5
No. 10	98.96	50.6	3.3

$\phi'_{t,SDS}$ = The friction angle using the Mohr-Coulomb (MC) approach.
c'_{SDS} = The shear stress intercept from the best-fit linear MC failure envelope.
— = Not measured.

Note that using a linear MC interpretation results in a cohesion value for each test because the y-intercept of the best-fit approximation is not zero (figure 19, for example); however, these aggregates are cohesionless. This inconsistency is attributed to the fact that the failure envelope is actually nonlinear; there is also aggregate interlocking and dilation that occurs during shearing, depending on the applied normal stress.[54] In reality, the friction angle decreases with increased applied normal stress in a logarithmic function. For the range of stresses tested, the secant friction angle corresponding to the peak for each applied normal stress was larger than that approximated from the MC approach. Because of these issues, the use of an alternative ZDA method is proposed to determine the design friction angle, which is based on the critical state or constant volume concept.[3]

ZDA Approach: The ZDA method requires knowledge about the dilation behavior of the sample. The vertical displacement during the consolidation and shearing phases was measured using an LVDT. Comparing the vertical displacement to the horizontal displacement during shear provides an indication of the dilation behavior of the aggregates. An example for the No. 57 aggregate is shown in figure 20. Positive vertical displacement indicates compression of the sample, whereas negative displacement indicates dilation. The dilation angle (ψ) is found according to equation 14.

$$\tan\psi = \frac{\Delta v}{\Delta h} \quad (14)$$

Where:

Δv = The change in vertical displacement.
Δh = The change in horizontal displacement.

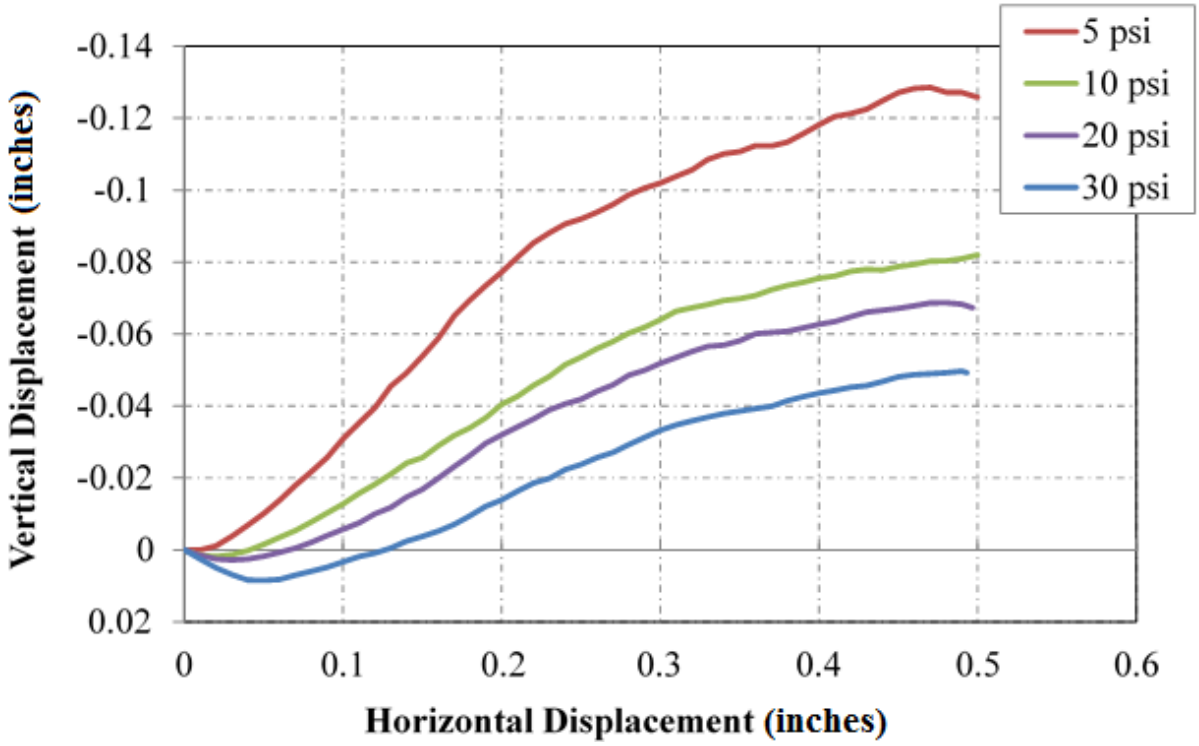

Figure 20. Chart. Deformation behavior of No. 57 during SDS testing.

Data for the DS testing is provided at every 0.01 inch of horizontal displacement, so Δh is constant. As the sample is sheared, Δv will change for each horizontal displacement increment. The maximum dilation angle for the aggregate is therefore found when the maximum change in vertical displacement occurs. A three-point moving average of the change in vertical displacement was taken to smooth the data and eliminate any misleading sharp peaks.

There is generally a linear relationship between the measured dilation angles and the peak friction angles. The intercept at zero dilation is the constant volume friction angle (ϕ'_{cv}) found using the ZDA approach. For example, ϕ'_{cv} is equal to 49 degrees for the No. 57 aggregate (figure 21). The resulting friction angle for each aggregate is shown in table 12; however, when combining the aggregates together (figure 22), there is no clear relationship. It was observed that the dilation angles measured during testing were sporadic and not as expected, likely a result of the considerable scalping performed on the aggregates, which changes its dilative behavior.

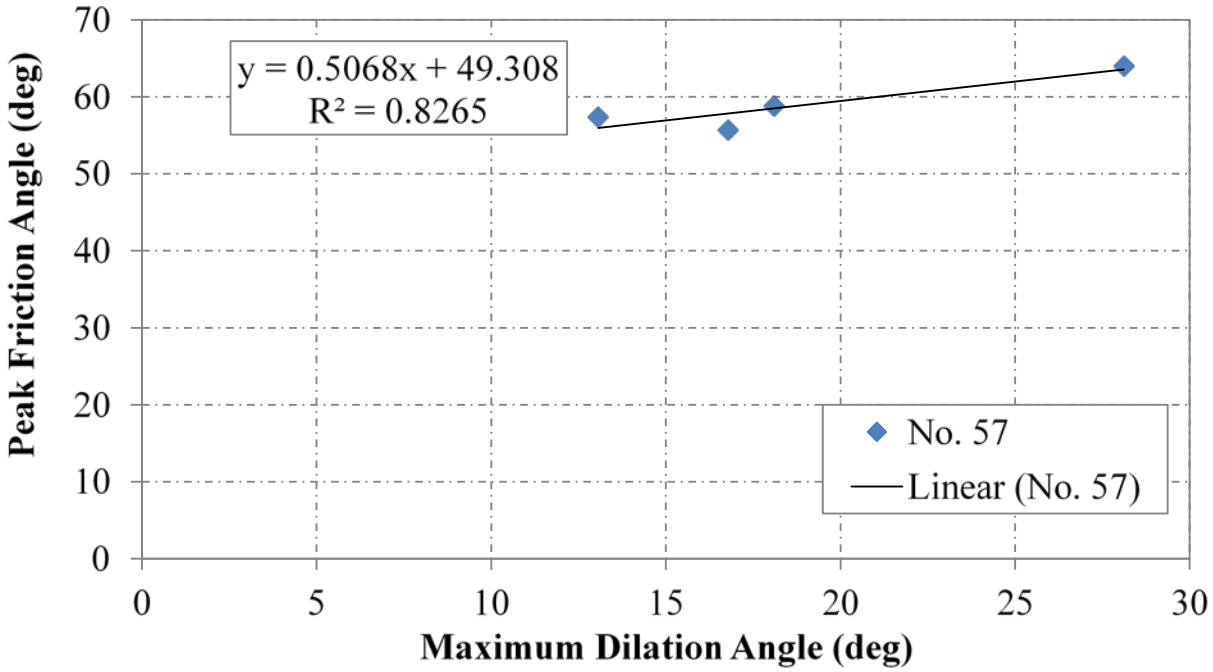

Figure 21. Chart. Friction angle versus dilation angle for No. 57 using SDS.

Table 12. SDS test results using the ZDA approach.

Sample	$\phi'_{cv,SDS}$ (degree)
No. 5	50.6*
No. 56	37.7
No. 57	49.0
No. 6	53.9
No. 67	49.1
No. 68	36.9
No. 7	51.3
No. 78	44.2
No. 8A	37.3
No. 8B	—
No. 8C	—
No. 8D	—
No. 8E	—
No. 89	42.3
No. 9	52.0
No. 10	39.0

*Modified zero dilation angle approach whereby the stress-strain curves were used to determine constant volume friction angle.

— = Not measured.

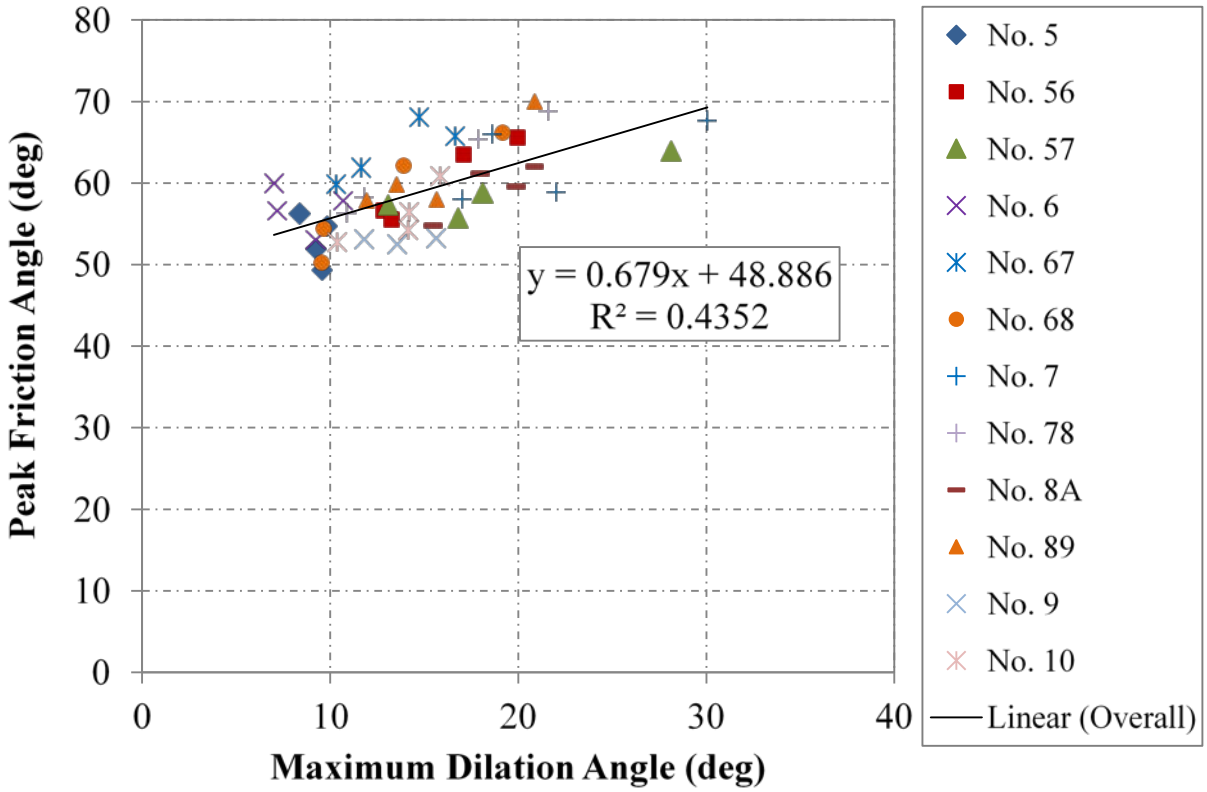

Figure 22. Chart. Relationship between friction and dilation angles in SDS testing.

Summary: The results from the standard direct shear testing on the scalped samples are shown in figure 23. The scalped samples all had friction angles higher than 34 degrees. Using the MC approach, friction angles ranged from 43 to 57 degrees, with a mean across all different sample aggregates of 52 degrees, a standard deviation of about 4 degrees, and a coefficient of variation (COV) of 7.2 percent. Using the ZDA approach, friction angles ranged from 38 to 54 degrees, with an overall mean of 45 degrees, a standard deviation of 6 degrees, and a COV of 13.6 percent.

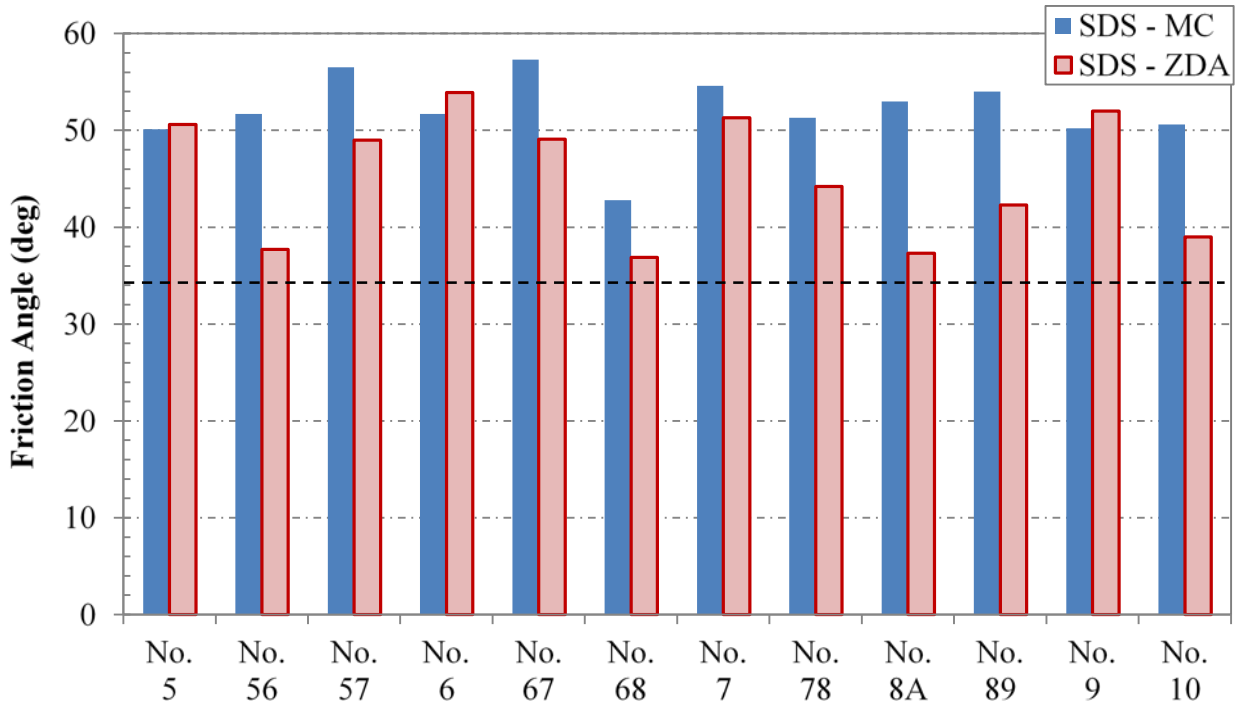

Figure 23. Chart. Summary of SDS testing.

LSDS Tests

To evaluate the strength properties of the AASTHO OG aggregates, a DS test is needed that is large enough to avoid scalping. At TFHRC, a 12- by 12- by 8-inch DS box is available to perform LSDS testing on aggregates of up to 1.2-inch maximum particle size (figure 24). This device was used to measure the strength of the 12 classifications of AASHTO aggregates (table 4) under both dry and saturated conditions. Note that the SDS tests were only tested under dry conditions.

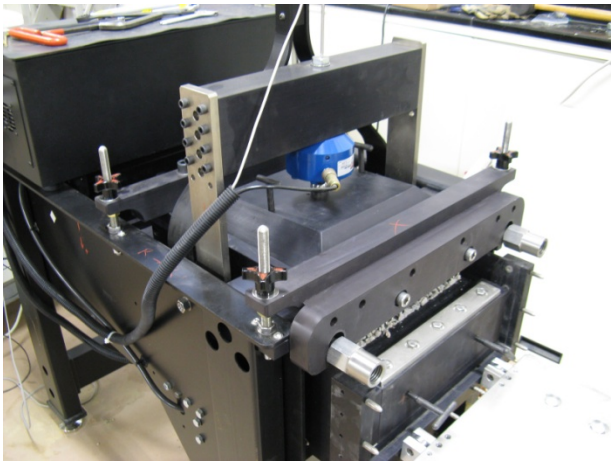

Figure 24. Photo. LSDS device at TFHRC.

Test Setup: The ASTM D3080 test method was followed for LSDS testing with the exception of the gap size between the top and bottom shear boxes. ASTM D3080 was originally developed for SDS testing, which designated the gap size as 0.025 inches.[75] Because the LSDS device and the aggregates tested in this research are considerably larger, the gap size was instead set to d_{85} (the aggregate size in which 85 percent of the material is smaller) for each sample based on the sieve analysis (table 6). This setting was determined from review of test methods outlined in ASTM D5321 and trial runs at various gap sizes, and to it was used to avoid frictional interference from either the two shear boxes or larger particles that may fall within the gap during testing.[78,79]

The shear strain displacement rate was set at 0.015 inches/min for the OGAs based on the results obtained during the compression phase of testing. The samples were sheared to a maximum of 20 percent of the device length for a total shear displacement of 2.4 inches. Because the friction angle increases with relative density for sands and gravels, an assumed worst-case condition was used by placing the samples with no compactive effort into the shear box.[79] Similar to the SDS tests, each aggregate was tested at normal stresses of 5, 10, 20, and 30 psi to determine the internal friction angle, which is a typical stress range for most wall and bridge applications.

Note that before testing, the load cells and LVDTs were calibrated. In addition, the LSDS device was also calibrated for displacement and shear resistance. With no sample in the shear box and no shear deformation occurring, the vertical displacement during loading and unloading was measured to account for box compression. The resulting calibration equation (figure 25) is then subtracted from the raw data to obtain a true displacement of the sample itself.

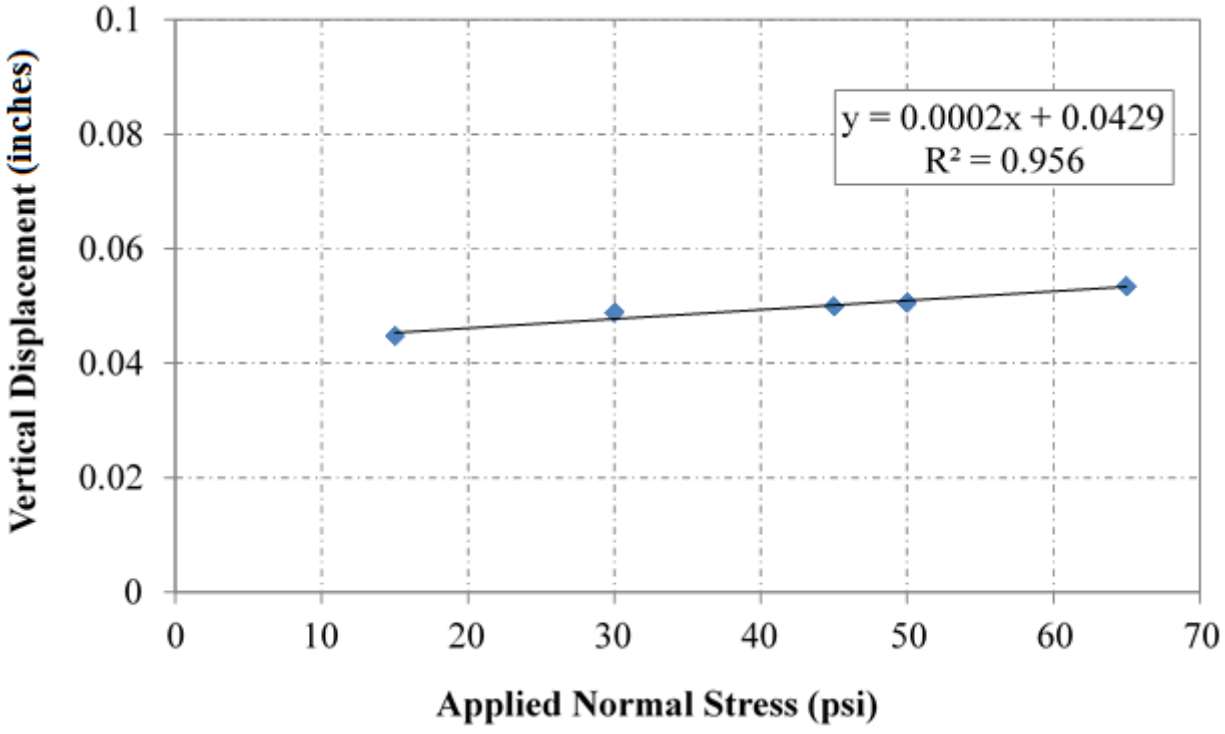

Figure 25. Chart. Vertical displacement calibration for LSDS device.

Similarly, the shear resistance of the rollers to movement must be subtracted from the measured shear stress. To do this, dead load was put in the shear box to equal the normal stresses tested in the program (5, 10, 20, and 30 psi), and the average shear stress was computed (table 13).

Table 13. LSDS resistance calibration values.

Normal Stress (psi)	Average Shear Stress (psi)
5	0.0307
10	0.0287
20	0.0481
30	0.0303

The area correction factor (F) for the applied normal load during testing is found in a different manner from that in equation 11 because the device is square, instead of circular like the SDS tests performed (equation 15).

$$F = 1 - \frac{h}{B} \tag{15}$$

Where:

h = horizontal displacement.
B = Sample side dimension.

The correction factor is then applied to the original sample area (A_o) to determine the corrected area (A_c) (equation 12).

Similar to the verification of the SDS device, tests were performed using the LSDS device on Ottawa sand to demonstrate the repeatability and validity of the device. This material was evaluated at 5 psi; the average secant friction angle across two sets of tests is 30.4 degrees. (Each test was about 1 percent from the average.) The results of the LSDS test are approximately 2 degrees less than the SDS tests at the same applied pressure. These results are consistent with results showing that LSDS devices produce a lower friction angle than SDS devices for the same material.[54]

MC Approach: After taking into account the calibrations and corrections, the results of LSDS testing using the linear MC approach for all of the aggregates are presented in table 14. The cohesion values are omitted because the materials are cohesionless; however, the entire set of results can be found in appendix A and are visualized in figure 26. While there is a large amount of scatter across the entire series of AASHTO OGAs tested, a linear fit can be made to determine a global tangent friction angle: 49 and 48 degrees for dry and saturated conditions, respectively.

Table 14. LSDS Test results using MC approach.

AASHTO Gradation	Dry	Saturated
	$\phi'_{t,LSDS,dry}$ (degree)	$\phi'_{t,LSDS,sat}$ (degree)
No. 5	47.6	55.3
No. 56	56.0	54.4
No. 57	48.9	52.1
No. 6	56.4	57.5
No. 67	53.2	57.3
No. 68	47.3	48.7
No. 7	54.0	48.9
No. 78	50.6	44.9
No. 8A	52.3	46.9
No. 8B	43.4	41.6
No. 8C	48.3	41.9
No. 8D	37.8	37.5
No. 8E	52.2	46.8
No. 89	44.8	41.2
No. 9	50.5	42.9
No. 10	42.9	37.1

AASHTO = American Association of State Highway and Transportation Officials.

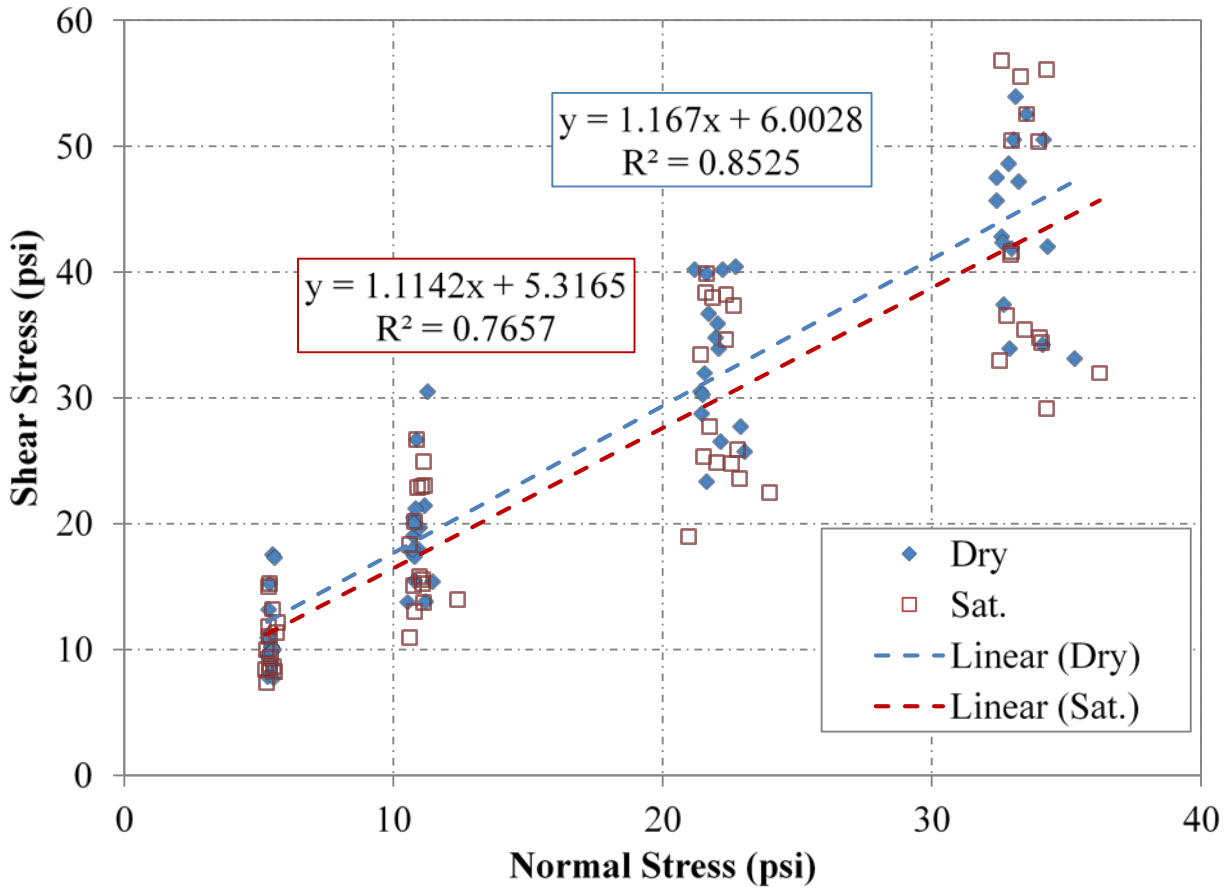

Figure 26. Chart. Global MC envelope for all AASHTO OGAs tested under both dry and saturated conditions.

ZDA Approach: Using the ZDA approach, the CV friction angle from LSDS testing was found for each aggregate (table 15).

Table 15. LSDS test results using ZDA approach.

AASHTO Gradation	Dry	Saturated
	$\phi'_{cv,LSDS,\ dry}$ (degree)	$\phi'_{cv,LSDS,\ sat}$ (degree)
No. 5	48.1	44.6
No. 56	50.3	52.9
No. 57	43.2	52.9
No. 6	45.2	51.7
No. 67	49.9	53.7
No. 68	47.0	47.9
No. 7	50.9	49.0
No. 78	49.2	45.5
No. 8A	51.8	50.3
No. 8B	45.7	45.5
No. 8C	46.6	45.8
No. 8D	44.4	42.1
No. 8E	50.4	45.6
No. 89	45.6	45.8
No. 9	49.8	45.5
No. 10	43.0	42.0

AASHTO = American Association of State Highway and Transportation Officials.

Comparing the relationship between peak friction angle and maximum dilation angle for all of the aggregates yields a reasonable linear trend for the entire AASHTO OGA dataset evaluated in this study (figure 27). This relationship is better than that found from SDS testing (figure 22) and is considered more accurate because no scalping was necessary.

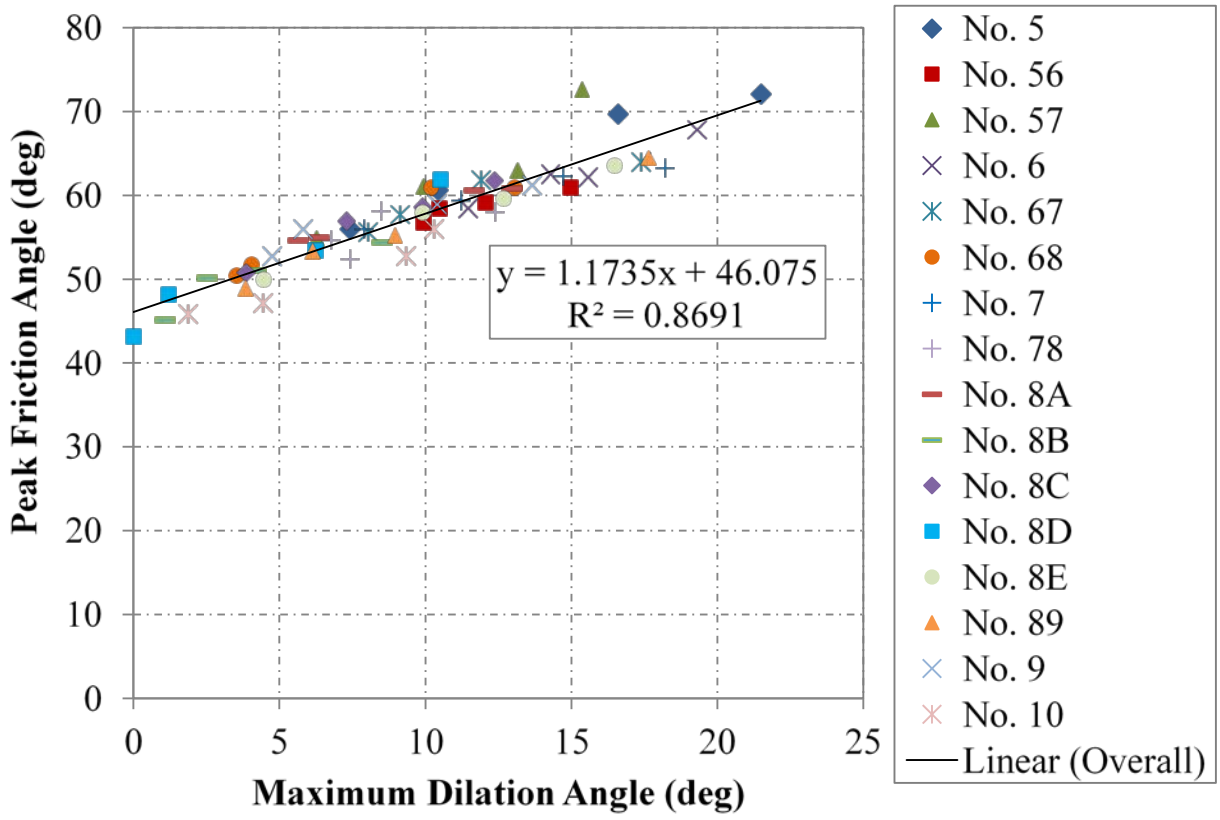

Figure 27. Chart. Relationship between friction and dilation angles in LSDS testing.

Summary: The results from the LSDS testing on the unscalped samples are shown in figure 28 for dry conditions and figure 29 for saturated conditions. The samples all had friction angles higher than 34 degrees. Using the MC approach, friction angles ranged from 37.1 to 57.5 degrees, with a mean across all different sample aggregates of 48.2 degrees, a standard deviation of 5.9 degrees, and a COV of 12.3 percent. The average friction angle under dry and saturated conditions is 49.1 and 47.2 degrees, respectively, so there is little impact resulting from saturation.

Using the ZDA approach, friction angles ranged from 42.0 to 53.7 degrees, with an overall mean of 47.6 degrees, a standard deviation of 3.3 degrees, and a COV of 6.9 percent. Saturation had no impact on the mean overall. It is interesting to note that the secant friction angles (ϕ'_s) for the range of confining stresses tested are all higher than the tangent friction angle (ϕ'_t).

By comparing the COV for the secant friction angles (ϕ'_s) over the range of confining stresses tested with the variation between the average ϕ'_s and the corresponding ϕ'_t under dry and saturated conditions, a general linear relationship is observed (figure 39). The scatter in saturated conditions is larger, but the general trend is the same. No relationship was found between ϕ'_s values and ϕ'_{cv} values; however, using the ZDA approach across all samples tested, the peak friction angle is 46.1 degrees (figure 27).

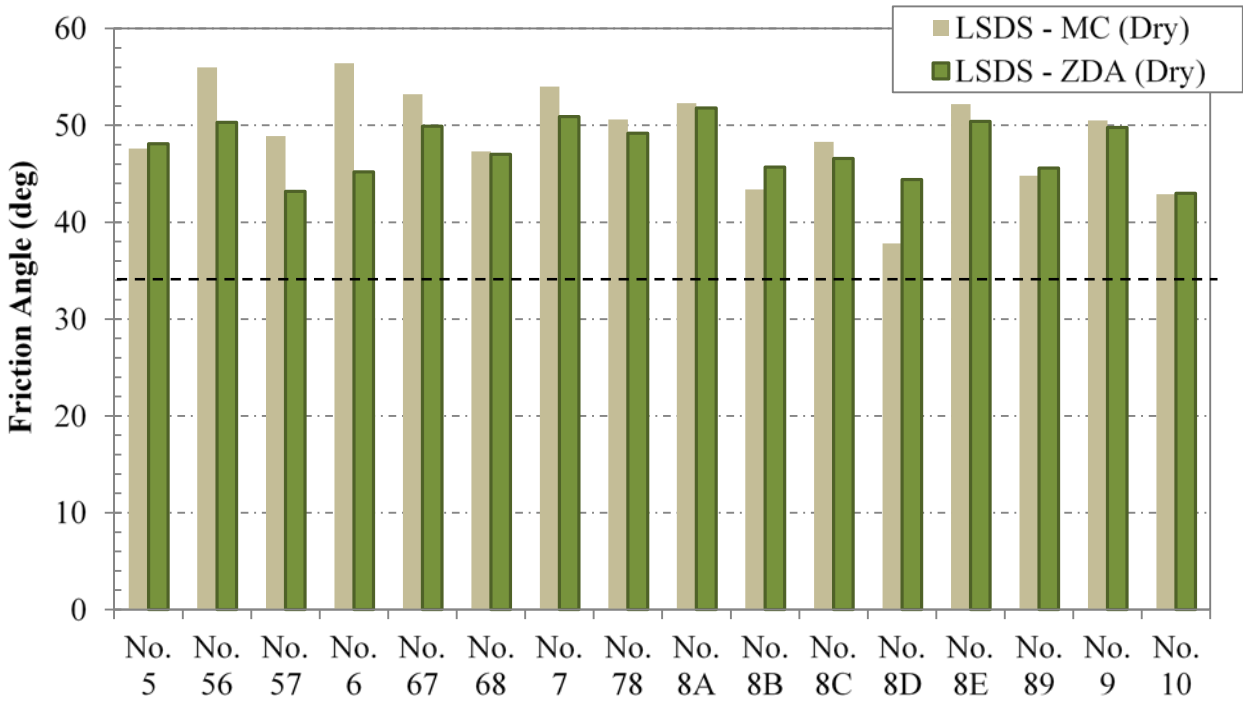

Figure 28. Chart. Summary of LSDS testing under dry conditions.

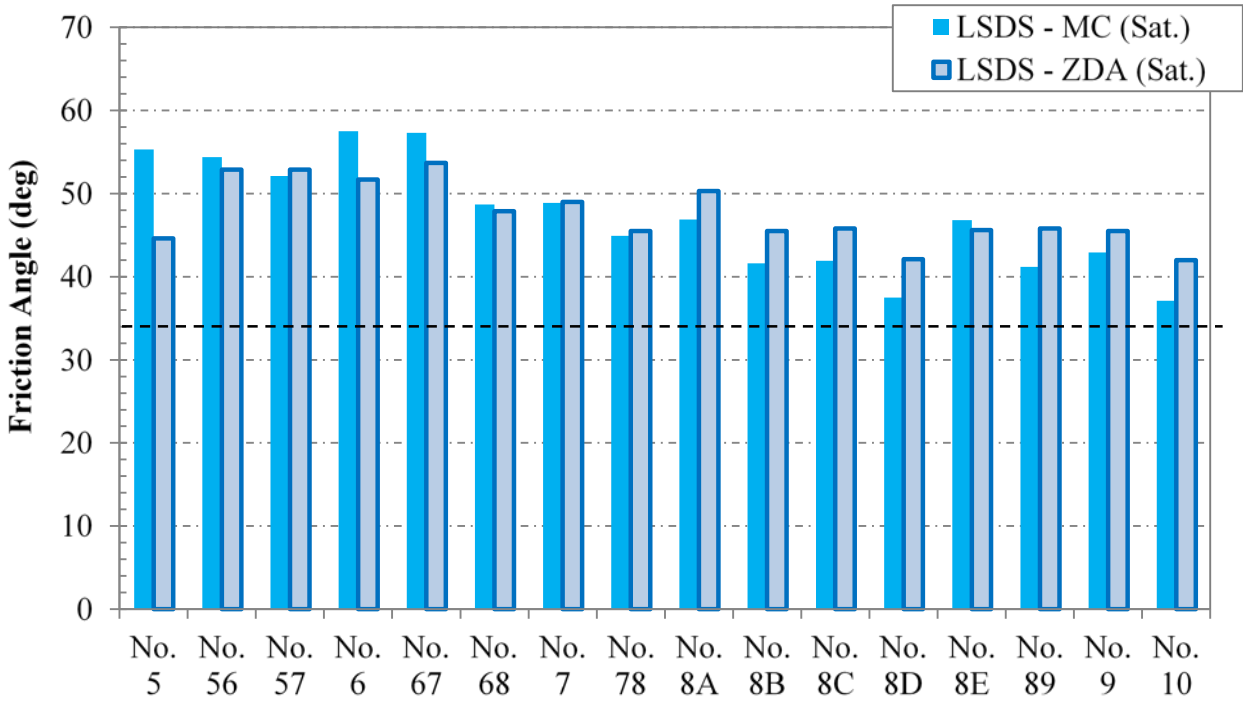

Figure 29. Chart. Summary of LSDS testing under saturated conditions.

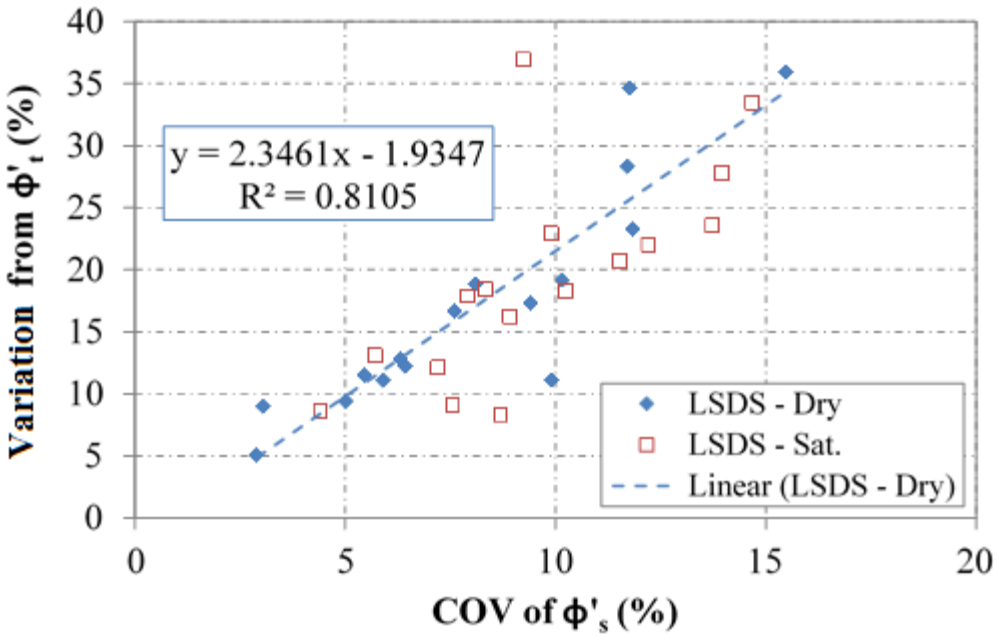

Figure 30. Chart. Comparison of the effective tangent and secant friction angles for LSDS testing.

LDTX Tests

At TFHRC, a 6-inch diameter TX unit is available to conduct large-scale consolidated drained/undrained compression testing on aggregates of up to 1-inch maximum particle size. A consolidated drained TX compression test was conducted according to ASTM D7181 to determine the strength of the 12 primary AASHTO aggregates.[800] The same series of aggregates tested in the LSDS device were tested with the LDTX device; however, only No. 8E was examined from the five types of No. 8 aggregates (table 5).

Test Setup: All of the tests were conducted at loose compaction with relative density of 30 percent to simulate the worse-case scenario for strength characterization of granular materials. The dry mass needed for each test to achieve the target value of compaction was determined based on the performed funnel and vibratory table tests according to ASTM D4254 and ASTM D4253, respectively.[68,69] The overall steps starting from sample preparation to the end of the LDTX test are illustrated in figure 31.

Sample preparation for the loose condition consisted of pouring a known mass of OGAs through a funnel into the split mold from nearly zero drop height. The nominal diameter and height of the prepared sample was 6 inches and 12 inches, respectively; the height-to-diameter ratio is 2, as recommended by ASTM.[800] The stability of the samples throughout the sample preparation phase, prior to mounting into the load frame, was maintained by applying partial suction to the specimen through one of the drainage valves located on the base of the pedestal.

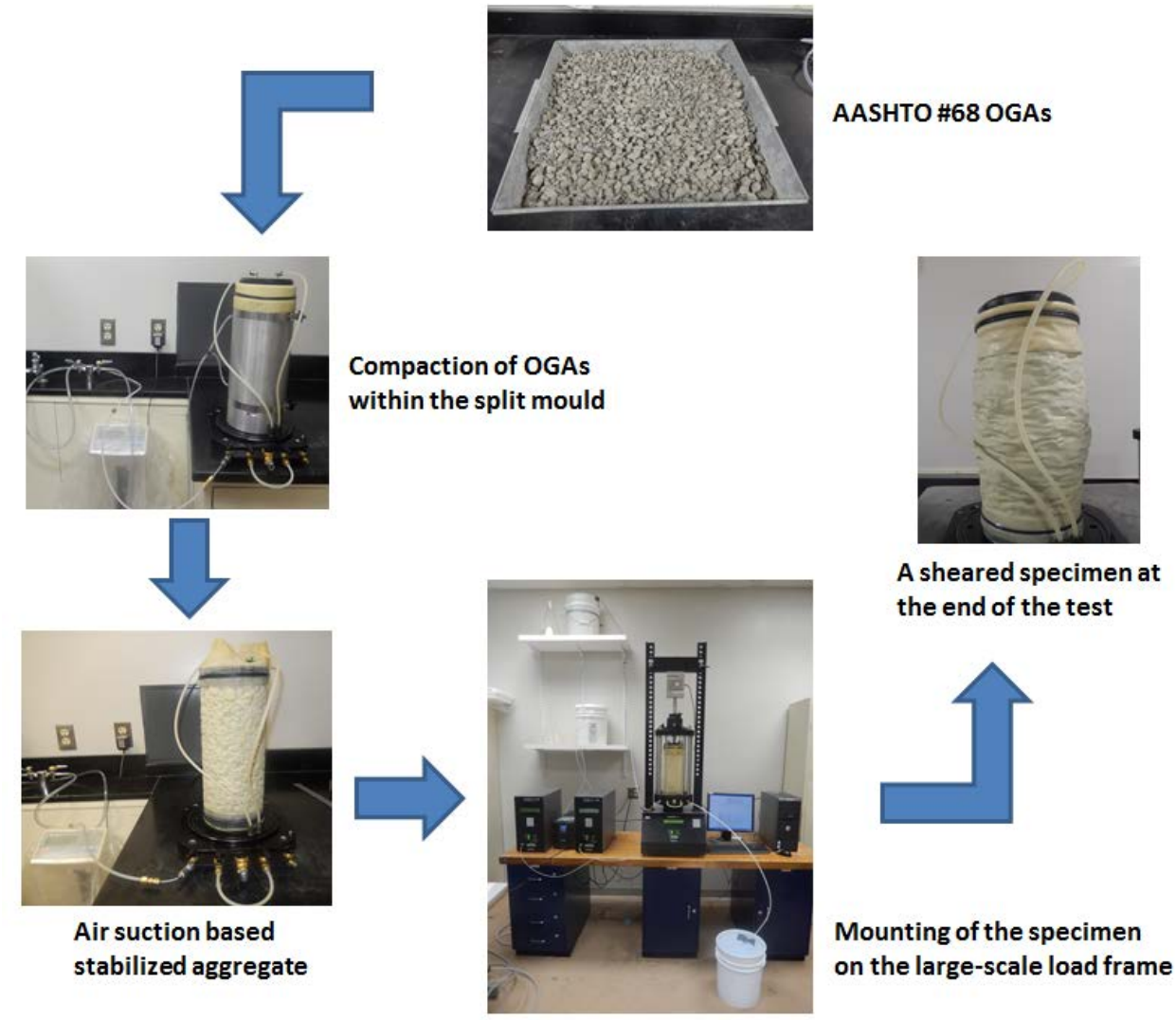

Figure 31. Diagram. Overview of the adopted procedure for LDTX testing.

To minimize the risk of membrane puncture during shearing by the coarse aggregates, two 0.025-inch-thick membranes were used; the inner membrane was used as a sacrificial membrane during compaction, and the second membrane was placed once compaction was completed. The stiffness of the individual and double membranes was measured to determine the appropriate membrane correction for the test results. The results yielded a Young's modulus for the double membrane of 11.1 kip/ft^2.

The compacted sample housed under the properly tightened chamber was mounted on the load frame, and the test chamber was filled with tap water. The sample was gravity presaturated through the tube connected to the bottom of the drainage valve prior to the initiation of the test. The water was also allowed to run through the drainage lines and the two tubes that connect these lines to remove the trapped air bubbles within the system. These steps helped reduce the back pressure required for saturation, and, as a result, the saturation period decreased. Furthermore, the pumps connected to the cell and the sample have a limited capacity; without the

presaturation procedure, the pumps have to be filled multiple times while the test is running, which interrupts the experiment and further increases the duration of the experiment.

The next step was to connect the cell and pore pressure pumps to the base of the TX setup and open a new file for each new test with the right values of dry mass of the aggregates and the diameter and height of the specimen. To achieve the acceptable minimum Skempton's B-value of 0.95 during the saturation phase, a back-pressure saturation in the range of 4.2 to 7.5 kip/ft^2 was employed.

Following saturation, the specimen was subjected to isotropic consolidation to the desired effective confining stress (5, 10, 20, or 30 psi) before the onset of the strain-controlled shear stage. The strain rate used for the shear phase was computed based on the estimated time needed to achieve 90 percent of the total consolidation (t_{90}).[800] The shear tests terminated when 15 percent axial strain was reached.

At the end of each test, the provided outputs include: axial (ε_1) and volumetric (ε_V) strain, major (σ'_1) and minor (σ'_3) effective principal stresses, and pore pressure. The difference between the major and minor principal stresses is termed the deviator stress (σ'_d). This parameter is then plotted against the axial strain; an example for the No. 57 aggregate is shown in figure 32 for each of the four effective confining pressures. The deformation behavior is shown in the relationship between volumetric strain and axial strain; an example for the No. 57 aggregate is shown in figure 33.

The secant, or peak, friction angle for each test was computed from the measured σ'_1 and σ'_3 values corresponding to the maximum σ'_d for each test (equation 6). The maximum dilation angle (ψ_{max}) is computed using equation 16 based on the measured volumetric and axial deformation behavior.[81]

$$\psi_{max} = \sin^{-1}\left[\frac{(d\varepsilon_1 + 2 \times d\varepsilon_3)}{(d\varepsilon_1 - 2 \times d\varepsilon_3)}\right]_{max} \quad (16)$$

Where:

$d\varepsilon_1$ = The incremental axial strain.
$d\varepsilon_3$ = the incremental lateral strain (equation 17).

$$\varepsilon_3 = \frac{(\varepsilon_V - \varepsilon_1)}{2} \quad (17)$$

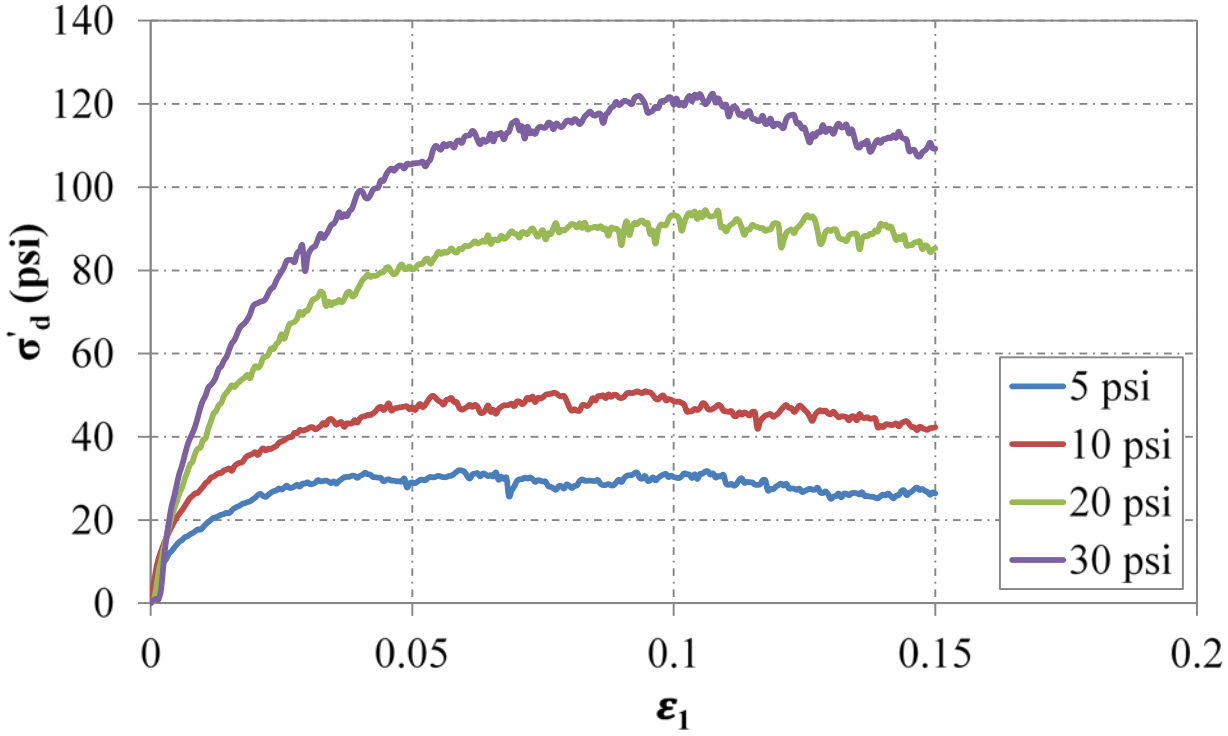

Figure 32. Chart. The effective deviator stress versus axial strain for No. 57 from LDTX testing.

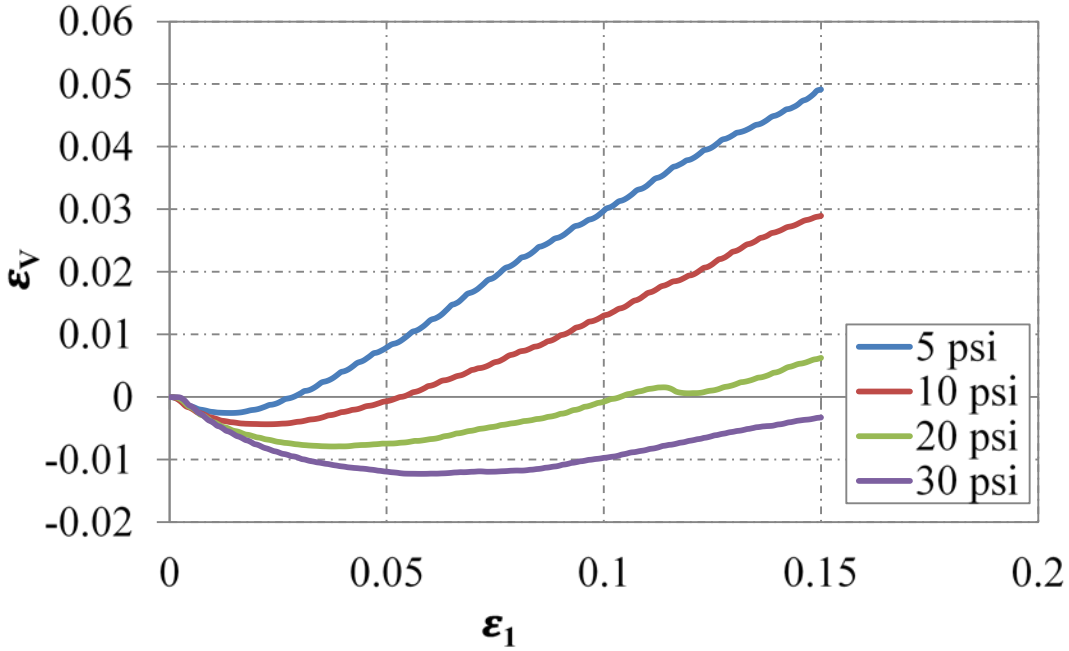

Figure 33. Chart. Volumetric strain versus axial strain for No. 57 from LDTX testing.

The reliability and repeatability of the TX apparatus was verified by conducting a drained consolidated test for Ottawa 20/30 sand and a AASHTO No. 68 sample, respectively. The Ottawa sands were subjected to various stress levels, and the resulting secant friction angles and the tangent angle are shown in table 1. The resulting ϕ'_t is very close to the well-recorded friction angle values of the uniform Ottawa sands. In addition, three replicates of fresh No. 68 OGAs with the same compaction state were subjected to the same stress level (5 psi) to verify the repeatability of the test; the measured peak friction angles has a standard deviation of 0.5, and all values are within less than 1.3 percent of the average (50.5 degrees).

Table 16. LDTX test results for Ottawa sand and AASHTO No. 68.

Sample Type	Effective Confining Stress (psi)	ϕ'_s (degree)	ϕ'_t (degree)
Ottawa	5	33.7	32.7
	10	33.9	
	20	31.8	
	30	33.1	
AASHTO #68	5	49.9	—
	5	50.7	
	5	50.9	

AASHTO = American Association of State Highway and Transportation Officials.
— = Not measured.

Prior to determining the strength parameters, correction procedures were performed on the raw data collected from the LDTX software. The corrections are conducted to minimize the errors that could be incurred because of (1) the changing cross-sectional area during the consolidation and shearing phase, (2) the membrane stiffness, and (3) the considerable change of volume due to membrane penetration during the consolidation phase.

A bulging type area correction (equation 18) method was implemented to determine the corrected cross-sectional area of the specimen as the sample deformed during the shearing process.[82]

$$A_c = A_o \times \left[\frac{1-\varepsilon_v}{1-(a \times \varepsilon_1)}\right] \quad (18)$$

Where:

A_c = Corrected area.
A_o = Initial area before correction.
ε_V = Volumetric strain.
a = Experimental constant normally between 1 and 2.
ε_1 = Axial strain.

For the experimental constant, a value of 1.67 was used.[83]

The extra radial stress added to the effective confining stress due to the membrane stiffness was also corrected according to equation 19.[80] The computed value from equation 19 was then subtracted from the measured deviator stress.

$$\Delta(\sigma_1 - \sigma_3) = \frac{4 \times E_m \times t_m \times \varepsilon_1}{D_c} \quad (19)$$

Where:

$\Delta(\sigma_1\text{-}\sigma_3)$ = Change in effective deviator stress due to the membrane correction.
E_m = Young's modulus for the membrane material (11.1 kip/ft^2).
t_m = Thickness of the membrane (0.025 inches).
ε_1 = Axial strain.
D_c = The specimen's diameter at the end of the consolidation phase.

The other potential error during the shear test is the significant volume reduction due to membrane penetration, which could be wrongly assumed as sample volume reduction. This phenomenon is more pronounced in samples with coarse grain sizes during the isotropic consolidation stage, especially after the application of high confining pressures. A graphical method proposed by Noor et al. was adopted to correct these potential errors in sample volume changes.[84] The approach assumes that the occurrence of membrane penetration and specimen compression is a consecutive process because the compression is only triggered after the membrane penetration has been fully mobilized. As a result, the initial sharp decrease in volume that is measured could be attributed to the membrane penetration (figure 32).

As demonstrated in figure 34, two straight (dashed) lines are drawn to best fit the initial and tail parts of the consolidation curve (CC).[84] A bisector line originating from the intersection of these lines is then made to connect to the CC; the distance from the intersection to the curve is found (L). A line with an equal distance of L is drawn away from the CC along the bisector line; from there, a perpendicular line is drawn until it intersects the initial part of the CC. This point marks the volume of the membrane reduction, which is deducted from the total reduced volume to determine the correct value of sample volume at the end of the consolidation phase. It is clear from figure 34 that the volume reduction due to membrane penetration increased significantly with the increase in grain size (AASHTO No. 5 > No. 8 > No. 10). Similarly, the correction increases with the increase of effective confining stress, the highest being for 30 psi (figure 35).

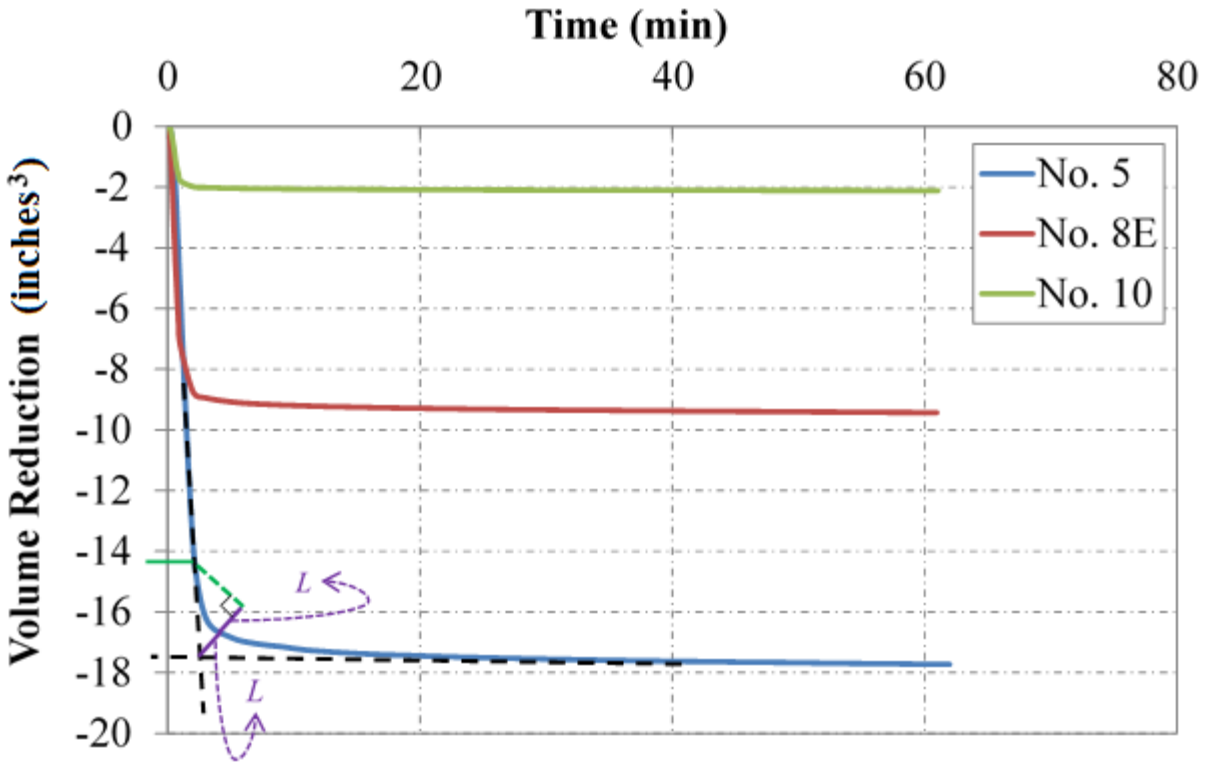

Figure 34. Chart. Graphical method to determine membrane penetration correction and the effect of aggregate size on volume reduction during LDTX testing.

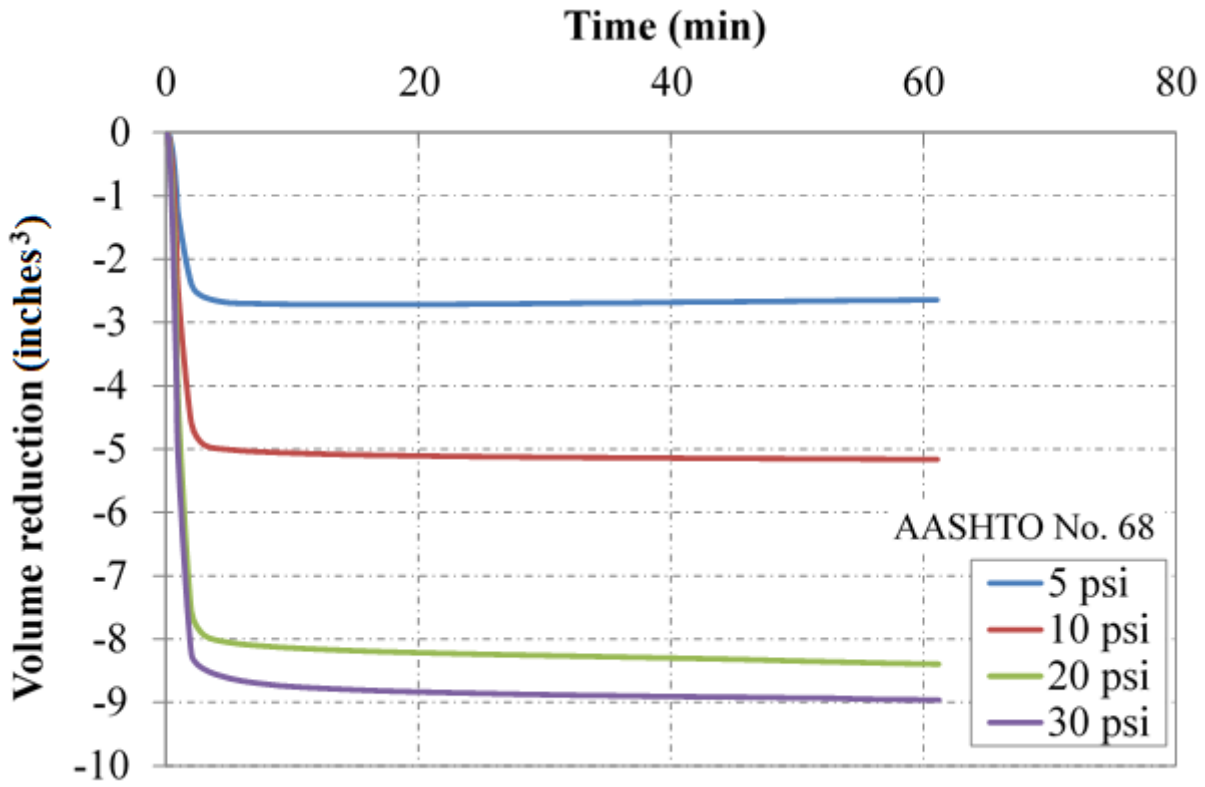

Figure 35. Chart. Effect of confining stress on volume reduction for AASHTO No. 68 sample during LDTX testing.

MC Approach: The linear MC approach presented in equation 5 for LDTX testing was used to compute ϕ'_t for the 12 tested OGAs. The summarized results are displayed in table 17. The full results displaying the individual ϕ'_s, ψ_{max}, and corresponding shear and normal stresses at failure for each test can be found in appendix A. The individual p' and q stress path values for the entire database tested were plotted together, and a good correlation is found for the entire series of OGAs tested with the LDTX device (figure 36). Using a linear regression, the overall computed friction angle is 39.1 degrees. An apparent cohesion is still observed because of the limitation of the MC approach for OGAs; however, if the linear regression is force-fit to zero, then q would equal about two-thirds p', with the friction angle slightly higher at 41.5 degrees.

Table 17. LDTX test results using MC approach.

AASHTO Gradation	$\phi'_{t,LDTX}$ (degree)
No. 5	36.5
No. 56	39.5
No. 57	40.5
No. 6	36.4
No. 67	39.0
No. 68	38.1
No. 7	38.4
No. 78	34.9
No. 8A	—
No. 8B	—
No. 8C	—
No. 8D	—
No. 8E	39.3
No. 89	38.3
No. 9	38.4
No. 10	40.1

AASHTO = American Association of State Highway and Transportation Officials.
— = Not measured.

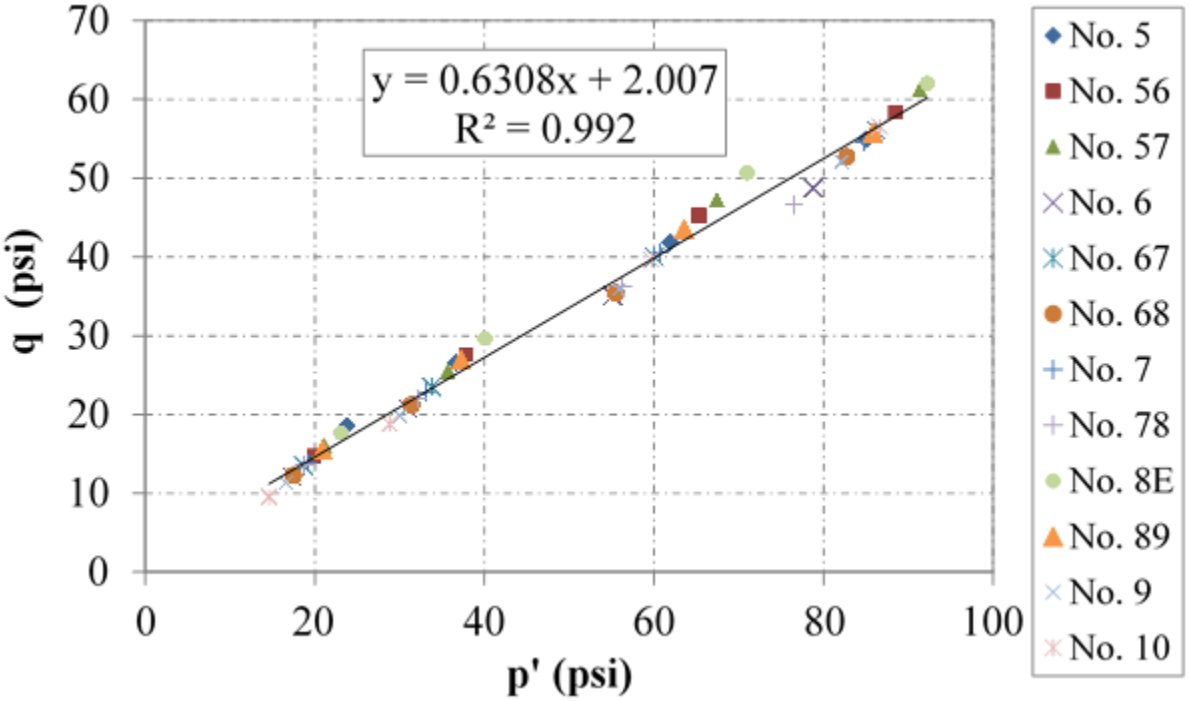

Figure 36. Chart. Relationship between *p'* and *q* values in LDTX testing series.

ZDA Approach: The constant volume friction angle (ϕ'_{cv}), which corresponds to the friction angle at which the dilation angle is zero, is determined using the ZDA approach. The results for each tested aggregate are presented in table 18. Similar to the LSDS results, the relationship between peak friction angle and maximum dilation angle for all of the aggregates yields a reasonable linear trend for the entire AASHTO OGA dataset evaluated in this study (figure 37). The resulting friction angle is 38.9, which is close to the value computed from the MC approach above.

Table 18. LDTX test results using ZDA approach.

AASHTO Gradation	$\phi'_{cv,LDTX}$ (degree)
No. 5	39.7
No. 56	39.4
No. 57	38.4
No. 6	36.8
No. 67	36.6
No. 68	38.7
No. 7	36.9
No. 78	38.3
No. 8A	—
No. 8B	—
No. 8C	—
No. 8D	—
No. 8E	37.5
No. 89	40.3
No. 9	39.4
No. 10	34.8

AASHTO = American Association of State Highway and Transportation Officials.
— = Not measured.

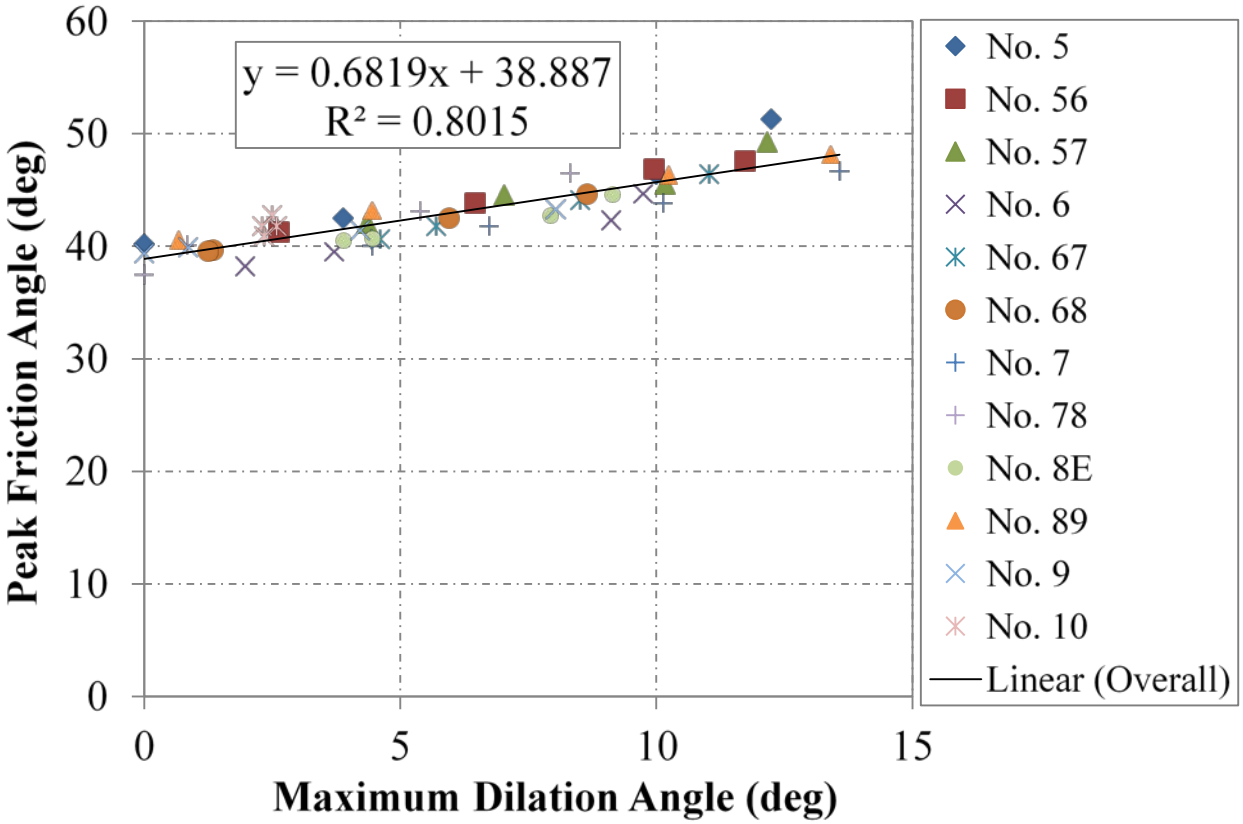

Figure 37. Chart. Relationship between friction and dilation angles in LDTX testing.

Summary: The results for both the tangent and CV friction angles for all conducted LDTX tests were marginally higher than the commonly adopted design value of 34 degrees (figure 38). The average and COV values for ϕ'_t for the entire series tested are 38.4 degrees and 4.6 percent, respectively; similarly for ϕ'_{cv}, they are 38.1 degrees and 4.2 percent, respectively. It is interesting to note that the secant friction angles (ϕ'_s) for the range of confining stresses tested are typically higher than the tangent friction angle (ϕ'_t).

By comparing the COV for the secant friction angles (ϕ'_s) over the range of confining stresses tested with the variation between the average ϕ'_s and the corresponding ϕ'_t, a linear relationship is again observed (figure 39). The highest COV (11 percent) corresponds to the largest sample (i.e., No. 5), while the lowest (2 percent) corresponds to the smallest sample (i.e., No. 10). Despite high values of individual ϕ'_s for sample No. 5, the ϕ'_t was the lowest (appendix A). This trend was not observed for the ϕ'_{cv} values using the ZDA approach.

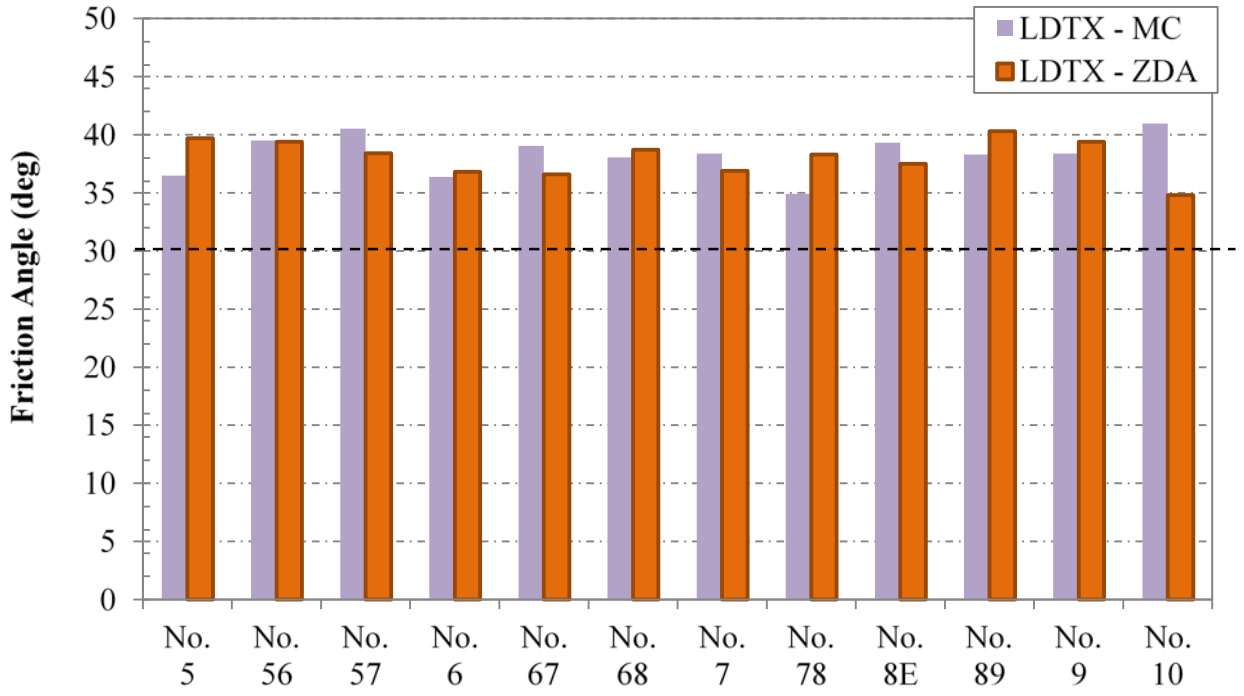

Figure 38. Chart. Summary of LDTX testing.

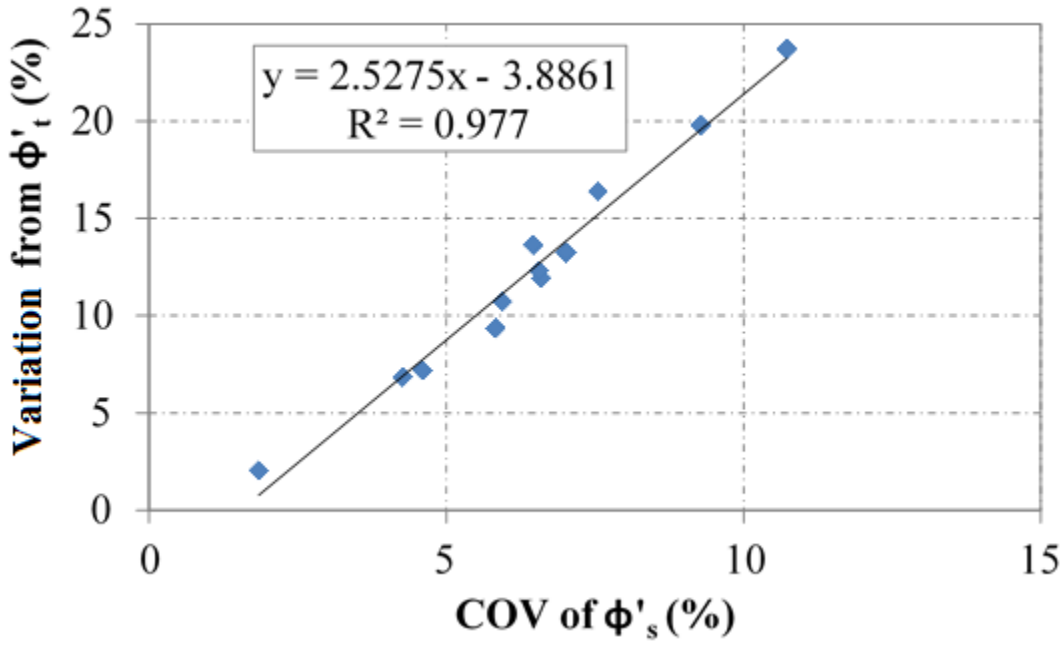

Figure 39. Chart. Comparison of the effective tangent and secant friction angles for LDTX testing.

CHAPTER 4. ANALYSIS OF RESULTS

4.1 DETERMINATION OF STRENGTH PROPERTIES

A total of sixteen different OGAs were tested in this study. From these series of tests, the strength parameters were found (table 11 through table 18). The strength of the aggregates was determined using three different devices: (1) SDS, (2) LSDS, and (3) LDTX. The choice of testing device plays a major role in the measured strength parameters.

4.2 TESTING DEVICE

To compare the testing devices, the measured friction angles were first investigated. Because the LDTX testing is performed saturated, the comparison focused on the LSDS test results under saturated conditions. Findings show that testing with the LSDS device produces higher measured friction angles than when compared with the LDTX device, regardless of the method of data interpretation, the MC or the ZDA approach (table 19 and table 20, respectively). In general, LSDS test results are generally between 8 and 52 percent higher than the LDTX test results. One exception is the No. 10 aggregate when using the MC approach; however, further study is needed to determine the reason for this smallest and most uniform aggregate tested.

Table 19. LSDS versus LDTX measured friction angles using MC approach.

	MC Tangent Friction Angle		LSDS Relationship to LDTX	
Sample	LSDS (degree)	LDTX (degree)	Total Difference (LSDS-LDTX) (degree)	Percent Difference (LSDS/LDTX - 1)*100 (percent)
No. 5	55.3	36.5	18.8	51.5
No. 56	54.4	39.5	14.9	37.7
No. 57	52.1	40.5	11.6	28.6
No. 6	57.5	36.4	21.1	58.0
No. 67	57.3	39.0	18.3	46.9
No. 68	48.7	38.1	10.6	27.8
No. 7	48.9	38.4	10.5	27.3
No. 78	44.9	34.9	10.0	28.7
No. 8A	46.9	—	—	—
No. 8B	41.6	—	—	—
No. 8C	41.9	—	—	—
No. 8D	37.5	—	—	—
No. 8E	46.8	39.3	7.5	19.1
No. 89	41.2	38.3	2.9	7.6
No. 9	42.9	38.4	4.5	11.7
No. 10	37.1	40.1	-3.0	-7.5

LDTX = Large-diameter triaxial.
LSDS = Large-scale direct shear.
MC = Mohr-Coulomb
— = Not measured.

Table 20. LSDS versus LDTX measured friction angles using ZDA approach.

	ZDA CV Friction Angle (degree)		LSDS Relationship to LDTX	
Sample	LSDS	LDTX	Total Difference (LSDS-LDTX) (degree)	Percent Difference (LSDS/LDTX - 1)*100 (percent)
No. 5	44.6	39.7	4.9	12.3
No. 56	52.9	39.4	13.5	34.3
No. 57	52.9	38.4	14.5	37.8
No. 6	51.7	36.8	14.9	40.5
No. 67	53.7	36.6	17.1	46.7
No. 68	47.9	38.7	9.2	23.8
No. 7	49.0	36.9	12.1	32.8
No. 78	45.5	38.3	7.2	18.8
No. 8A	50.3	—	—	—
No. 8B	45.5	—	—	—
No. 8C	45.8	—	—	—
No. 8D	42.1	—	—	—
No. 8E	45.6	37.5	8.1	21.6
No. 89	45.8	40.3	5.5	13.6
No. 9	45.5	39.4	6.1	15.5
No. 10	42.0	34.8	7.2	20.7

LDTX = Large-diameter triaxial.
LSDS = Large-scale direct shear.
MC = Mohr-Coulomb
— = Not measured.

The mean size of the aggregate plays a role in the percent increase for LSDS test results as compared with LDTX test results (figure 40). As the aggregate gets larger, the percent difference typically increases. Overall, however, there is no observed relationship between friction angles measured using LDTX and LSDS testing for the range of OGAs tested (figure 41).

Looking at the range of aggregates tested, from the No. 5 to the No. 10, the mean tangent friction angle using the LSDS device under saturated conditions is 47.2 degrees, with a COV of 14.2 percent. The tests using the LDTX device, however, resulted in a mean tangent friction of 38.4 degrees and a COV of 4.6 percent. For the CV friction angle, the mean and COV using the LSDS device is 47.6 degrees, with a COV of about 7 percent; with the LDTX device, the values are 38.1 degrees and 4.2 percent, respectively. The aggregate type (i.e., size) had more of an impact with LSDS testing than with LDTX testing under loose compaction, likely as a result of the different boundaries conditions between the two tests.

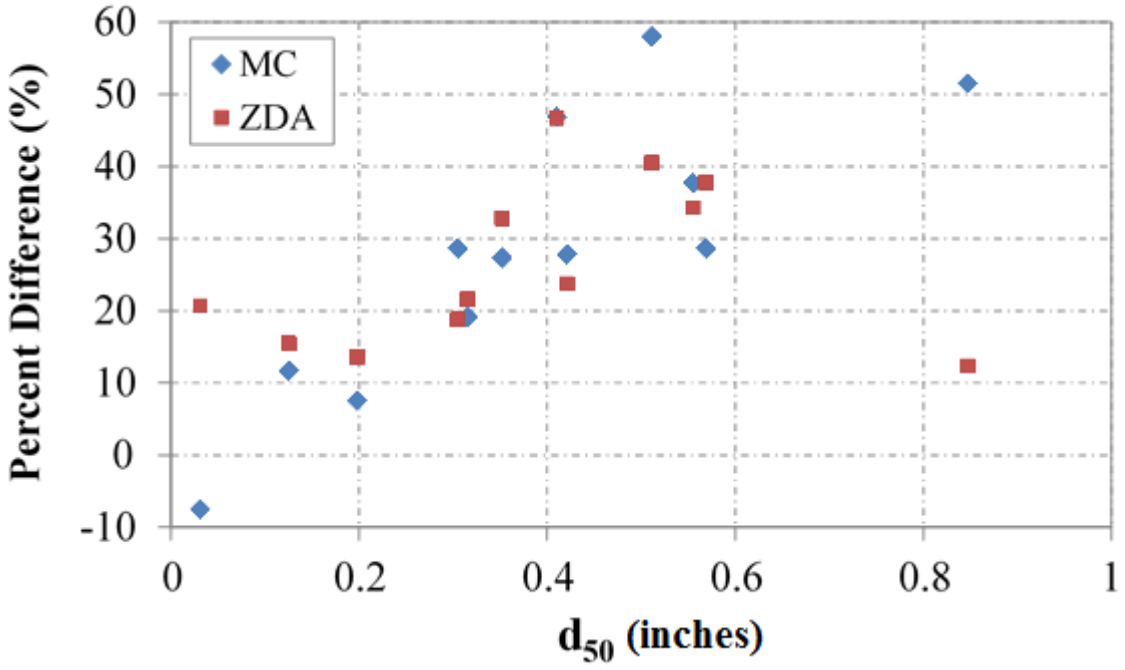

Figure 40. Chart. Difference between LSDS and LDTX as a function of mean aggregate size.

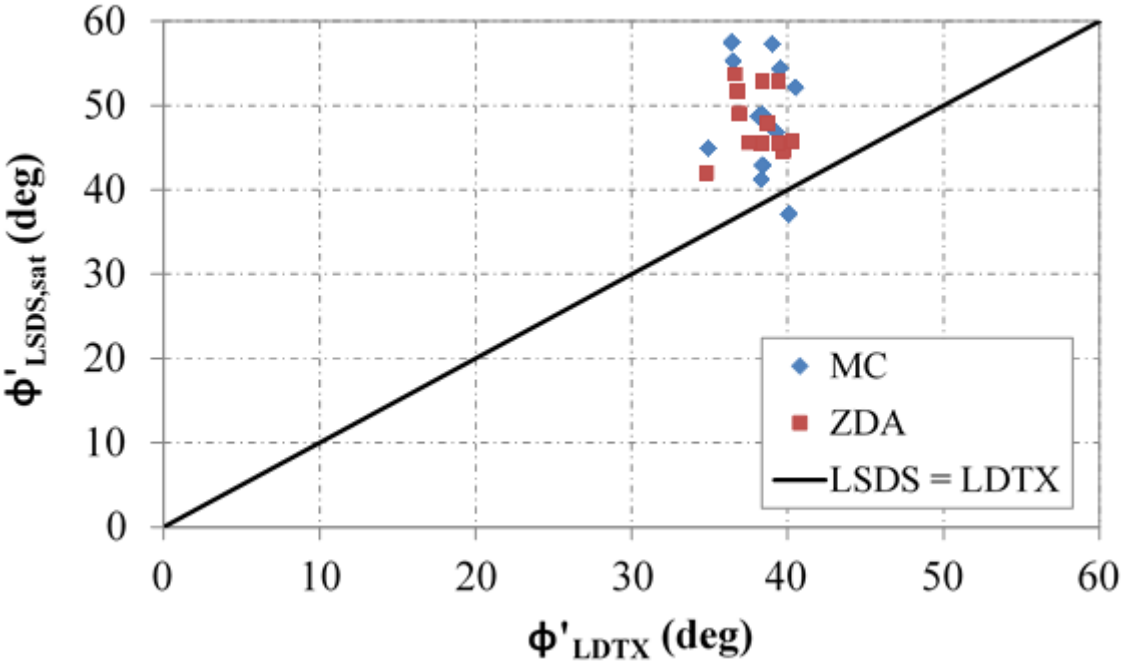

Figure 41. Chart. Relationship between LSDS and LDTX friction angles.

A similar observation is made for the measured secant friction angles; however, the difference between LDTX and LSDS testing tends to decrease with increasing confining stress (figure 42). This observation again may be related to the reduced dilative behavior at higher confining

stresses. The linear relationship found between the COV of the secant friction angles for a particular aggregate and the variation of the tangent friction angle from the average secant angle was found for both LSDS (figure 30) and LDTX testing (figure 39). The LDTX testing produces results that are considerably less scattered than the LSDS testing, thus reducing the variability across all samples tested.

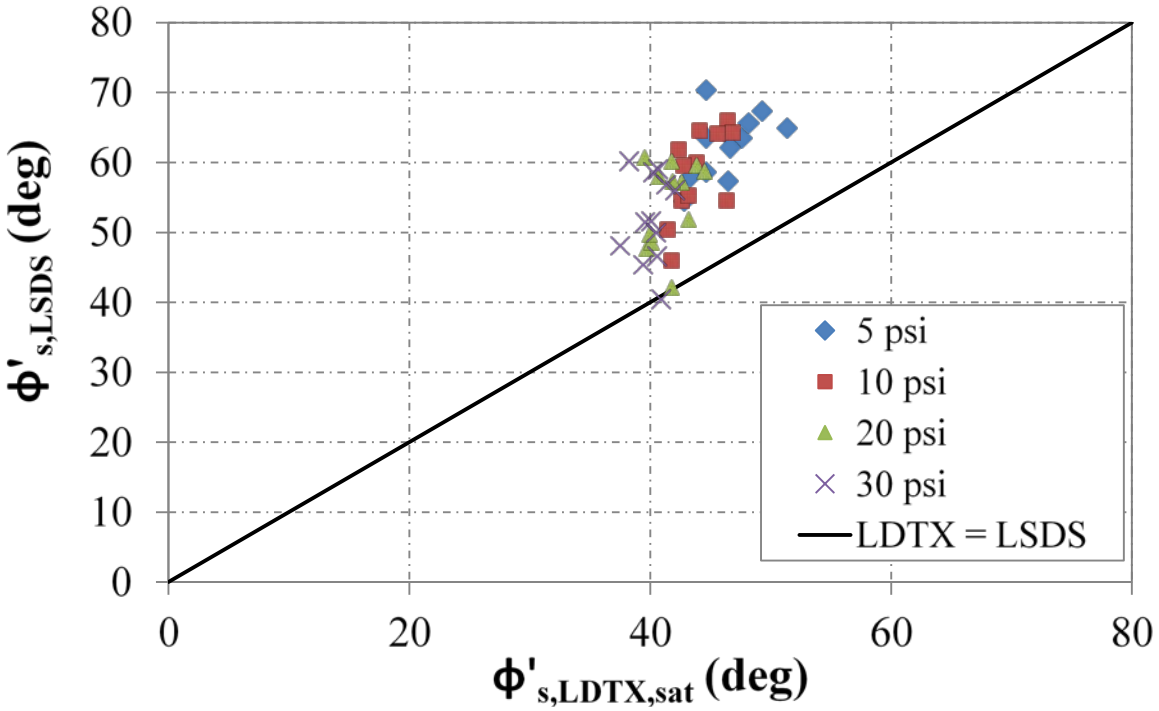

Figure 42. Chart. Relationship between LSDS and LDTX effective secant friction angles.

When looking at the dilation angle, those measured with the LDTX device are also lower than those measured with the LSDS device (figure 43). This result is expected because of the forced failure plane that the aggregates must displace over in the LSDS device, causing more dilation. There is a general trend observed for dilation angles measured with the different large-scale devices; the dilation angle measured with LDTX is approximately 60 percent of that measured with LSDS. This result also explains the lower friction angles measured with LDTX because dilation behavior plays a big role in the strength of aggregates. Considering there is a trend with dilation but not with tangent or CV friction angles between LDTX and LSDS results, it is clear that more factors are contributing to the strength between the two test methods.

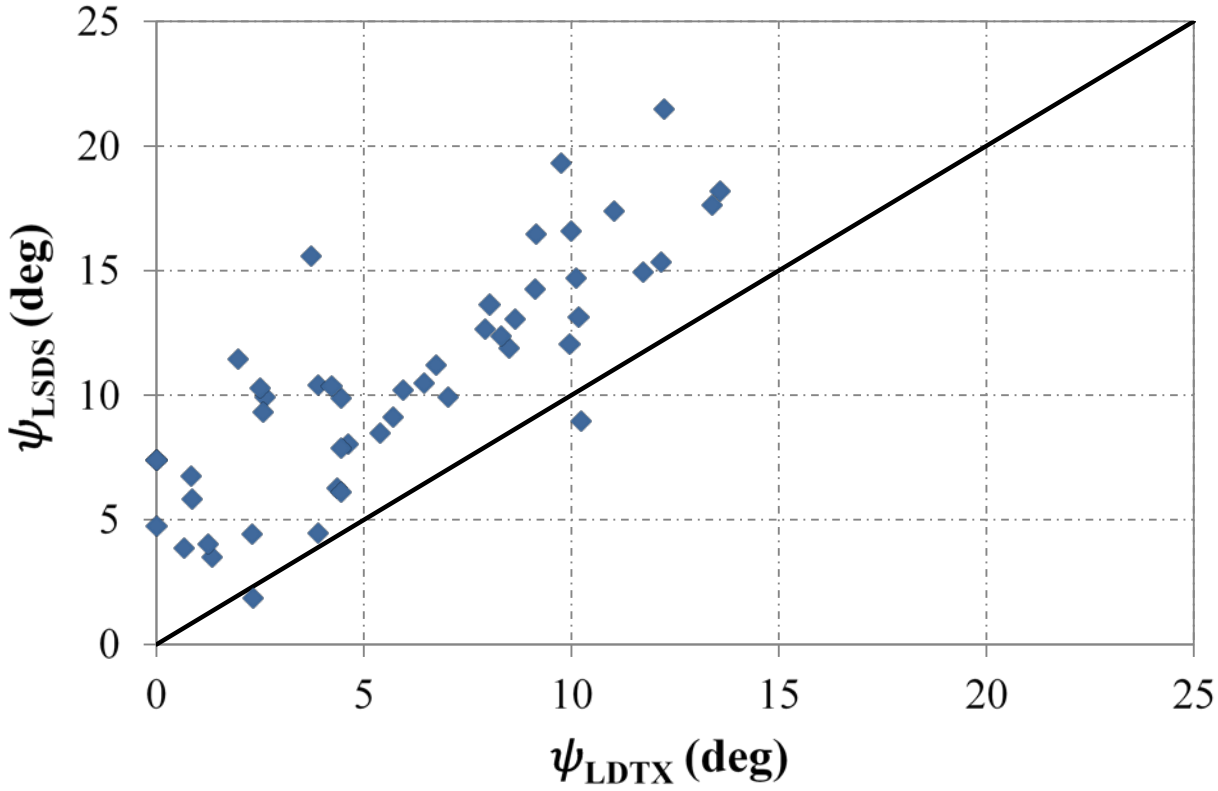

Figure 43. Chart. Relationship between LDTX and LSDS measured dilation angles.

Scale Effects

One parameter investigated in this study was scale of the direct shear testing device used to measure the strength of the aggregates. A 2.5-inch-diameter SDS device and a 12-inch-square LSDS device were used in the comparison. To ensure that the ASTM standard was met for each test, the samples were scalped prior to testing in the SDS device; no scalping was needed for the LSDS tests.[(75)] Tests were performed uncompacted under dry conditions.

Some samples measured with the LSDS results show higher strength than the SDS results; however, the differences largely lie within 10 to 20 percent (figure 44). The difference in the measured tangent friction angle when conducting SDS tests on scalped samples versus LSDS tests on complete samples ranged from 0 to 9.2 degrees when evaluating the results using the MC approach (table 21). When using the ZDA approach, the difference is greater, up to 14.5 degrees, and the LSDS results are about 40 percent higher than the SDS results (table 22).

The larger difference using the ZDA approach is explained by the variation and scatter in measured dilation angles between scalped and unscalped samples (see figure 22 and figure 27). The scalping process changes the dilation properties of the aggregates, with relative differences ranging from 15 to 65 percent; no trend was found (figure 45). The initial void ratio for testing is also changed, which has an impact on strength. Overall, scalped samples are unrepresentative of field behavior; results from strength testing cannot be relied upon.

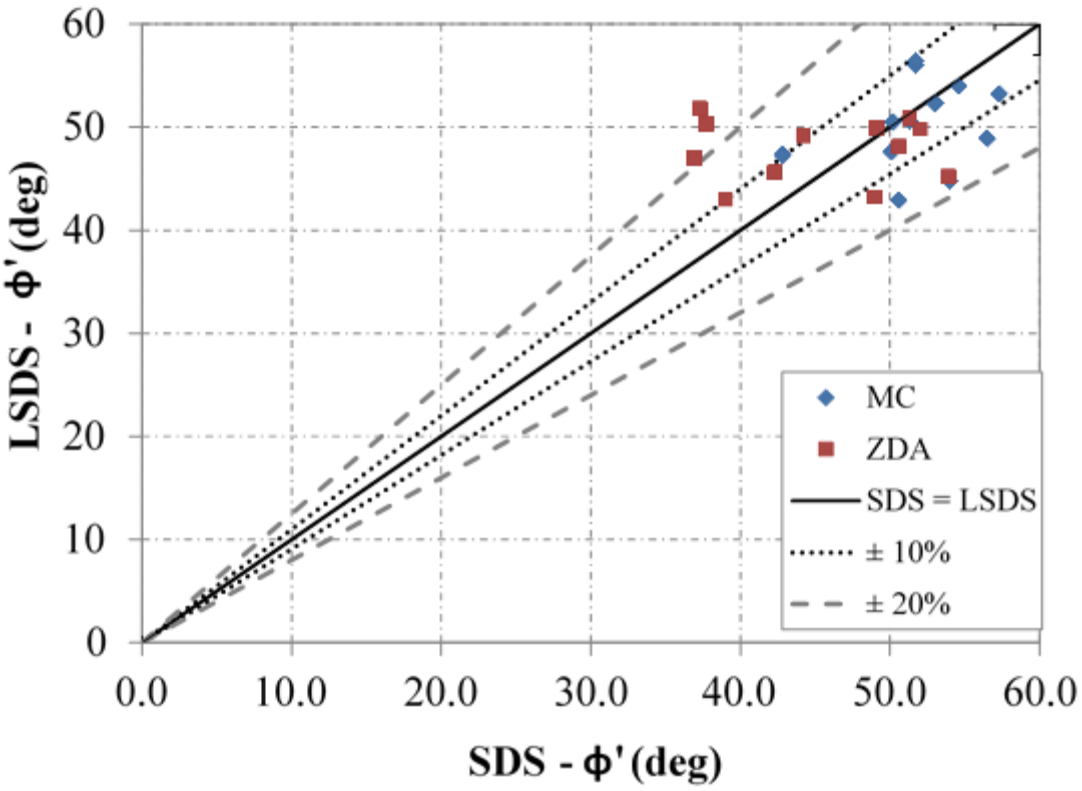

Figure 44. Chart. Relationship between LSDS and SDS measured friction angles.

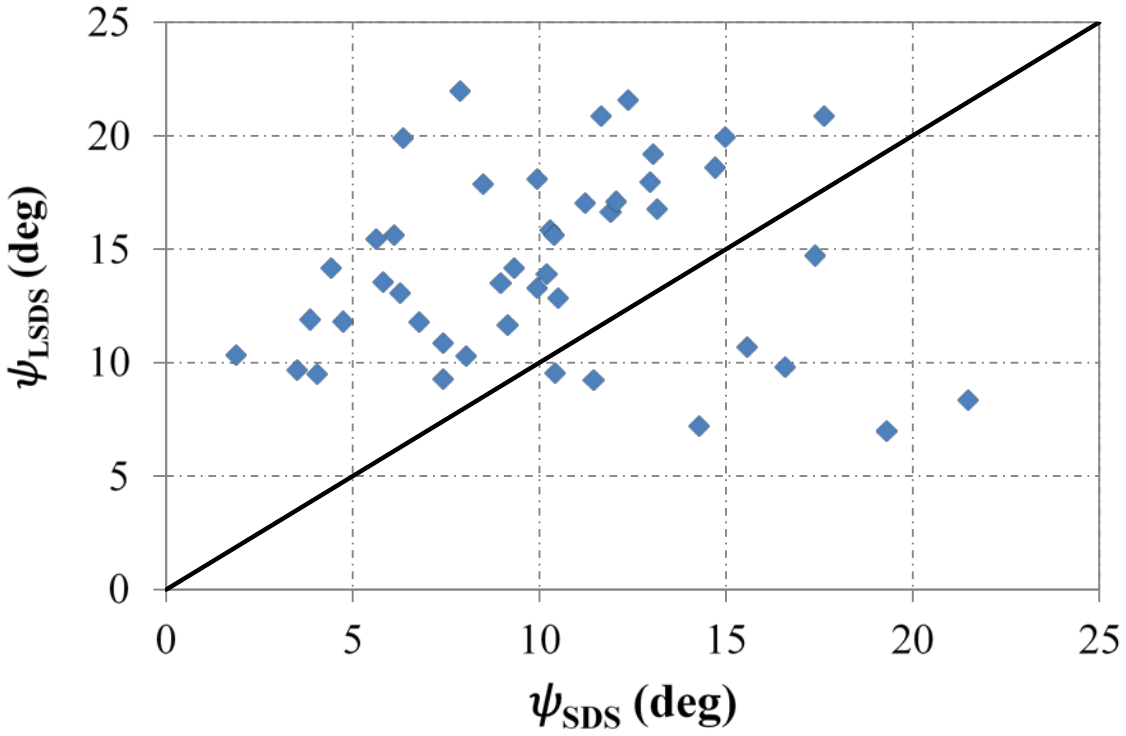

Figure 45. Chart. Relationship between LSDS and SDS measured dilation angles.

Table 21. SDS versus LSDS friction angles using MC approach.

AASHTO Gradation	MC Friction Angle (degree)		LSDS Relationship to SDS	
	SDS	LSDS	Total Difference (LSDS-SDS) (degree)	Percent Difference (LSDS/SDS - 1)*100 (percent)
No. 5	50.1	47.6	-2.5	-5.0
No. 56	51.7	56.0	4.3	8.3
No. 57	56.5	48.9	-7.6	-13.5
No. 6	51.7	56.4	4.7	9.1
No. 67	57.3	53.2	-4.1	-7.2
No. 68	42.8	47.3	4.5	10.5
No. 7	54.6	54.0	-0.6	-1.1
No. 78	51.3	50.6	-0.7	-1.4
No. 8A	53.0	52.3	-0.7	-1.3
No. 8B	—	43.4	—	—
No. 8C	—	48.3	—	—
No. 8D	—	37.8	—	—
No. 8E	—	52.2	—	—
No. 89	54.0	44.8	-9.2	-17.0
No. 9	50.2	50.5	0.3	0.6
No. 10	50.6	42.9	-7.7	-15.2

AASHTO = American Association of State Highway and Transportation Officials.
LSDS = Large-scale direct shear.
MC = Mohr-Coulomb.
SDS = Standard direct shear.
— = Not measured.

Table 22. SDS versus LSDS friction angles using ZDA approach.

AASHTO Gradation	ZDA Friction Angle (degree)		LSDS Relationship to SDS	
	SDS	LSDS	Total Difference (LSDS-SDS) (degree)	Percent Difference (LSDS/SDS - 1)*100 (percent)
No. 5	50.6	48.1	-2.5	-4.9
No. 56	37.7	50.3	12.6	33.4
No. 57	49.0	43.2	-5.8	-11.8
No. 6	53.9	45.2	-8.7	-16.1
No. 67	49.1	49.9	0.8	1.6
No. 68	36.9	47.0	10.1	27.4
No. 7	51.3	50.9	-0.4	-0.8
No. 78	44.2	49.2	5	11.3
No. 8A	37.3	51.8	14.5	38.9
No. 8B	—	45.7	—	—
No. 8C	—	46.6	—	—
No. 8D	—	44.4	—	—
No. 8E	—	50.4	—	—
No. 89	42.3	45.6	3.3	7.8
No. 9	52.0	49.8	-2.2	-4.2
No. 10	39.0	43.0	4	10.3

AASHTO = American Association of State Highway and Transportation Officials.
LSDS = Large-scale direct shear.
SDS = Standard direct shear.
ZDA = Zero dilation angle.
— = Not measured.

The results of the Ottawa sand and the No. 10 aggregate tests can more directly be compared for scale effects because no or very little scalping was needed. The average secant friction angle from SDS testing of Ottawa sand at 5 psi was 32.2 degrees; from LSDS testing, it was 30.4 degrees. For the No. 10 aggregates, the difference is larger, up to 15.2 percent, with the SDS results also higher than the LSDS results. These findings are relatively consistent with research on sands in which larger devices resulted in lower measured friction angles for the same material.[(54)]

In contrast, the difference for the CV friction angles measured from SDS and LSDS tests is approximately 4 degrees, with the LSDS device producing a higher friction angle than that measured with the SDS device. This difference is considered negligible, however, because it is about 10 percent.[(85)] With dilation negated through the ZDA approach, it is expected that the aggregate would have similar strength regardless of the size of the device, assuming that all other aspects are constant.

Data Interpretation

The use of the traditional MC approach results in the peak, or secant, friction angle at each applied normal stress, which can provide the tangent friction angle over the range tested. The ZDA approach, however, results in the constant volume friction angle, which is a measure at the critical state. The tangent and constant volume friction angle are not equivalent parameters. A comparison between the friction angles resulting from the MC and ZDA approaches indicates that the difference between the two is within 20 percent regardless of testing device (figure 46).

The choice of data interpretation method, unless specified, will often default to the MC approach because it is the most common. The linear MC interpretation, however, results in measured cohesion for each test because the y-intercept of the best-fit approximation is not zero. This inconsistency for these cohesionless materials is attributed to the fact that the failure envelope is actually nonlinear; there is also aggregate interlocking and dilation that occurs during shearing, depending on the applied normal stress. In reality, the friction angle decreases with increased applied normal stress in a logarithmic function.

For the range of stresses tested, the secant friction angle corresponding to the peak for each applied normal stress was larger than that approximated from the MC approach. Because of these issues, an alternative ZDA method is proposed to determine the design friction angle. The ZDA approach reduces the friction angle to the critical state, thereby negating the effect of dilation from peak conditions. This approach helps reduce the amount of factors affecting the measured strength of aggregates and is theoretically the worst-case scenario.

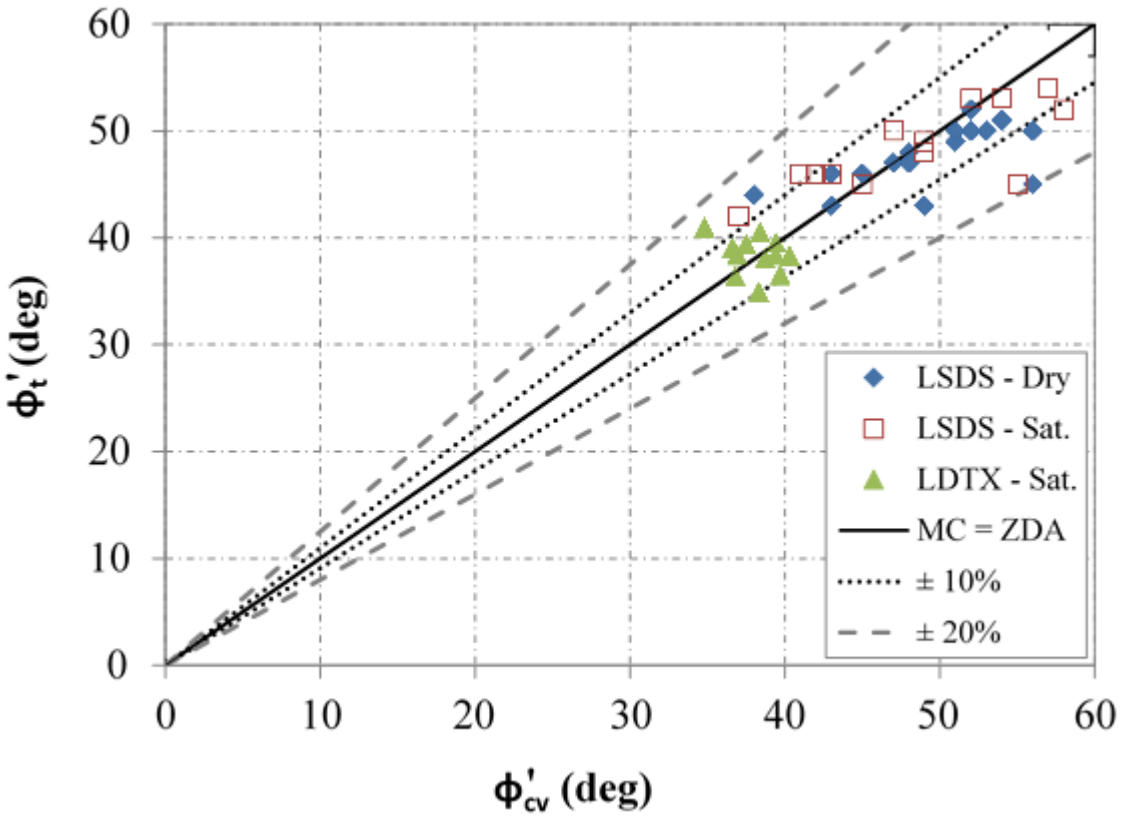

Figure 46. Chart. Relationship between measured tangent and CV friction angles.

Effect of Saturation

Saturation was investigated in the LSDS device by performing tests under both dry and saturated conditions. Tests with saturation are considered drained tests because the material is free-draining, the water is free to move into and out of the sample, and the strain rate is relatively low to prevent build-up of pore pressures during testing. The measured friction angle results are shown in table 14 and table 15. Generally, for the samples larger than the No. 7 aggregates (d_{max} > 0.75 inches), the friction angles measured from the saturated tests using the MC approach were higher than from the dry tests, up to 15 percent (figure 47). The reverse trend was found for No. 7 and smaller aggregates ($d_{max} \leq 0.75$ inches), where saturated testing produced lower friction angles. The biggest difference was for the No. 9 and No. 10 aggregates, where differences were up to 16 percent. Similar results are seen using the ZDA approach (figure 48).

For two-thirds of the aggregates (10 out of 15), the difference in measured tangent friction angles is within 10 percent. The results are similar for a larger population, almost 90 percent of the samples (13 out of 15), when using the ZDA approach. It is thought that saturation affects the dilative behavior, which is why the ZDA approach shows more negligible results. Overall, however, the difference between friction angles under dry and saturated conditions is within 20 percent for all samples regardless of test method (figure 49). While saturated tests take longer to perform than dry tests because of the time needed to achieve saturation and to drain the water

after testing, the test should ideally mimic in-service conditions; however, the effect for OGAs appears to be minimal.

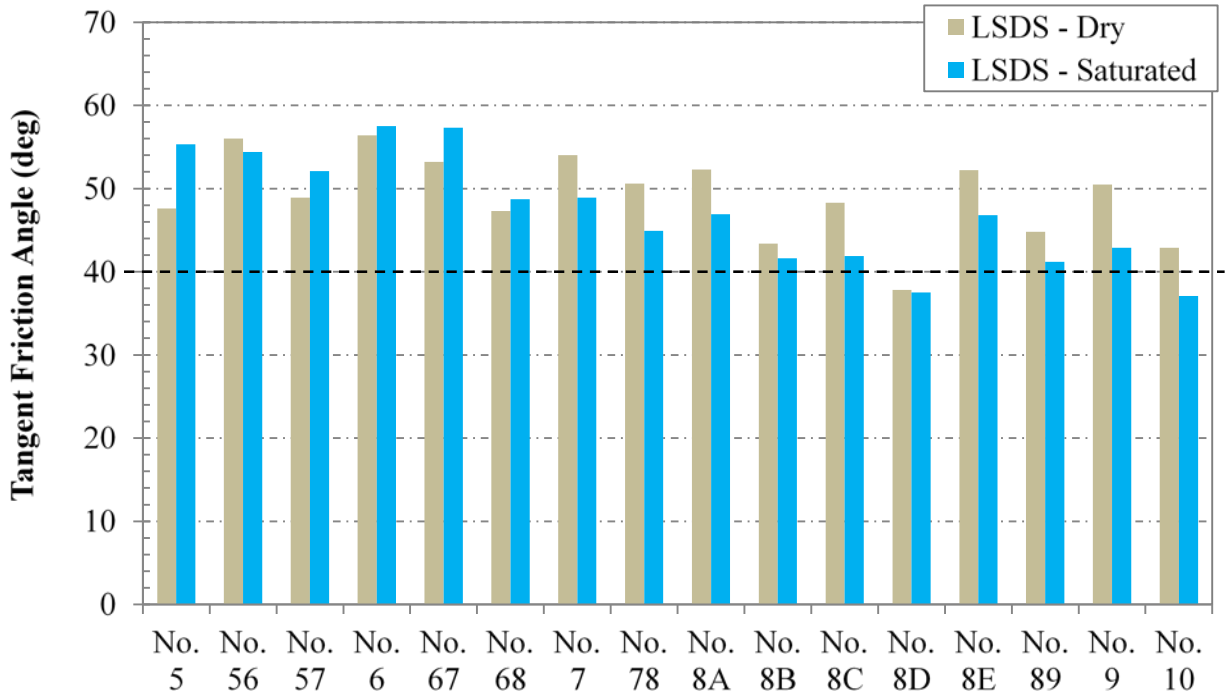

Figure 47. Chart. Measured friction angles under dry and saturated LSDS testing using the MC approach.

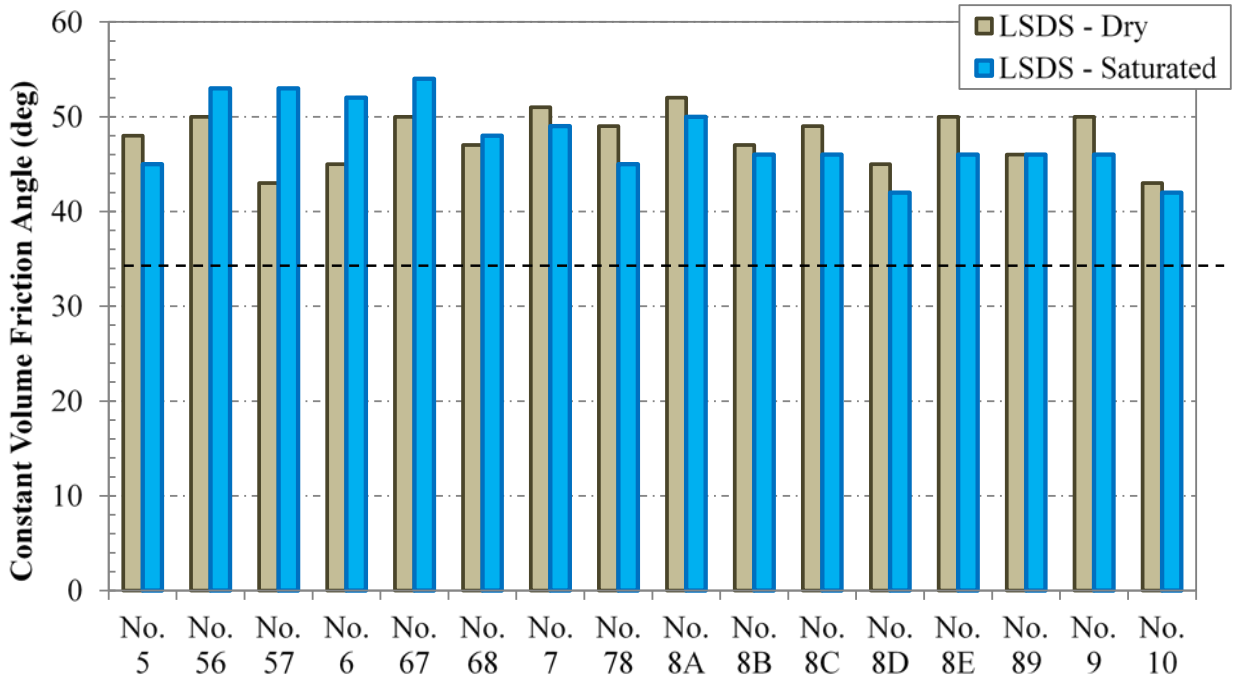

Figure 48. Chart. Measured friction angles under dry and saturated LSDS testing using the ZDA approach.

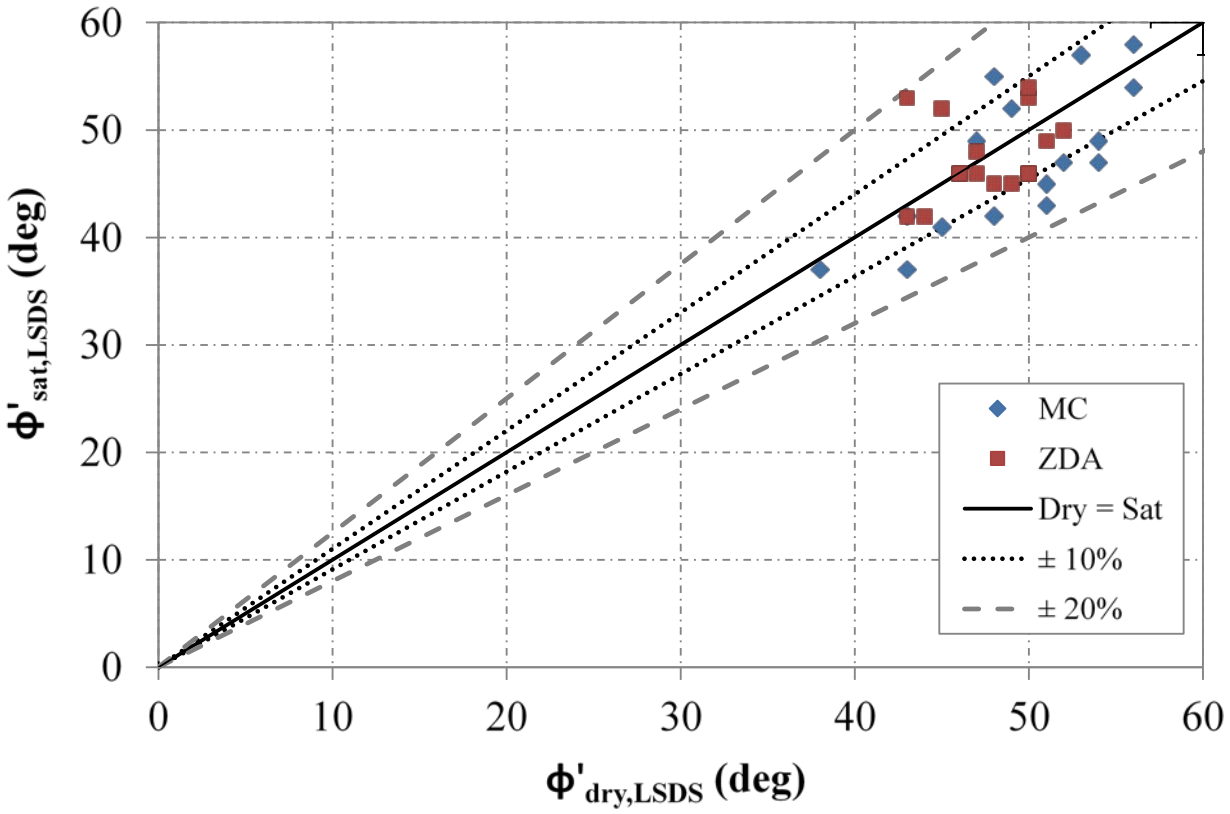

Figure 49. Chart. Relationship between measured friction angles under dry and saturated conditions in the LSDS device.

4.3 STRENGTH CORRELATIONS

In the absence of shear testing, designers will sometimes refer to correlations between other measured parameters and the friction angle of the material. The results were therefore compared with standard testing parameters to determine whether simple trends or correlations exist for OGAs.

Gradation

It was found that when comparing the measured tangent and CV friction angles with the mean aggregate size (d_{50}, see table 6), there is a general trend whereby as the mean size increases, the friction angle also increases under LSDS testing (figure 50 and figure 51, respectively). This result is not observed for LDTX testing in which the tangent friction angle is independent of mean aggregate size; however, when looking at the secant friction angles results from LDTX testing, a small positive relationship is observed that diminishes as confining stress increases (figure 52). This relationship may be the result of the low relative density under which testing occurred (about 30 percent). For the LSDS testing confined in a rigid box, the friction angle may not be affected as much for this reason as with LDTX testing, which has a more flexible boundary. Similar relationships are found with other gradation limits (e.g., d_{10}, d_{30}, d_{60}, d_{85}) and with the FM.

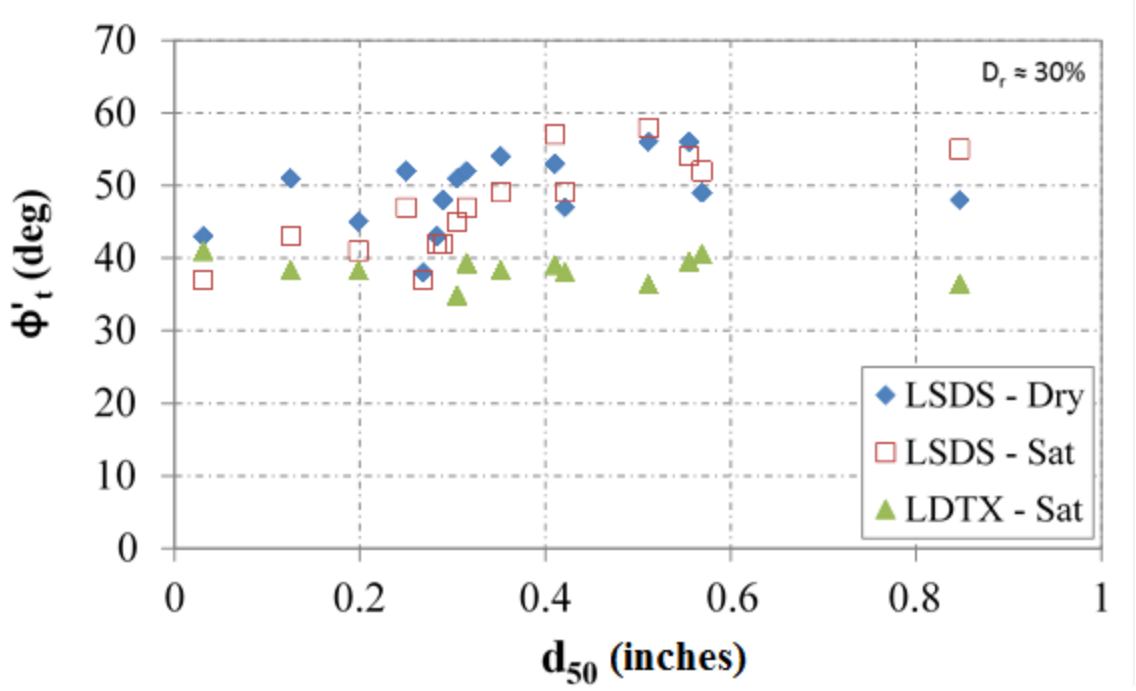

Figure 50. Chart. Relationship between tangent friction angle and median grain size.

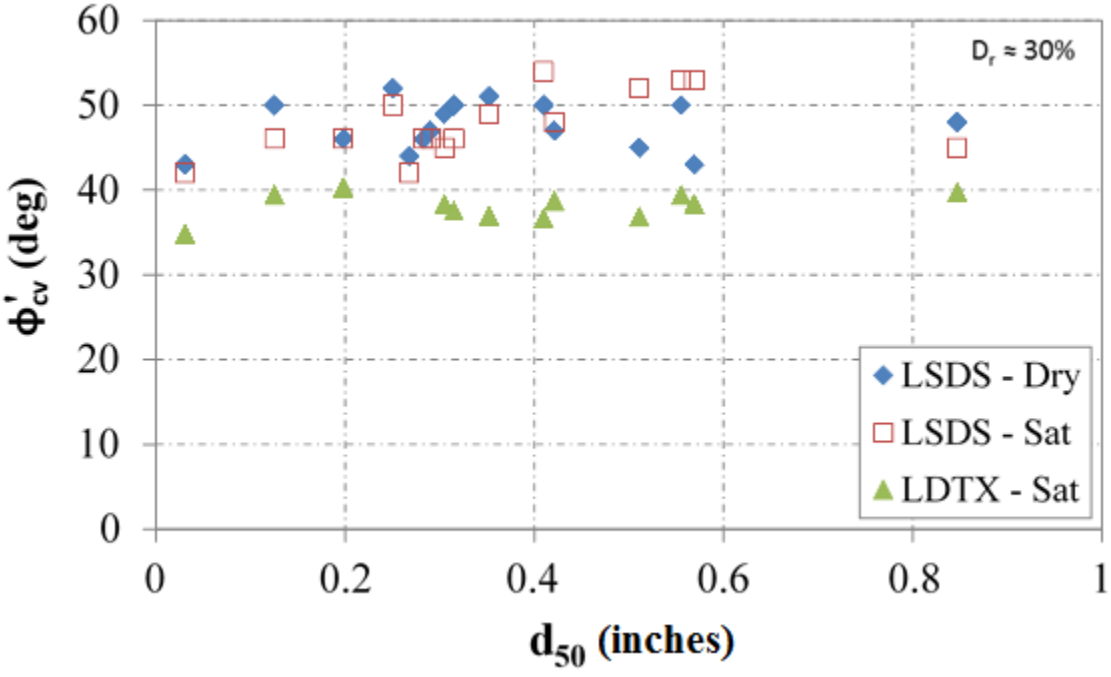

Figure 51. Chart. Relationship between CV friction angle and median grain size.

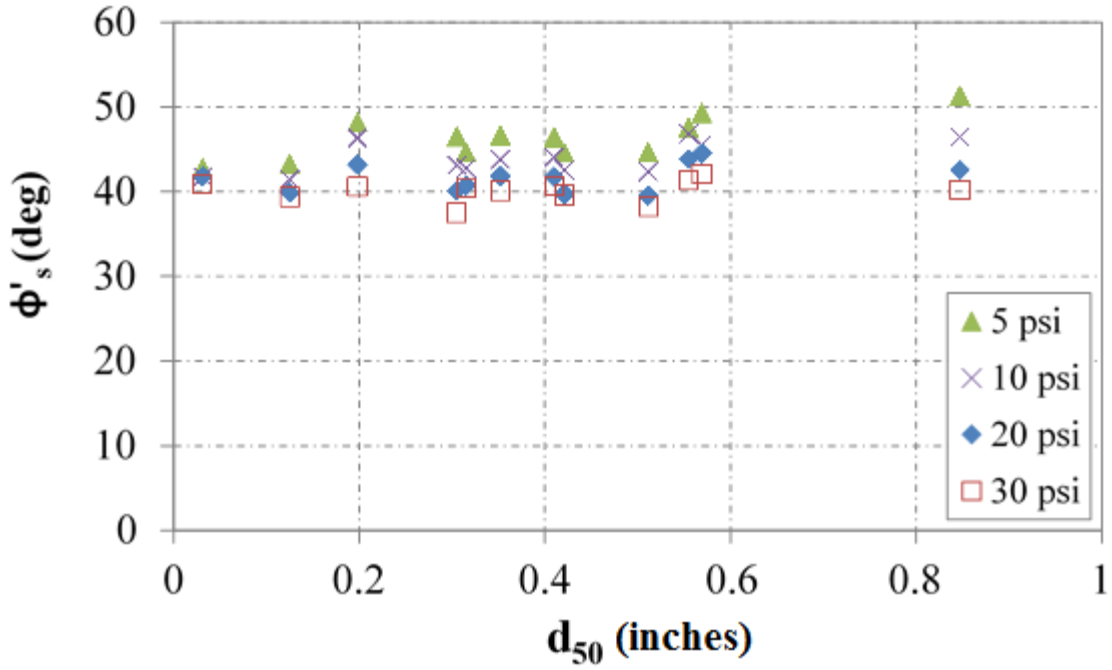

Figure 52. Chart. Relationship between secant friction angle and median grain size for LDTX testing.

The coefficient of uniformity (C_u) is another important parameter; it helps describe whether a material is OG or well-graded. Based on the findings of this study, a clear relationship was not found between the measured friction angles and the C_u for the materials (figure 53 and figure 54). For OGAs, this lack of a relationship indicates that aggregate size plays more of a role than the overall gradation; however, the range of C_u values examined is relatively narrow.

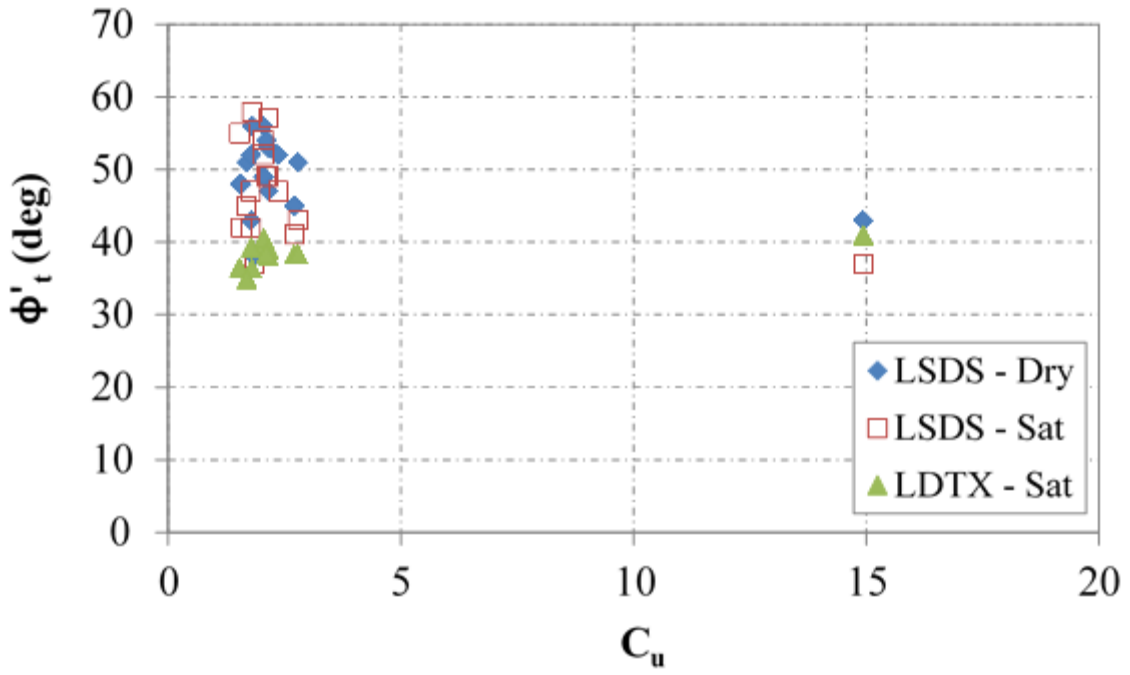

Figure 53. Chart. Relationship between tangent friction angle and C_u.

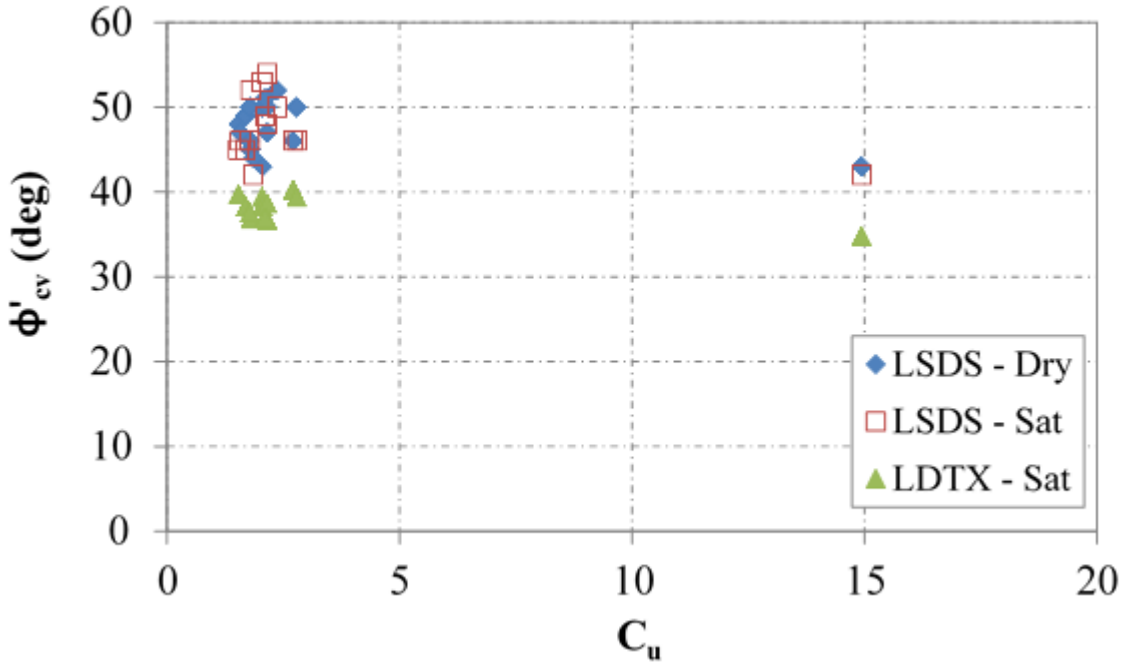

Figure 54. Chart. Relationship between CV friction angle and C_u.

Maximum Unit Weight

The samples were tested uncompacted at about 30 percent relative density, which was determined using the minimum and maximum unit weight of the OGAs found through vibratory table testing, described previously (table 7). By comparing the results for both LSDS and LDTX testing, it is found that the tangent friction angle is independent of the maximum density of the material (figure 55). A similar result is found when comparing the CV friction angle determined using LSDS testing and maximum unit weight (figure 56); however, there is a trend for the TX results whereby as maximum unit weight increases, the constant volume decreases.

These results are contrary to the Naval Facilities Engineering Command (NAVFAC) correlation that shows friction angle increasing with increasing dry unit weight for a given relative density.[86] Also contrary is that the estimated friction angle for a poorly graded gravel classified soil at 30 percent relative density is shown by NAVFAC as about 32 degrees, which is on the low side based on the measured test results in this study. More testing is needed on OGAs to investigate this discrepancy.

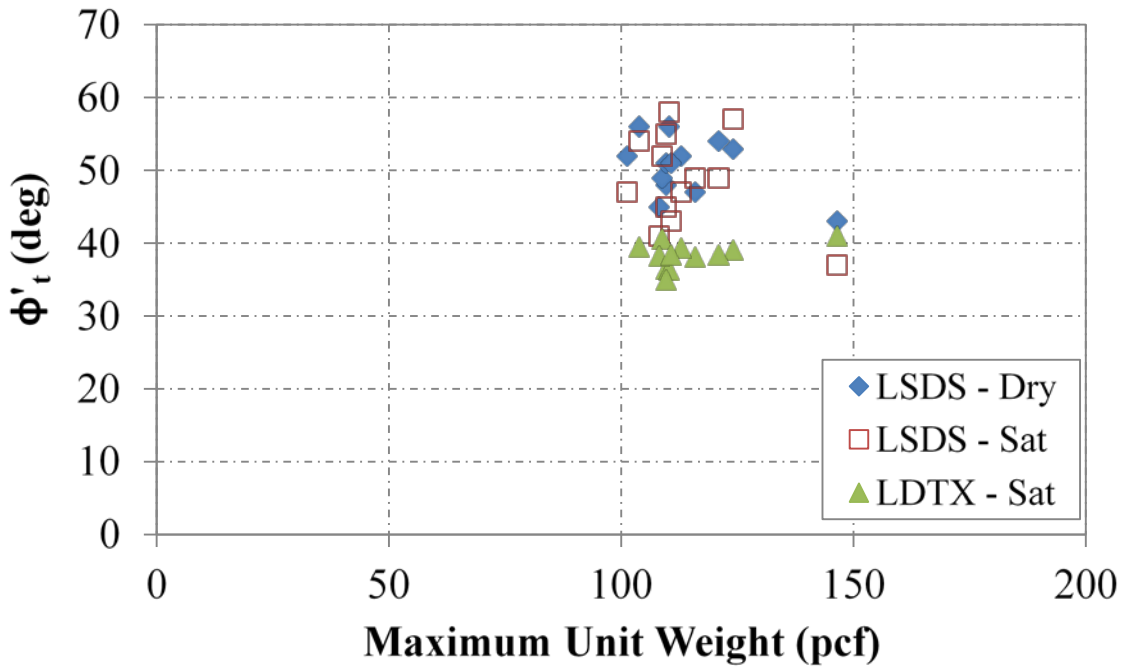

Figure 55. Chart. Relationship between tangent friction angle and maximum unit weight.

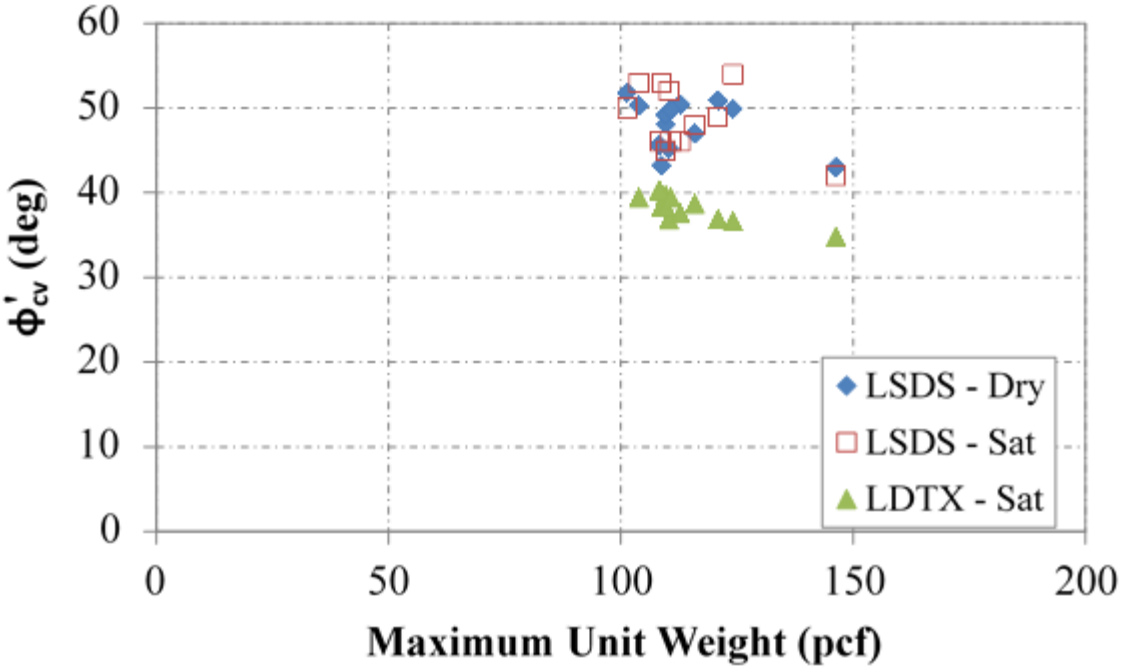

Figure 56. Chart. Relationship between CV friction angle and maximum unit weight.

Repose Angle

Others have postulated that the repose angle is equal to the constant volume friction angle; however, this theory is based on the behavior of soils.[10,87] For the OGAs tested, however, the CV friction angle is greater than the repose angle, with no clear relationship found between the measured repose angle and CV friction angle (figure 57).

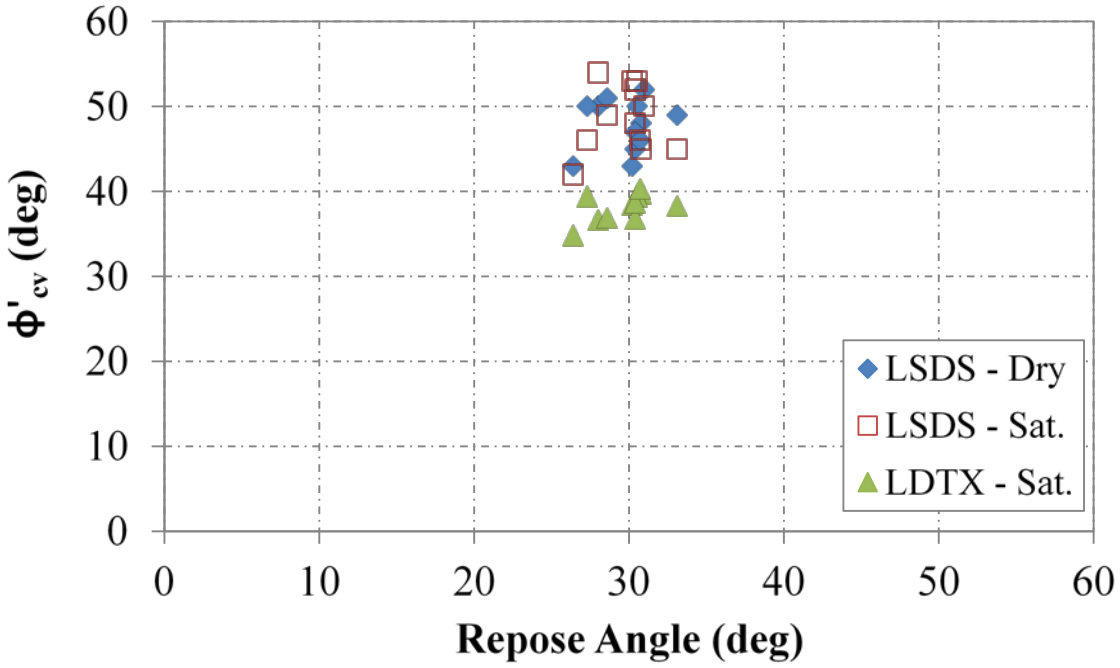

Figure 57. Chart. Relationship between CV friction angle and repose angle.

Angularity, Texture, and Sphericity

Angularity, texture, and sphericity were all described in this study with AIMS2 (table 9). The tangent and CV friction angles measured with the LSDS device show an inverse relationship with the average angularity index (figure 58 and figure 59, respectively). While this result is contrary to expectations, it is postulated that as the aggregates get more angular, there is less contact area between the particles and a higher void ratio (i.e., less dense). Higher void ratios typically result in lower friction angles (figure 60).

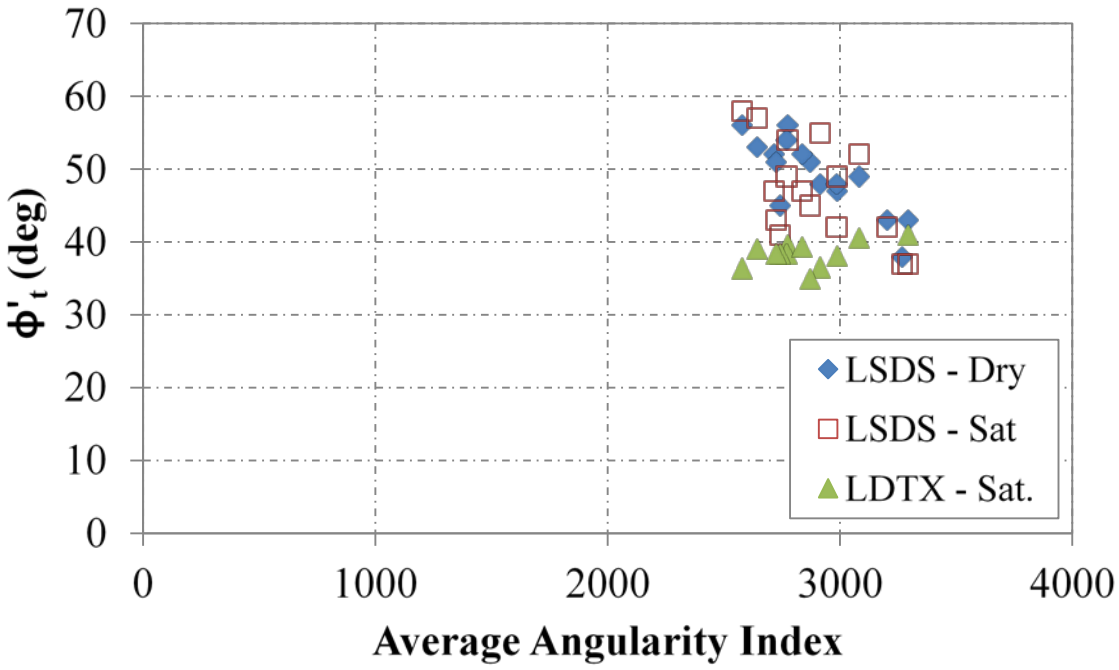

Figure 58. Chart. Relationship between tangent friction angle and angularity.

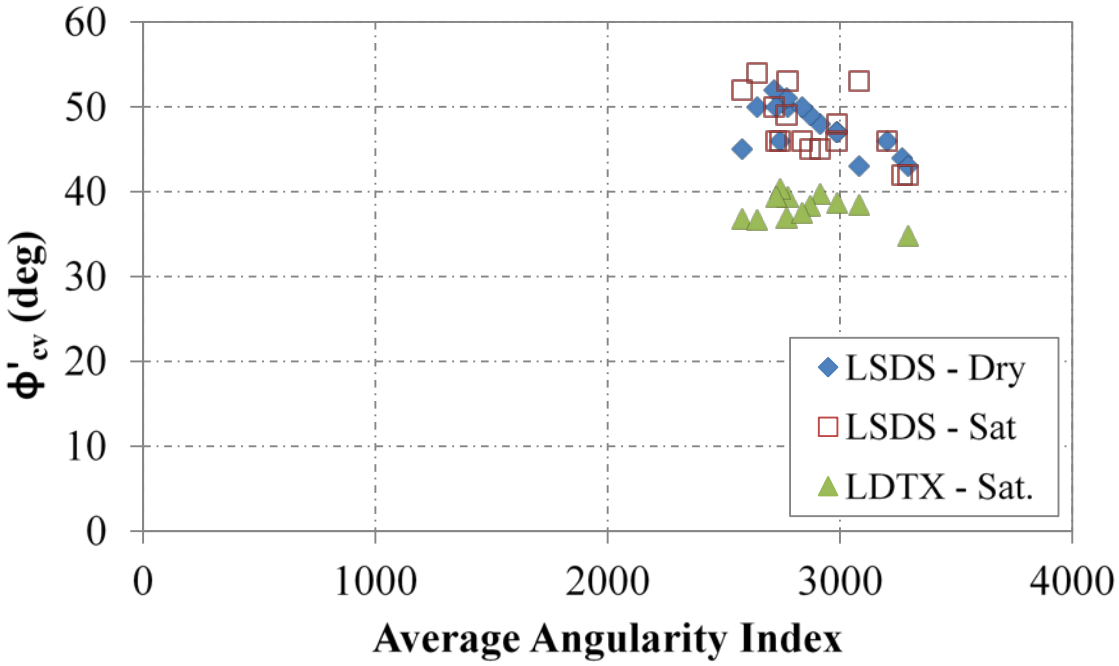

Figure 59. Chart. Relationship between CV friction angle and angularity.

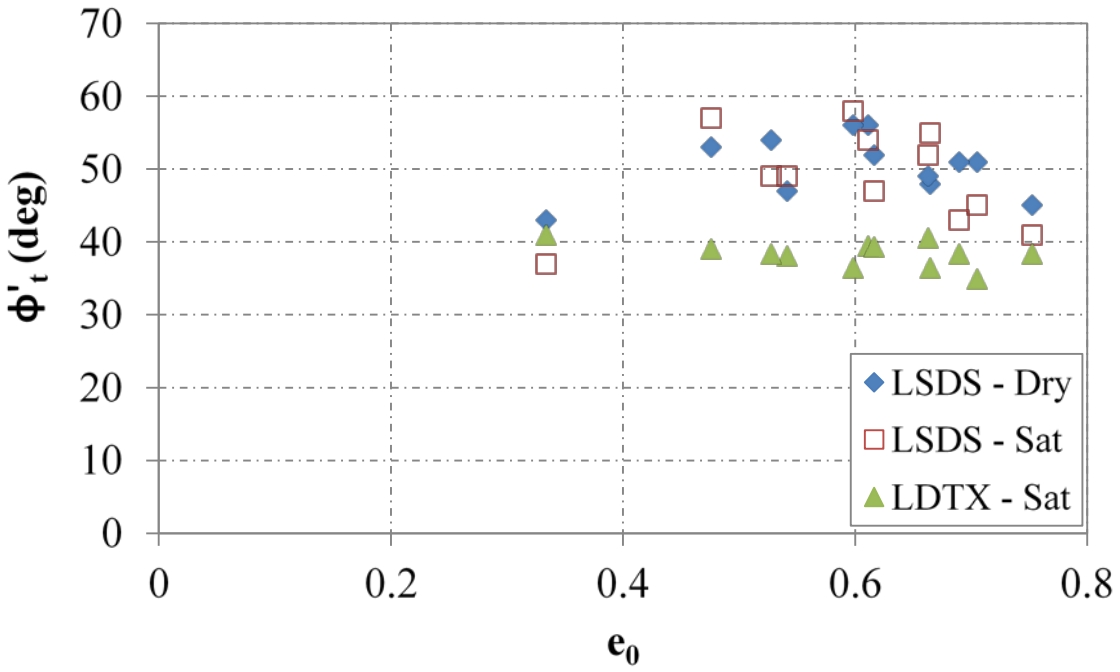

Figure 60. Relationship between initial void ratio and tangent friction angle.

Because all of the aggregates have the same classification for angularity, however, it is difficult to make a definitive conclusion. Texture was found to not influence the measured tangent friction angle (figure 61) or the CV friction angle.

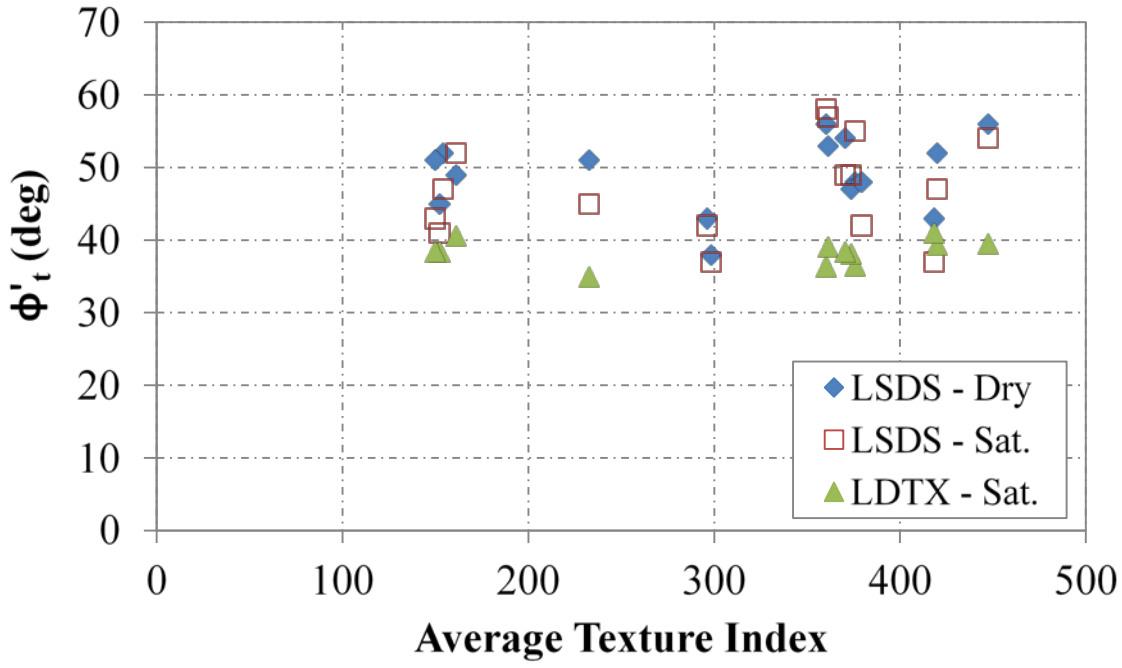

Figure 61. Chart. Relationship between CV friction angle and texture.

Sphericity does play a role in LSDS test results; as the average sphericity index increases, the friction angle also increases (figure 62 and figure 63). As with many of the other parameters, the LDTX results are independent of the sphericity. With the forced failure plane in LSDS testing, sphericity (the general roundness of the aggregates) affects the amount of dilation that occurs. Assuming the same angularity, flat/elongated particles will more easily slide past one another than rounded particles.

The measured angularity indexes help explain the variation between the various No. 8 aggregates tested, regardless of data interpretation (figure 64 and figure 65). To a lesser extent, sphericity influences the results as well (figure 66). Additional testing is needed to expand the database and develop design equations to correlate angularity with friction angle for all relevant AASHTO OGAs.

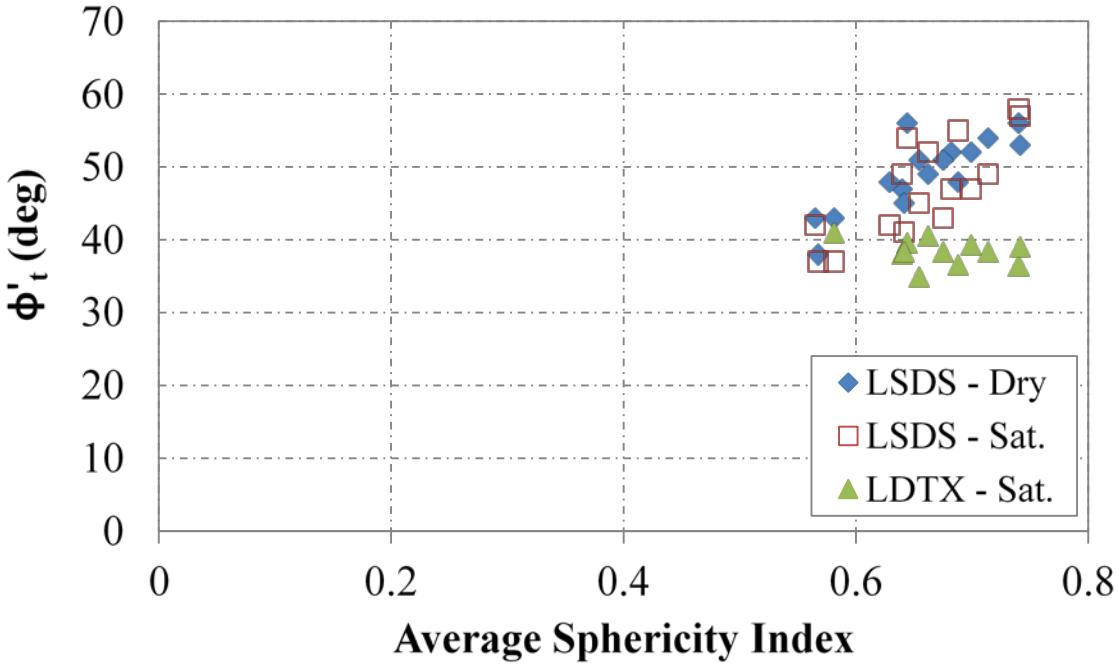

Figure 62. Chart. Relationship between tangent friction angle and sphericity.

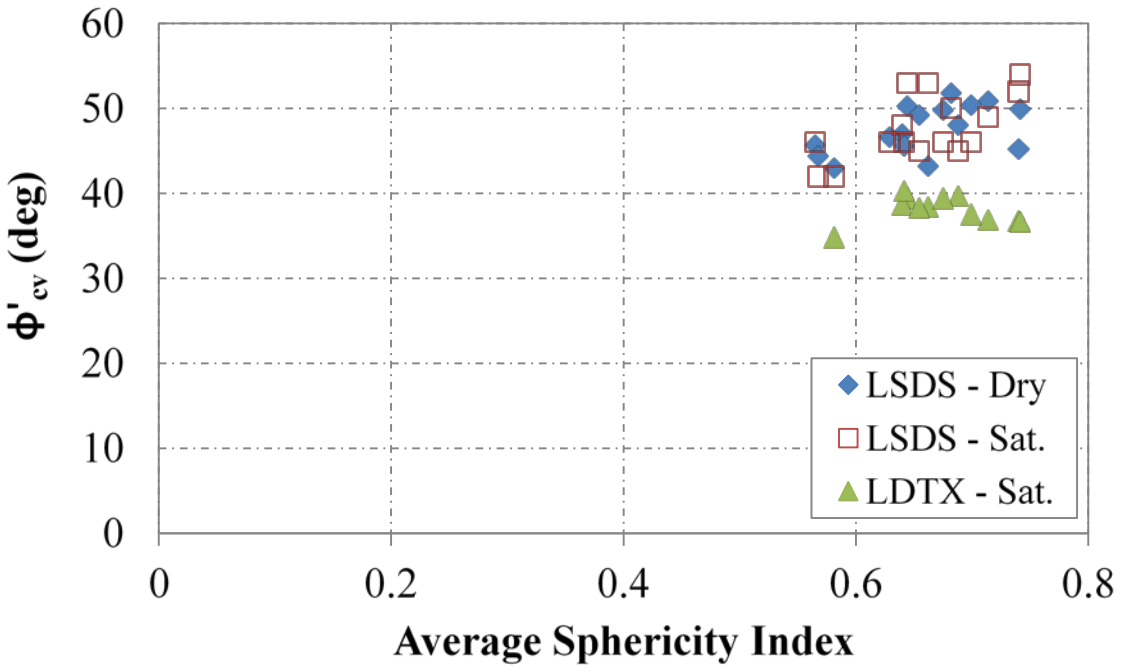

Figure 63. Chart. Relationship between CV friction angle and sphericity.

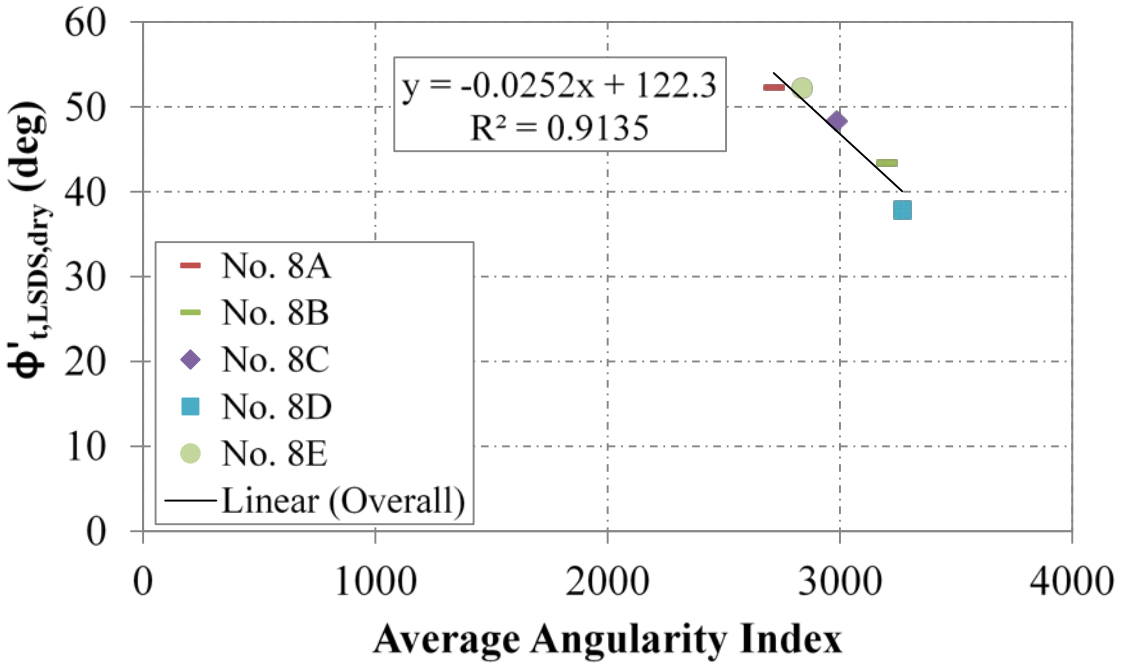

Figure 64. Chart. Relationship between tangent friction angle and angularity in LSDS testing for AASHTO No. 8 aggregates.

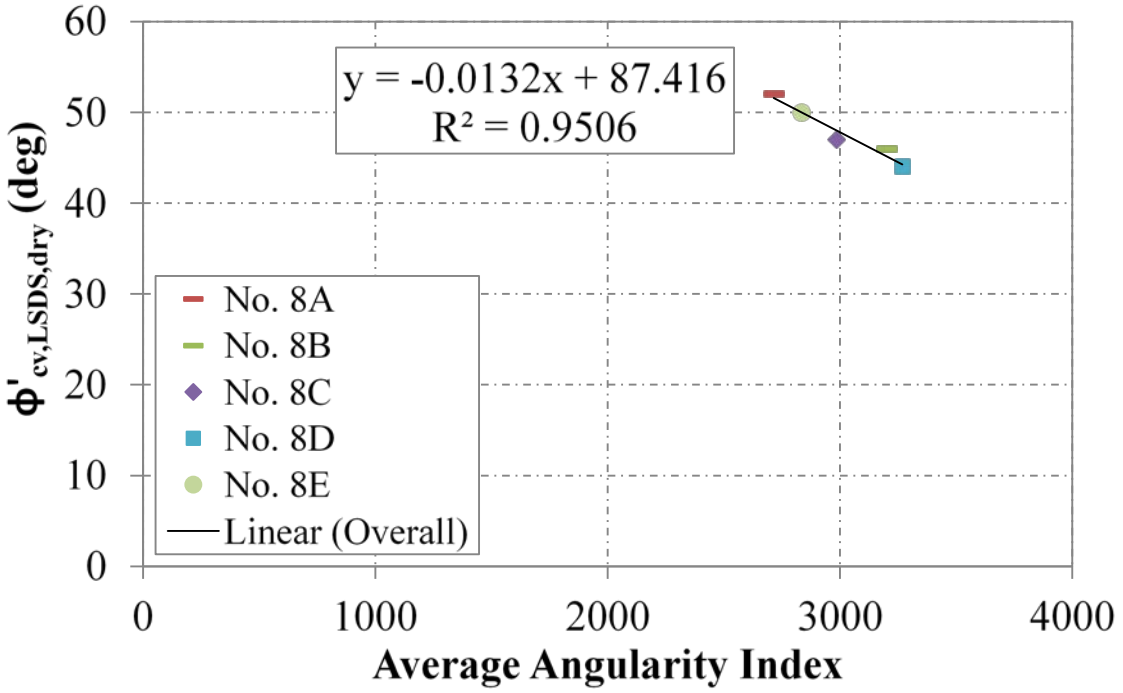

Figure 65. Chart. Relationship between CV friction angle and angularity in LSDS testing for AASHTO No. 8 aggregates.

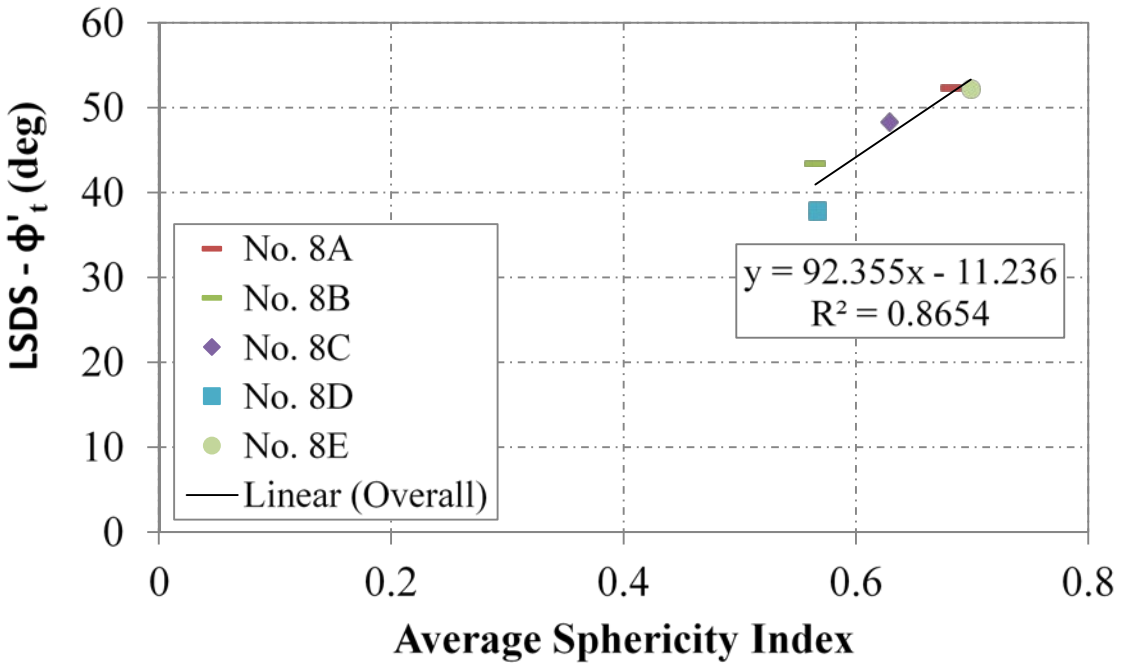

Figure 66. Chart. Relationship between tangent friction angle and sphericity in LSDS testing for AASHTO No. 8 aggregates.

CHAPTER 5. CONCLUSIONS

Sixteen AASHTO M43 gradations, ranging from an AASHTO No. 10 to an AASHTO No. 5 aggregate, were characterized in this study, including their gradation, minimum and maximum density, repose angle, angularity, and texture. In addition, LSDS and LDTX tests were conducted on the samples, compacted at a relative density of approximately 30 percent, to evaluate the strength. The results provide insight into the strength behavior of manufactured OGAs.

5.1 FRICTION ANGLE

Transportation agencies use OGAs as structural backfill for road and bridge construction, yet their strength parameters are not fully understood. To address this need, a comprehensive study was initiated, with the primary objectives to quantify the strength parameters, evaluate different conventional testing devices, and determine the influence of various factors on strength. The results indicate that the typical default friction angle of 34 degrees is a conservative measure (table 23). It is important to note that the reported friction angles are from samples tested at 30 percent relative density. In the field, compaction would result in added strength; therefore, the friction angles reported herein are considered conservative.

Table 23. Summary of LSDS and LDTX testing.

	MC Tangent Friction Angle		ZDA CV Friction Angle (degree)	
Sample	LSDS (degree)	LDTX (degree)	LSDS	LDTX
No. 5	55.3	36.5	44.6	39.7
No. 56	54.4	39.5	52.9	39.4
No. 57	52.1	40.5	52.9	38.4
No. 6	57.5	36.4	51.7	36.8
No. 67	57.3	39.0	53.7	36.6
No. 68	48.7	38.1	47.9	38.7
No. 7	48.9	38.4	49.0	36.9
No. 78	44.9	34.9	45.5	38.3
No. 8A	46.9	—	50.3	—
No. 8B	41.6	—	45.5	—
No. 8C	41.9	—	45.8	—
No. 8D	37.5	—	42.1	—
No. 8E	46.8	39.3	45.6	37.5
No. 89	41.2	38.3	45.8	40.3
No. 9	42.9	38.4	45.5	39.4
No. 10	37.1	40.1	42.0	34.8

CV = Constant volume.
LDTX = Large-diameter triaxial.
LSDS = Large-scale direct shear.
MC = Mohr-Coulomb.
ZDA = Zero dilation angle.
— = Not measured.

Two methods for determining the friction angle were investigated for comparison: (1) the slope of the best-fit linear MC failure envelope as in current practice, and (2) the ZDA approach. When combining all the results from every aggregate, the tangent friction angle was 48.2 and 38.4 degrees for LSDS and LDTX testing, respectively. Similarly, the CV friction angle from the ZDA method was 46.1 and 38.9 degrees for LSDS and LDTX testing, respectively (figure 67). Based on a typical COV of 5 to 10 percent for lab testing, and using the ZDA method for LSDS testing, the recommended default friction angle for AASHTO OGAs is 41 degrees.[85]

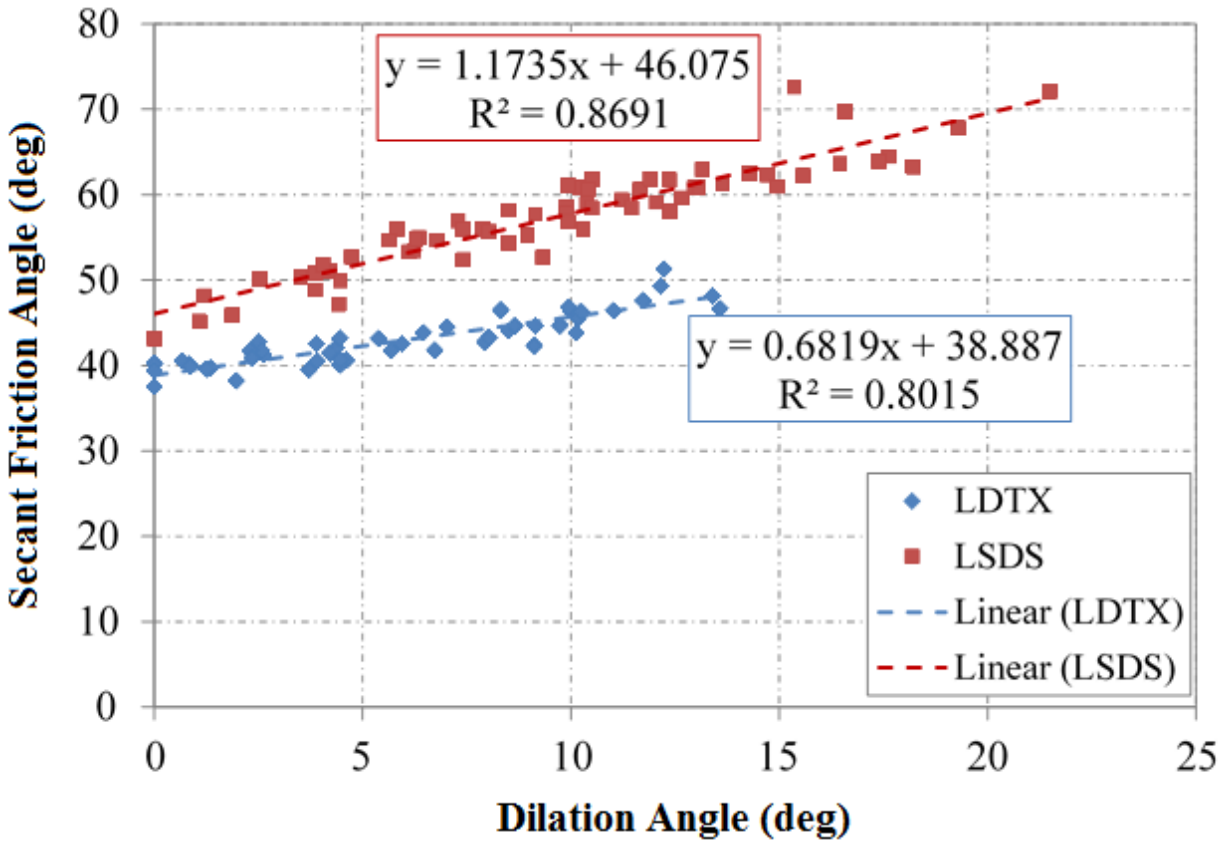

Figure 67. ZDA Approach for LDTX and LSDS testing.

Regardless of the approach, the results are similar; however, the ZDA method offers more confidence as a conservative estimate for strength. The linear MC method resulted in more data scatter and produces a measured cohesion value for a cohesionless material. The ZDA method also provides a consistent basis for obtaining the friction angle at the critical state but requires an extra step in the analysis to determine the dilation angle. Other methods such as measuring the secant friction angle at a given confining stress are available but rely on a design assumption that confining stress will remain constant throughout the life of the structure.

5.2 TEST METHOD

The selection of the test device to measure strength plays an important role. The LDTX device resulted in strengths that were considerably lower than those measured in the LSDS device. The difference in results generally increases with increasing aggregate size. The dilation angles

determined from the LDTX device are also lower than those measured with the LSDS device (about 60 percent) because there is a forced failure plane during the LSDS test, causing more dilation. The difference in dilatancy from each test device helps explain the lower friction angles measured with LDTX because dilation is a component in the strength of aggregates. Because the contribution of dilation is different depending on whether the LDTX or LSDS test is employed (which suggests that there is a trend with dilation but not with tangent or CV friction angles between LDTX and LSDS results), it is clear that more factors are contributing to the strength between the two devices.

The SDS device was also investigated to evaluate a common practice of scalping the sample. To use a 2.5-inch-diameter SDS device, aggregates larger than 0.25 inches must be removed from each test sample. The SDS results of the scalped samples indicated friction angles that were still considerably greater than the default of 34 degrees. There was no clear relationship between the scalped and unscalped results determined from SDS and LSDS testing, respectively, with friction angles largely between 10 and 20 percent different. While the overall strength values were similar, the scalping process changes the dilation properties of the aggregates, with relative differences ranging from 15 to 65 percent; no trend was found. In addition, the initial void ratio also changed, which has an impact on strength. Overall, scalped samples are unrepresentative of field behavior and lead to uncertainty in the results.

The effect of saturation was evaluated in the LSDS device. For two-thirds of the aggregates (10 out of 15), the difference in the tangent friction angles between saturated and dry conditions was within 10 percent. The results were similar for a larger population—almost 90 percent of the samples (13 out of 15)—when using the ZDA method. It is thought that saturation reduces the dilative behavior, which is why the ZDA approach shows more negligible results. Overall, the difference between friction angles under dry and saturated conditions was within 20 percent for all samples regardless of test method. While the test should ideally mimic in-service conditions, the effect of saturation for OGAs appears minimal.

To take advantage of the strength of these engineered aggregates for more cost-effective designs, large-scale testing is recommended. The selection of LSDS versus LDTX testing depends on the use of the results and other factors. For example, if the friction angle is the only parameter needed, then the LSDS device is quicker and simpler to perform. The LDTX test can offer more information about the deformation behavior but is more complex, time consuming, and costly to perform.

Both the LSDS and LDTX devices produce friction angles that are theoretically less than PS conditions. The result from either device is appropriate in design; however, in most cases, the LSDS results would produce more cost-effective structures. In typical applications utilizing OGAs, such as in reinforced soil retaining walls and bridge foundations, the aggregates will be confined in a PS condition, which the LSDS device would more adequately mimic as compared with the LDTX device

5.3 STRENGTH CORRELATIONS

Correlations between various soil properties and parameters were investigated, but no direct relationship was found that designers can use in the absence of strength testing. LDTX results

were independent of the various parameters; however, there were general trends found for LSDS testing. The strongest relationships were observed when comparing the aggregate size, angularity, void ratio, and sphericity to strength. There was no relationship between the measured friction angle and the coefficient of uniformity, maximum unit weight, repose angle, and aggregate texture; however, these poor correlations could potentially be the result of the relatively small differences between the physical parameters for the aggregates tested in this study.

As the mean aggregate size increased, the friction angle also increased. The tangent and CV friction angles measured with the LSDS device show an inverse relationship with the average angularity index. While this result is contrary to expectations, it is postulated that as the aggregates gets more angular, there is less contact area between the particles and a higher void ratio (i.e., less dense), and higher void ratios typically result in lower friction angles. There is a positive trend with sphericity, however, whereby as the average sphericity index increases, the friction angle also increases. With the forced failure plane in LSDS testing, sphericity affects the amount of dilation that occurs.

5.4 FUTURE RESEARCH

This study was the first to systematically test and characterize AASHTO OGAs. While many insightful results were produced, additional research is needed before concrete design recommendations can be proposed. A database of multiple sources of each OGA is needed to quantify the material variability to determine appropriate confidence intervals. The impact of relative density on the strength will also be investigated. In addition, the results presented utilized material that was retested for each confining stress; the influence and practicality of using virgin material for each test will be studied. Until this range of research is conducted, readers are encouraged to understand and take advantage of the strength of these OGAs in design. Testing can then be used to facilitate the use of higher than 34-degree default values

APPENDIX A. RAW DATA

NO. 5

Figure 68. Photo. No. 5 aggregate sample.

Table 24. No. 5 gradation.

Sieve No.	Sieve Size (inches)	Mass of Soil + Pan (g)	Mass of Pan (kg)	Mass of Soil (kg)	Percent Retained	Percent Passing
1.5	1.5	1,476	1,476	0	0.00	100.00
1	1	2,443.8	1,453	990.8	13.06	86.94
0.75	0.75	5,974.3	1,393.2	4,581.1	60.36	26.58
0.50	0.5	2,955.3	1,087.8	1,867.5	24.61	1.98
0.375	0.375	1,208.3	1,102.6	105.7	1.39	0.58
4	0.187	1,524.3	1,515	9.3	0.12	0.46
8	0.0937	1,129.2	1,129.2	0	0.00	0.46
16	0.0469	910.1	909.8	0.3	0.00	0.46
200	0.0029	930.7	916.4	14.3	0.19	0.27
Pan	—	690.2	669.8	20.4	0.27	0.00

Table 25. No. 5 density.

Sample	Minimum Density (pfc) ASTM D4254					Maximum Density (pcf) ASTM D4253			
	Test 1	Test 2	Test 3	Average	Standard Deviation	Test 1	Test 2	Average	Standard Deviation
No. 5	94.7	95.6	94.5	94.9	0.6	109.8	109.3	109.6	0.4

Table 26. No. 5 repose angle.

	Angle Finder						String Method			Average Repose Angle
Test	1	2	3	4	5	Average	Circumference (inches)	Angle	Average	
1	30	30	35	32	32	30.13	50	32.74	31.53	30.83
2	30	31	28	30	32		51.375	30.65		
3	28	30	26	29	29		51	31.21		

Table 27. No. 5 standard DS results.

Normal Stress (psi)	Max Shear (psi)	Peak Friction Angle (degree)	Max Dilation Angle (degree)
5.13	8.74	59.61	8.37
10.05	18.62	61.64	9.82
20.02	31.04	57.18	9.55
30.07	49.57	58.76	9.28

Table 28. No. 5 LSDS results—dry.

Normal Stress (psi)	Max Shear (psi)	Peak Friction Angle (degree)	Max Dilation Angle (degree)
5.59	17.30	72.10	21.48
11.27	30.53	69.74	16.58
22.72	40.45	60.68	10.42
34.17	50.55	55.94	7.41

Table 29. No. 5 LSDS results—saturated.

Normal Stress (psi)	Max Shear (psi)	Peak Friction Angle (degree)	Max Dilation Angle (degree)
5.69	12.17	64.93	15.86
11.10	24.91	65.99	14.75
22.36	34.62	57.15	10.92
34.24	56.10	58.60	9.46

Table 30. No. 5 LDTX results.

σ'_1 (psi)	σ'_3 (psi)	ϕ'_s (degree)	ψ_{max} (degree)
5.22	42.32	51.31	12.23
10.12	63.25	46.42	9.99
20.05	103.81	42.55	3.88
30.01	139.98	40.25	0.00

NO. 56

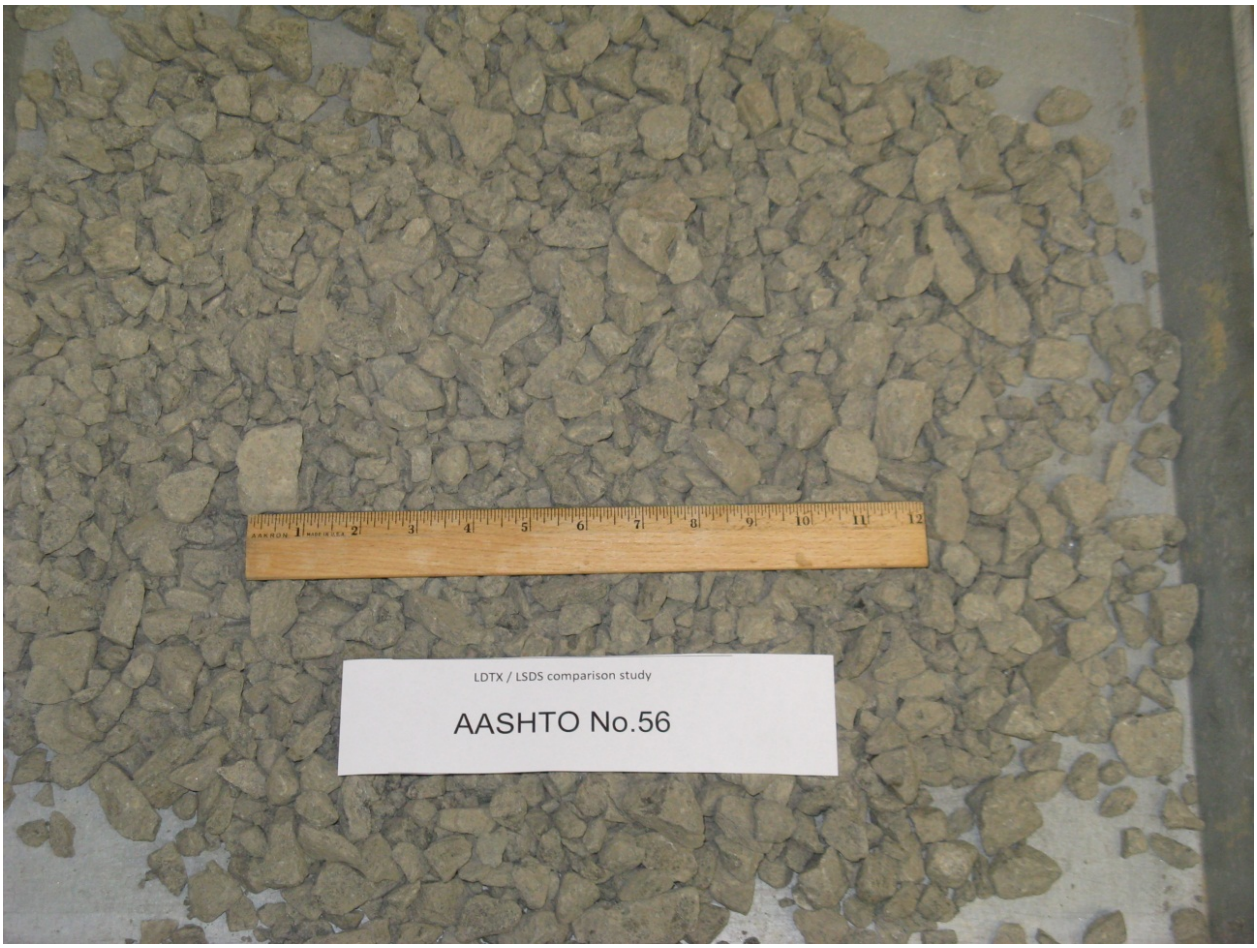

Figure 69. Photo. No. 56 aggregate sample.

Table 31. No. 56 gradation.

Sieve No.	Sieve Size (inches)	Mass of Soil + Pan (g)	Mass of Pan (kg)	Mass of Soil (kg)	Percent Retained	Percent Passing
1.5	1.5	1,475.9	1,475.9	0	0.00	100.00
1	1	1,421	1,127.1	293.9	4.27	95.73
0.75	0.75	2,109.9	1,393.21	716.69	10.42	85.31
0.50	0.5	4,203.1	1,087.95	3,115.15	45.27	40.04
0.375	0.375	2,821.4	1,102.79	1,718.61	24.98	15.07
4	0.187	2,374.5	1,514.98	859.52	12.49	2.58
8	0.0937	1,253.2	1,129.04	124.16	1.80	0.77
16	0.0469	922.5	909.95	12.55	0.18	0.59
50	0.0117	749.9	741.69	8.21	0.12	0.47
200	0.0029	928.4	916.46	11.94	0.17	0.30
Pan	—	620.9	600.56	20.34	0.30	0.00

Table 32. No. 56 density.

Sample	Minimum Density (pfc) ASTM D4254					Maximum Density (pcf) ASTM D4253			
	Test 1	Test 2	Test 3	Average	Standard Deviation	Test 1	Test 2	Average	Standard Deviation
No. 56	100.4	100.4	101.8	100.9	0.8	108.5	99.1	103.8	6.6

Table 33. No. 56 repose angle.

Test	Angle Finder						String Method			Average Repose Angle
1	35	35	32	28	33		52.75	28.70		
2	32	30	27	25	30	31.4	53	28.36	29.55	30.48
3	33	30	33	34	34		50.75	31.59		

Table 34. No. 56 standard DS results.

Normal Stress (psi)	Max Shear (psi)	Peak Friction Angle (degree)	Peak Dilation Angle (degree)
5.43	12.81	67.03	19.94
10.05	22.17	65.61	17.10
20.24	34.26	59.43	12.85
30.14	50.04	58.94	13.28

Table 35. No. 56 LSDS results—dry.

Normal Stress (psi)	Max Shear (psi)	Peak Friction Angle (degree)	Peak Dilation Angle (degree)
5.54	9.97	60.94	14.96
10.72	17.91	59.10	12.05
22.03	35.91	58.47	10.49
33.04	50.52	56.82	9.94

Table 36. No. 56 LSDS results—saturated.

Normal Stress (psi)	Max Shear (psi)	Peak Friction Angle (degree)	Peak Dilation Angle (degree)
5.66	11.34	63.47	15.15
11.05	22.98	64.32	14.46
22.36	38.18	59.65	7.14
32.98	50.44	56.82	7.44

Table 37. No. 57 LDTX results.

σ'_1 (psi)	σ'_3 (psi)	ϕ'_s (degree)	ψ_{max} (degree)
34.59	5.21	47.58	11.73
65.42	10.23	46.85	9.95
110.50	20.05	43.86	6.46
146.86	30.12	41.27	2.63

NO. 57

Figure 70. Photo. No. 57 aggregate sample.

Table 38. No. 57 gradation.

Sieve No.	Sieve Size (inches)	Mass of Soil + Pan (g)	Mass of Pan (kg)	Mass of Soil (kg)	Percent Retained	Percent Passing
1	1	1,127.1	1,127.1	0	0.00	100.00
0.75	0.75	2,311	1,393.4	917.6	12.09	87.91
0.50	0.5	5,052.1	1,087.8	3,964.3	52.22	35.69
0.375	0.375	2,739.5	1,102.7	1,636.8	21.56	14.13
4	0.187	2,308.8	1,514.8	794	10.46	3.67
8	0.0937	1,224.5	1,128.9	95.6	1.26	2.41
16	0.0469	981.1	909.8	71.3	0.94	1.47
200	0.0029	974.5	916.7	57.8	0.76	0.71
Pan	—	723.3	669.7	53.6	0.71	0.00

Table 39. No. 57 density.

	Minimum Density (pfc) ASTM D4254					Maximum Density (pcf) ASTM D4253			
Sample	Test 1	Test 2	Test 3	Average	Standard Deviation	Test 1	Test 2	Average	Standard Deviation
No. 57	95.1	96.0	95.1	95.4	0.5	108.1	109.3	108.7	0.8

Table 40. No. 57 repose angle.

Test	Angle Finder						String Method			Average Repose Angle
1	30	30	30	32	30		50.75	31.59		
2	31	30	27	30	26	29.67	52	29.75	30.79	30.23
3	27	29	29	34	30		51.125	31.02		

Table 41. No. 57 standard DS results.

Normal Stress (psi)	Max Shear (psi)	Peak Friction Angle (degree)	Peak Dilation Angle (degree)
5.74	12.59	65.48	28.11
10.29	16.88	58.64	16.79
20.51	37.50	61.33	18.10
29.73	52.45	60.45	13.06

Table 42. No. 57 LSDS results—dry.

Normal Stress (psi)	Max Shear (psi)	Peak Friction Angle (degree)	Peak Dilation Angle (degree)
5.49	17.55	72.62	15.36
10.81	21.19	62.96	13.15
22.23	40.21	61.07	9.93
33.22	47.19	54.85	6.28

Table 43. No. 57 LSDS results—saturated.

Normal Stress (psi)	Max Shear (psi)	Peak Friction Angle (degree)	Peak Dilation Angle (degree)
5.52	13.23	67.35	15.66
11.14	23.01	64.16	10.58
22.63	37.33	58.77	5.94
33.97	50.37	56.00	3.28

Table 44. No. 57 LDTX results.

σ'_1 (psi)	σ'_3 (psi)	ϕ'_s (degree)	ψ_{max} (degree)
37.09	5.11	49.28	12.15
61.16	10.21	45.55	10.17
114.64	20.15	44.51	7.03
152.52	30.12	42.08	4.35

NO. 6

Figure 71. Photo. No. 6 aggregate sample.

Table 45. No. 6 gradation.

Sieve No.	Sieve Size (inches)	Mass of Soil + Pan (kg)	Mass of Pan (kg)	Mass of Soil (kg)	Percent Retained	Percent Passing
1	1	1,127.1	1,127.1	0	0.00	100.00
0.75	0.75	1,640.8	1,393.3	2,47.5	3.83	96.17
0.50	0.5	4,210.5	1,087.8	3,122.7	48.27	47.91
0.375	0.375	3,365	1,102.5	2,262.5	34.97	12.94
4	0.187	2,110.7	1,514.6	596.1	9.21	3.72
8	0.0937	1,207.1	1,129.1	78	1.21	2.52
200	0.0029	990.9	916.5	74.4	1.15	1.37
Pan	—	758	669.6	88.4	1.37	1.15

Table 46. No. 6 density.

	Minimum Density (pfc) ASTM D4254					Maximum Density (pcf) ASTM D4253			
Sample	Test 1	Test 2	Test 3	Average	Standard Deviation	Test 1	Test 2	Average	Standard Deviation
No. 6	100.8	100.8	101.3	101.0	0.3	116.3	104.2	110.3	8.6

Table 47. No. 6 repose angle.

Test	Angle Finder						String Method			Average Repose Angle
1	33	33	31	33	32	31.2	52.175	29.50	29.67	30.43
2	32	31	28	29	30		52	29.75		
3	31	35	36	25	29		52	29.75		

Table 48. No. 6 standard DS results.

Normal Stress (psi)	Max Shear (psi)	Peak Friction Angle (degree)	Peak Dilation Angle (degree)
5.134	11.86186	66.60	7.00
10.13	20.50297	63.71	7.20
20.14	38.43	62.34	10.68
30.13	53.4429	60.59	9.22

Table 49. No. 6 LSDS results—dry.

Normal Stress (psi)	Max Shear (psi)	Peak Friction Angle (degree)	Peak Dilation Angle (degree)
5.36	13.16	67.83	19.30
11.13	21.42	62.54	14.28
21.18	40.18	62.21	15.57
33.10	53.92	58.45	11.45

Table 50. No. 6 LSDS results—saturated.

Normal Stress (psi)	Max Shear (psi)	Peak Friction Angle (degree)	Peak Dilation Angle (degree)
5.35	15.00	70.36	17.30
10.78	20.17	61.88	15.83
21.58	38.40	60.67	11.26
32.57	56.84	60.19	8.28

Table 51. No. 6 LDTX results.

σ'_1 (psi)	σ'_3 (psi)	ϕ'_s (degree)	ψ_{max} (degree)
29.43	5.13	44.66	9.74
51.71	10.09	42.33	9.12
90.16	20.04	39.52	3.71
127.48	30.05	38.21	1.97

NO. 67

Figure 72. Photo. No. 67 aggregate sample.

Table 52. No. 67 gradation.

Sieve No.	Sieve Size (inches)	Mass of Soil + Pan (g)	Mass of Pan (kg)	Mass of Soil (kg)	Percent Retained	Percent Passing
1	1	1,127.1	1,127.1	0	0.00	100.00
0.75	0.75	1,622.1	1,393.3	228.8	3.09	96.91
0.50	0.5	3,356.9	1,087.8	2269.1	30.67	66.24
0.375	0.375	2,783.2	1,102.7	1680.5	22.71	43.52
4	0.187	4,442.4	1,514.9	2927.5	39.57	3.96
8	0.0937	1,345.1	1,128.9	216.2	2.92	1.03
16	0.0469	914.2	909.9	4.3	0.06	0.98
50	0.0117	745	741.6	3.4	0.05	0.93
200	0.0029	928.6	916.7	11.9	0.16	0.77
Pan	—	726.6	669.7	56.9	0.77	0.00

Table 53. No. 67 density.

	Minimum Density (pfc) ASTM D4254					Maximum Density (pcf) ASTM D4253			
Sample	Test 1	Test 2	Test 3	Average	Standard Deviation	Test 1	Test 2	Average	Standard Deviation
No. 67	105.8	107.7	105.1	106.2	1.3	122.9	125.2	124.1	1.6

Table 54. No. 67 repose angle.

Test	Angle Finder						String Method			Average Repose Angle
1	28	27	28	29	29		52.25	29.40		
2	29	27	29	30	26	27.6	52.75	28.70	28.38	27.99
3	27	27	25	26	27		54	27.04		

Table 55. No. 67 standard DS results.

Normal Stress (psi)	Max Shear (psi)	Peak Friction Angle (degree)	Peak Dilation Angle (degree)
5.311	15.2042	70.75	14.72
10.25	28.5173	70.23	16.62
20.04	49.13	67.81	11.65
30.25	65.2277	65.12	10.30

Table 56. No. 67 LSDS results—dry.

Normal Stress (psi)	Max Shear (psi)	Peak Friction Angle (degree)	Peak Dilation Angle (degree)
5.34	10.93	63.94	17.39
10.73	20.05	61.84	11.90
21.97	34.77	57.71	9.15
32.41	47.48	55.68	8.03

Table 57. No. 67 LSDS results—saturated.

Normal Stress (psi)	Max Shear (psi)	Peak Friction Angle (degree)	Peak Dilation Angle (degree)
5.41	11.03	63.89	15.34
10.89	22.87	64.55	12.69
21.84	37.99	60.10	11.11
33.29	55.53	59.06	7.41

Table 58. No. 67 LDTX results.

σ'_1 (psi)	σ'_3 (psi)	ϕ'_s (degree)	ψ_{max} (degree)
32.13	5.13	46.42	11.02
57.28	10.28	44.09	8.50
100.00	20.05	41.76	5.70
142.31	30.05	40.64	4.61

NO. 68

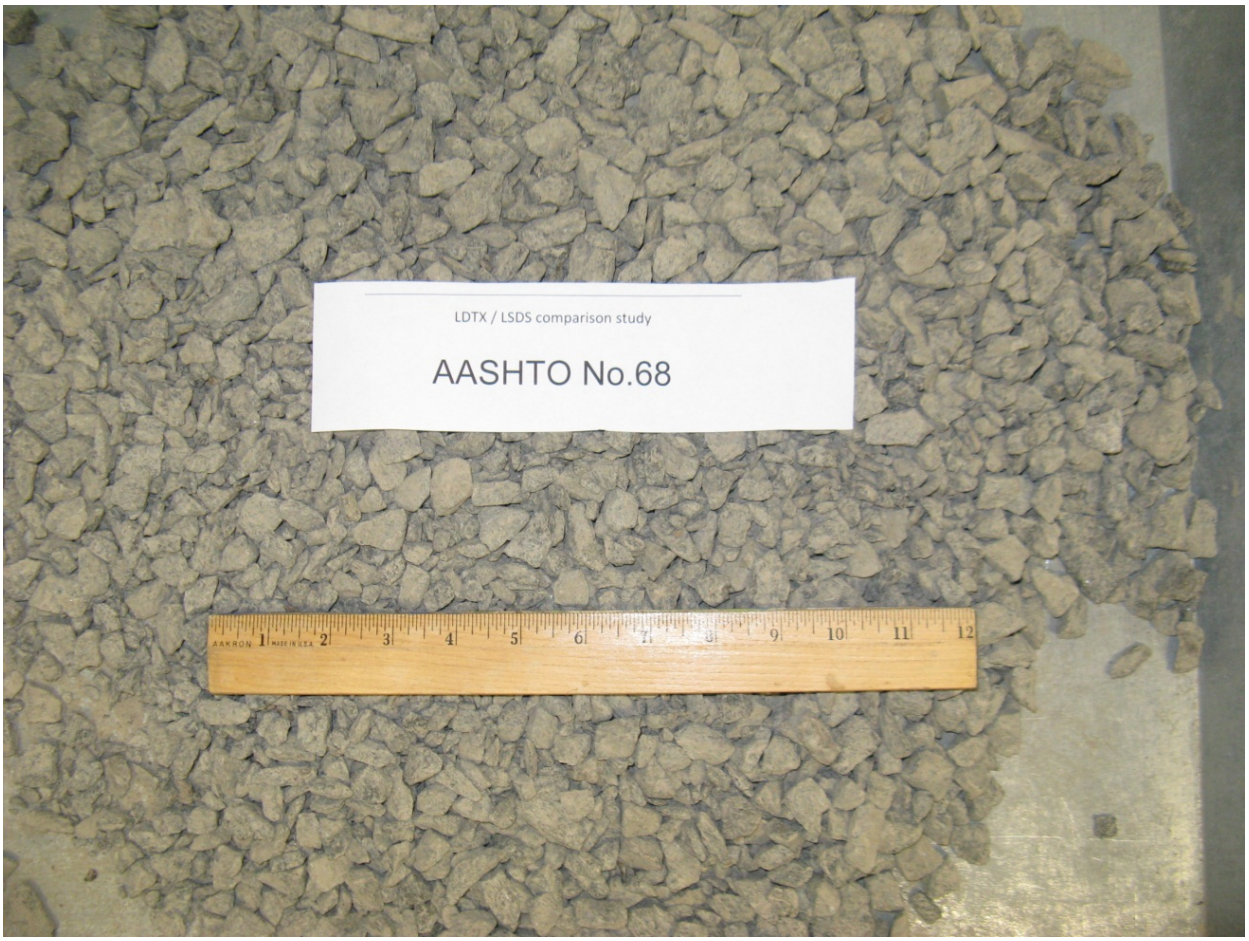

Figure 73. Photo. No. 68 aggregate sample.

Table 59. No. 68 gradation.

Sieve No.	Sieve Size (inches)	Mass of Soil + Pan (g)	Mass of Pan (kg)	Mass of Soil (kg)	Percent Retained	Percent Passing
0.75	0.75	1,393.4	1,393.4	0	0.00	100.00
0.50	0.5	2,943.3	1,088	1,855.3	31.56	68.44
0.375	0.375	2,818.9	1,102.7	1,716.2	29.19	39.25
4	0.187	3,387.1	1,514.8	1,872.3	31.85	7.40
8	0.0937	1,446.8	1,128.9	317.9	5.41	2.00
16	0.0469	938.5	909.8	28.7	0.49	1.51
50	0.0117	741.6	741.6	0	0.00	1.51
200	0.0029	949.7	918.2	31.5	0.54	0.97
Pan	—	727.1	670	57.1	0.97	0.00

Table 60. No. 68 density.

Sample	Minimum Density (pfc) ASTM D4254					Maximum Density (pcf) ASTM D4253			
	Test 1	Test 2	Test 3	Average	Standard Deviation	Test 1	Test 2	Average	Standard Deviation
No. 68	98.1	96.2	96.4	96.9	1.0	116.6	115.1	115.9	1.1

Table 61. No. 68 repose angle.

Test	Angle Finder						String Method			Average Repose Angle
1	31	36	30	32	32		52.125	29.57		
2	33	30	33	29	33	31.27	52	29.75	29.46	30.36
3	29	32	31	28	30		52.5	29.05		

Table 62. No. 68 standard DS results.

Normal Stress (psi)	Max Shear (psi)	Peak Friction Angle (degree)	Peak Dilation Angle (degree)
5.456	13.60408	68.15	19.20
10.2	22.662	65.77	13.91
20.04	32.53	58.36	9.67
30.3	44.2085	55.57	9.52

Table 63. No. 68 LSDS results—dry.

Normal Stress (psi)	Max Shear (psi)	Peak Friction Angle (degree)	Peak Dilation Angle (degree)
5.48	9.85	60.90	13.05
10.95	19.70	60.92	10.19
22.90	27.71	50.42	3.51
32.98	41.90	51.79	4.04

Table 64. No. 68 LSDS results—saturated.

Normal Stress (psi)	Max Shear (psi)	Peak Friction Angle (degree)	Peak Dilation Angle (degree)
5.39	8.82	58.56	13.82
11.08	15.59	54.59	7.37
22.55	24.78	47.69	1.44
32.92	41.37	51.49	3.05

Table 65. No. 68 LDTX results.

σ'_1 (psi)	σ'_3 (psi)	ϕ'_s (degree)	ψ_{max} (degree)
29.73	5.20	44.61	8.64
52.60	10.16	42.54	5.95
90.90	20.04	39.70	1.34
135.42	30.01	39.58	1.25

NO. 7

Figure 74. Photo. No. 7 aggregate sample.

Table 66. No. 7 gradation.

Sieve No.	Sieve Size (inches)	Mass of Soil + Pan (kg)	Mass of Pan (kg)	Mass of Soil (kg)	Percent Retained	Percent Passing
0.75	0.75	1,393.3	1,393.3	0	0.00	100.00
0.50	0.5	1,398.8	1,087.8	311	5.28	94.72
0.375	0.375	3,408.1	1,102.6	2,305.5	39.17	55.55
4	0.187	4,180.3	1,514.7	2,665.6	45.28	10.26
8	0.0937	1,545.1	1,128.9	416.2	7.07	3.19
200	0.0029	1,014.3	916.4	97.9	1.66	1.53
Pan	—	759.9	669.8	90.1	1.53	1.66

Table 67. No. 7 density.

	Minimum Density (pfc) ASTM D4254					Maximum Density (pcf) ASTM D4253			
Sample	Test 1	Test 2	Test 3	Average	Standard Deviation	Test 1	Test 2	Average	Standard Deviation
No. 7	102.6	103.6	103.7	103.3	0.6	120.4	121.3	120.9	0.6

Table 68. No. 7 repose angle.

Test	Angle Finder						String Method			Average Repose Angle
1	29	28	28	32	25	29.3333	53.5	27.69	27.94	28.63
2	30	27	30	29	30		54.25	26.72		
3	33	31	31	29	28		52.25	29.40		

Table 69. No. 7 standard DS results.

Normal Stress (psi)	Max Shear (psi)	Peak Friction Angle (degree)	Peak Dilation Angle (degree)
5.81	15.9929	70.03	30.05
10.33	28.7211	70.22	18.61
20.26	39.15	62.64	17.03
30.63	60.6459	63.20	21.99

Table 70. No. 7 LSDS results—dry.

Normal Stress (psi)	Max Shear (psi)	Peak Friction Angle (degree)	Peak Dilation Angle (degree)
5.36	10.63	63.25	18.21
10.74	20.47	62.32	14.72
21.70	36.67	59.39	11.22
32.85	48.62	55.95	7.88

Table 71. No. 7 LSDS results—saturated.

Normal Stress (psi)	Max Shear (psi)	Peak Friction Angle (degree)	Peak Dilation Angle (degree)
5.30	10.03	62.15	16.88
10.62	18.37	59.98	12.80
21.41	33.41	57.34	8.48
32.98	41.58	51.58	4.39

Table 72. No. 7 LDTX results.

σ'_1 (psi)	σ'_3 (psi)	ϕ'_s (degree)	ψ_{max} (degree)
33.09	5.23	46.65	13.58
55.98	10.17	43.82	10.12
101.23	20.25	41.80	6.73
139.31	30.19	40.08	4.45

NO. 78

Figure 75. Photo. No. 78 aggregate sample.

Table 73. No. 78 gradation.

Sieve No.	Sieve Size (inches)	Mass of Soil + Pan (g)	Mass of Pan (kg)	Mass of Soil (kg)	Percent Retained	Percent Passing
0.75	0.75	0	1,393.3	0	0.00	100.00
0.50	0.5	1,096.3	1,087.9	8.4	0.12	99.88
0.375	0.375	2,791.8	1,102.7	1,689.1	24.07	75.81
4	0.187	6,401.5	1,515	4,886.5	69.63	6.18
8	0.0937	1,503.8	1,129	374.8	5.34	0.84
16	0.0469	929.6	910.2	19.4	0.28	0.57
50	0.0117	747.6	741.5	6.1	0.09	0.48
100	0.0059	814.6	809.4	5.2	0.07	0.41
200	0.0029	923.1	916.4	6.7	0.10	0.31
Pan	—	691.6	669.8	21.8	0.31	0.00

Table 74. No. 78 density.

	Minimum Density (pfc) ASTM D4254					Maximum Density (pcf) ASTM D4253			
Sample	Test 1	Test 2	Test 3	Average	Standard Deviation	Test 1	Test 2	Average	Standard Deviation
No. 78	93.2	92.5	91.2	92.3	1.0	110.1	109.1	109.6	0.7

Table 75. No. 78 repose angle.

Test	Angle Finder						String Method			Average Repose Angle
1	33	33	30	35	31		50.75	31.59		
2	34	34	35	30	33	33.6	50	32.74	32.62	33.11
3	36	34	35	36	35		49.5	33.53		

Table 76. No. 78 standard DS results.

Normal Stress (psi)	Max Shear (psi)	Peak Friction Angle (degree)	Peak Dilation Angle (degree)
5.608	16.1631	70.87	21.60
10.53	26.6066	68.41	17.87
20.37	42.82	64.56	11.81
30.26	56.4644	61.81	10.87

Table 77. No. 78 LSDS results—dry.

Normal Stress (psi)	Max Shear (psi)	Peak Friction Angle (degree)	Peak Dilation Angle (degree)
5.48	8.77	58.00	12.38
10.78	17.36	58.17	8.49
21.49	30.29	54.65	6.77
32.62	42.35	52.39	7.41

Table 78. No. 78 LSDS results—saturated.

Normal Stress (psi)	Max Shear (psi)	Peak Friction Angle (degree)	Peak Dilation Angle (degree)
5.40	8.43	57.32	9.42
10.98	15.81	55.22	6.07
21.99	24.90	48.56	3.02
32.77	36.55	48.12	1.93

Table 79. No. 78 LDTX results.

σ'_1 (psi)	σ'_3 (psi)	ϕ'_s (degree)	ψ_{max} (degree)
32.44	5.16	46.49	8.31
54.01	10.15	43.13	5.38
92.61	20.02	40.13	0.84
123.08	29.94	37.49	0.00

NO. 8A (DEFIANCE)

Figure 76. Photo. No. 8A aggregate sample.

Table 80. No. 8A gradation.

Sieve No.	Sieve Size (inches)	Mass of Soil + Pan (g)	Mass of Pan (kg)	Mass of Soil (kg)	Percent Retained	Percent Passing
0.50	0.5	0	1,087.9	0	0.00	100.00
0.375	0.375	1,314.4	1,102.7	211.7	3.01	96.99
4	0.187	6,469.6	1515	4,954.6	70.49	26.50
8	0.0937	2,666.2	1129	1,537.2	21.87	4.63
16	0.0469	1,105.3	910.2	195.1	2.78	1.85
50	0.0117	807.6	741.5	66.1	0.94	0.91
100	0.0059	820.1	809.4	10.7	0.15	0.76
200	0.0029	924.1	916.4	7.7	0.11	0.65
Pan	—	715.4	669.8	45.6	0.65	0.00

Table 81. No. 8A density.

Sample	Minimum Density (pfc) ASTM D4254					Maximum Density (pcf) ASTM D4253			
	Test 1	Test 2	Test 3	Average	Standard Deviation	Test 1	Test 2	Average	Standard Deviation
No. 8A	86.2	85.3	85.7	85.7	0.5	101.3	101.3	101.3	0.0

Table 82. No. 8A repose angle.

Test	Angle Finder						String Method			Average Repose Angle
1	30	32	30	30	32	31.1333	51.5	30.47	30.78	30.96
2	32	34	31	32	33		51.25	30.84		
3	30	30	30	31	30		51.125	31.02		

Table 83. No. 8A standard DS results.

Normal Stress (psi)	Max Shear (psi)	Peak Friction Angle (degree)	Peak Dilation Angle (degree)
5.41	10.77703	63.34	17.97
10.50	21.74814	64.23	20.87
20.56	38.72	62.03	19.89
30.4	47.9136	57.61	15.47

Table 84. No. 8A LSDS results—dry.

Normal Stress (psi)	Max Shear (psi)	Peak Friction Angle (degree)	Peak Dilation Angle (degree)
5.31	9.51	60.84	12.96
10.76	19.06	60.57	11.65
21.40	30.53	54.97	6.35
32.40	45.65	54.64	5.63

Table 85. No. 8A LSDS results—saturated.

Normal Stress (psi)	Max Shear (psi)	Peak Friction Angle (degree)	Peak Dilation Angle (degree)
5.36	10.08	61.98	11.06
10.89	14.32	52.74	5.58
21.71	26.68	50.87	1.70
33.16	39.28	49.83	1.93

NO. 8B (STAUNTON LIME)

Figure 77. Photo. No. 8B aggregate sample.

Table 86. No. 8B gradation.

Sieve No.	Sieve Size (inches)	Mass of Soil + Pan (g)	Mass of Pan (g)	Mass of Soil (g)	Percent Retained	Percent Passing
0.75	0.75	1,189.4	1,189.4	0	0.00	100.00
0.50	0.5	1,398.1	1,386.4	11.7	0.19	99.81
0.375	0.375	2,101.9	1,171.1	930.8	14.93	84.88
4	0.187	5,961.1	1,514.5	4,446.6	71.32	13.56
8	0.0937	1,774.1	1,041.7	732.4	11.75	1.82
16	0.0469	945.9	910.6	35.3	0.57	1.25
50	0.0117	811.9	799	12.9	0.21	1.04
100	0.0059	747.5	743	4.5	0.07	0.97
200	0.0029	745.6	737.4	8.2	0.13	0.84
Pan	—	739.9	687.6	52.3	0.84	0.00

Table 87. No. 8B LSDS results—dry.

Normal Stress (psi)	Max Shear (psi)	Peak Friction Angle (degree)	Peak Dilation Angle (degree)
5.55	7.73	54.35	8.50
11.18	13.84	51.06	4.20
22.15	26.53	50.14	2.53
34.09	34.26	45.14	1.08

Table 88. No. 8B LSDS results—saturated.

Normal Stress (psi)	Max Shear (psi)	Peak Friction Angle (degree)	Peak Dilation Angle (degree)
5.55	8.63	57.26	8.99
11.08	15.25	54.00	4.80
22.86	23.60	45.91	1.00
34.02	34.78	45.64	0.00

NO. 8C (FRAZIER)

Figure 78. Photo. No. 8C aggregate sample.

Table 89. No. 8C gradation.

Sieve No.	Sieve Size (inches)	Mass of Soil + Pan (g)	Mass of Pan (kg)	Mass of Soil (kg)	Percent Retained	Percent Passing
0.75	0.75	1,189.4	1,189.4	0	0.00	100.00
0.50	0.5	1,386.4	1,386.4	0	0.00	100.00
0.375	0.375	1,783.6	1,171.1	612.5	9.70	90.30
4	0.187	6,838	1,514.5	5,323.5	84.32	5.98
8	0.0937	1,355.2	1,041.7	313.5	4.97	1.02
16	0.0469	919.4	910.6	8.8	0.14	0.88
50	0.0117	801.9	799	2.9	0.05	0.83
100	0.0059	745.2	743	2.2	0.03	0.80
200	0.0029	743.5	737.5	6	0.10	0.70
Pan	—	750.4	669.8	80.6	0.88	0.00

Table 90. No. 8C LSDS results—dry.

Normal Stress (psi)	Max Shear (psi)	Peak Friction Angle (degree)	Peak Dilation Angle (degree)
5.45	10.16	61.77	12.35
10.94	17.93	58.60	9.90
22.07	33.96	56.98	7.29
34.30	42.03	50.79	3.85

Table 91. No. 8C LSDS results—saturated.

Normal Stress (psi)	Max Shear (psi)	Peak Friction Angle (degree)	Peak Dilation Angle (degree)
5.43	9.38	59.93	11.19
11.11	13.75	51.06	3.83
22.78	25.91	48.68	1.91
34.06	34.42	45.30	0.00

NO. 8D (VULCAN MATERIALS)

Figure 79. Photo. No. 8D aggregate sample.

Table 92. No. 8D gradation.

Sieve No.	Sieve Size (inches)	Mass of Soil + Pan (g)	Mass of Pan (g)	Mass of Soil (g)	Percent Retained	Percent Passing
0.50	0.5	1,386.4	1,386.4	0	0.00	100.00
0.375	0.375	1,550	1,171.1	378.9	5.97	94.03
4	0.187	6,416.4	1,514.5	4,901.9	77.18	16.86
8	0.0937	1,989.2	1,041.8	947.4	14.92	1.94
16	0.0469	973.6	910.6	63	0.99	0.95
50	0.0117	817.7	798.9	18.8	0.30	0.65
100	0.0059	747.3	742.9	4.4	0.07	0.58
200	0.0029	750.4	737.6	12.8	0.20	0.38
Pan	—	711.8	687.6	24.2	0.38	0.00

Table 93. No. 8D LSDS results—dry.

Normal Stress (psi)	Max Shear (psi)	Peak Friction Angle (degree)	Peak Dilation Angle (degree)
5.46	10.22	61.87	10.51
11.43	15.43	53.48	6.23
23.03	25.72	48.16	1.20
35.28	33.10	43.17	0.00

Table 94. No. 8D LSDS results—saturated.

Normal Stress (psi)	Max Shear (psi)	Peak Friction Angle (degree)	Peak Dilation Angle (degree)
5.57	8.28	56.08	7.33
12.37	13.99	48.51	3.81
23.99	22.48	43.15	0.00
36.24	31.96	41.41	0.00

NO. 8E (LUCK STONE)

Figure 80. Photo. No. 8E aggregate sample.

Table 95. No. 8E gradation.

Sieve No.	Sieve Size (inches)	Mass of Soil + Pan (g)	Mass of Pan (kg)	Mass of Soil (kg)	Percent Retained	Percent Passing
1	1	1,127.1	1,127.1	0	0.00	100.00
0.50	0.5	1,116.5	1,087.7	28.8	0.31	99.69
0.375	0.375	3,832	1,102.6	2,729.4	29.83	69.86
4	0.187	6,694.3	1,013.8	5,680.5	62.08	7.78
8	0.0937	1,688.5	1,128.7	559.8	6.12	1.66
10	0.079	1,398.7	1,374	24.7	0.27	1.39
16	0.0469	935	909.7	25.3	0.28	1.11
40	0.0165	810	793.1	16.9	0.18	0.93
50	0.0117	746.2	741.8	4.4	0.05	0.88
Pan	—	750.4	669.8	80.6	0.88	0.00

Table 96. No. 8E density.

	Minimum Density (pfc) ASTM D4254					Maximum Density (pcf) ASTM D4253			
Sample	Test 1	Test 2	Test 3	Average	Standard. Deviation.	Test 1	Test 2	Average	Standard Deviation
No. 8E	97.3	98.4	97.9	97.9	0.6	111.1	114.5	112.8	2.4

Table 97. No. 8E LSDS results—dry.

Normal Stress (psi)	Max Shear (psi)	Peak Friction Angle (degree)	Peak Dilation Angle (degree)
5.38	15.22	70.53	17.80
10.86	26.73	67.90	12.40
21.62	39.89	61.55	10.04
33.51	52.55	57.47	6.51

Table 98. No. 8E LSDS results—saturated.

Normal Stress (psi)	Max Shear (psi)	Peak Friction Angle (degree)	Peak Dilation Angle (degree)
5.46	11.00	63.59	16.46
10.89	18.57	59.60	12.66
22.07	35.24	57.94	9.89
33.38	39.74	49.97	4.47

Table 99. No. 8E LDTX results.

σ'_1 (psi)	σ'_3 (psi)	ϕ'_s (degree)	ψ_{max} (degree)
40.70	5.43	49.86	15.89
69.68	10.44	47.68	13.24
121.65	20.30	45.56	9.28
154.29	30.20	42.27	5.20

NO. 89

Figure 81. Photo. No. 89 aggregate sample.

Table 100. No. 89 gradation.

Sieve No.	Sieve Size (inches)	Mass of Soil + Pan (g)	Mass of Pan (kg)	Mass of Soil (kg)	Percent Retained	Percent Passing
0.75	0.75	0	1,393.2	0	0.00	100.00
0.50	0.5	1,092.6	1,087.8	4.8	0.08	99.92
0.375	0.375	1,280.5	1,102.7	177.8	2.93	96.99
4	0.187	4,543.2	1,514.7	3,028.5	49.98	47.01
8	0.0937	3,313.7	1,128.8	2,184.9	36.06	10.95
16	0.0469	1,312.3	909.7	402.6	6.64	4.31
50	0.0117	882	741.5	140.5	2.32	1.99
200	0.0029	937.9	916.4	21.5	0.35	1.63
Pan	—	768.7	669.8	98.9	1.63	0.00

Table 101. No. 89 density.

	Minimum Density (pfc) ASTM D4254					Maximum Density (pcf) ASTM D4253			
Sample	Test 1	Test 2	Test 3	Average	Standard Deviation	Test 1	Test 2	Average	Standard Deviation
No. 89	88.9	89.5	86.8	88.4	1.4	107.0	109.4	108.2	1.7

Table 102. No. 89 repose angle.

Test	Angle Finder						String Method			Average Repose Angle
1	32	30	29	30	31		51	31.21		
2	27	29	30	30	30	29.87	50	32.74	31.60	30.73
3	29	31	30	29	31		51.25	30.84		

Table 103. No. 89 standard DS results.

Normal Stress (psi)	Max Shear (psi)	Peak Friction Angle (degree)	Peak Dilation Angle (degree)
5.57	16.6604	71.51	20.87
10.4	19.9907	62.51	13.52
20.24	36.06	60.69	15.63
30.13	53.6784	60.69	11.91

Table 104. No. 89 LSDS results—dry.

Normal Stress (psi)	Max Shear (psi)	Peak Friction Angle (degree)	Peak Dilation Angle (degree)
5.35	11.20	64.46	17.62
10.78	15.51	55.21	8.95
21.42	28.76	53.32	6.11
32.68	37.40	48.86	3.85

Table 105. No. 89 LSDS results—saturated.

Normal Stress (psi)	Max Shear (psi)	Peak Friction Angle (degree)	Peak Dilation Angle (degree)
5.35	11.83	65.69	13.19
10.74	15.13	54.62	6.30
21.73	27.74	51.92	3.66
33.43	35.40	46.64	0.62

Table 106. No. 89 LDTX results.

σ'_1 (psi)	σ'_3 (psi)	ϕ'_s (degree)	ψ_{max} (degree)
36.41	5.32	48.17	13.39
64.16	10.29	46.34	10.24
107.05	20.05	43.19	4.45
141.61	30.00	40.57	0.67

NO. 9

Figure 82. Photo. No. 9 aggregate sample.

Table 107. No. 9 gradation.

Sieve No.	Sieve Size (inches)	Mass of Soil + Pan (g)	Mass of Pan (kg)	Mass of Soil (kg)	Percent Retained	Percent Passing
0.375	0.375	0	1,102.79	0	0.00	100.00
4	0.187	1,785.33	1,514.98	270.35	5.78	94.22
8	0.0937	4,236.2	1,129.04	3,107.16	66.47	27.75
16	0.0469	1,791.1	909.95	881.15	18.85	8.90
50	0.0117	986.6	741.69	2,44.91	5.24	3.66
100	0.0059	830	809.4	20.6	0.44	3.22
200	0.0029	934.9	916.46	18.44	0.39	2.82
Pan	—	732.6	600.56	132.04	2.82	0.00

Table 108. No. 9 density.

Sample	Minimum Density (pfc) ASTM D4254					Maximum Density (pcf) ASTM D4253			
	Test 1	Test 2	Test 3	Average	Standard Deviation	Test 1	Test 2	Average	Standard Deviation
No. 9	93.4	90.9	92.6	92.3	1.3	113.0	108.3	110.7	3.3

Table 109. No. 9 repose angle.

Test	Angle Finder						String Method			Average Repose Angle
1	29	26	24	26	27		53.75	27.36		
2	25	26	28	28	31	26.8	52.5	29.05	27.82	27.31
3	26	26	25	27	28		54	27.04		

Table 110. No. 9 standard DS results.

Normal Stress (psi)	Max Shear (psi)	Peak Friction Angle (degree)	Peak Dilation Angle (degree)
5.323	12.13962	66.32	1.53
10.08	17.8952	60.61	15.62
20.08	31.37	57.38	13.53
30.17	46.6205	57.09	11.82

Table 111. No. 9 LSDS results—dry.

Normal Stress (psi)	Max Shear (psi)	Peak Friction Angle (degree)	Peak Dilation Angle (degree)
5.35	9.73	61.22	13.64
10.66	17.70	58.93	10.38
21.57	31.97	55.99	5.82
32.60	42.84	52.73	4.73

Table 112. No. 9 LSDS results—saturated.

Normal Stress (psi)	Max Shear (psi)	Peak Friction Angle (degree)	Peak Dilation Angle (degree)
5.26	8.39	57.93	12.08
10.76	13.05	50.49	5.58
21.54	25.38	49.69	2.71
32.53	32.98	45.40	0.61

Table 113. No. 9 LDTX results.

σ'_1 (psi)	σ'_3 (psi)	ϕ'_s (degree)	ψ_{max} (degree)
27.85	5.20	43.27	8.03
49.83	10.14	41.44	4.22
91.75	20.03	39.92	0.86
134.13	30.01	39.37	0

NO. 10

Figure 83. Photo. No. 10 aggregate sample.

Table 114. No. 10 gradation.

Sieve No.	Sieve Size (inches)	Mass of Soil + Pan (g)	Mass of Pan (kg)	Mass of Soil (kg)	Percent Retained	Percent Passing
0.375	0.375	0	1,102.6	0	0.00	100.00
4	0.187	1,560.7	1,514.9	45.8	1.04	98.96
8	0.0937	1,821.7	1,128.9	692.8	15.78	83.18
16	0.0469	1,798.3	909.8	888.5	20.23	62.95
50	0.0117	2,022.6	741.5	1,281.1	29.17	33.78
100	0.0059	1,464.5	809.4	655.1	14.92	18.86
200	0.0029	1,267.7	916.4	351.3	8.00	10.86
Pan	—	1,146.6	669.8	476.8	10.86	0.00

Table 115. No. 10 density.

Sample	Minimum Density (pfc) ASTM D4254					Maximum Density (pcf) ASTM D4253			
	Test 1	Test 2	Test 3	Average	Standard Deviation	Test 1	Test 2	Average	Standard Deviation
No. 10	114.9	116.4	116.0	115.8	0.8	146.4	146.2	146.3	0.1

Table 116. No. 10 repose angle.

Test	Angle Finder						String Method			Average Repose Angle
1	32	30	28	28	31	27.4	54	27.04	25.32	26.36
2	28	25	28	26	25		55.625	25.03		
3	26	24	28	27	25		56.625	23.88		

Table 117. No. 10 standard DS results.

Normal Stress (psi)	Max Shear (psi)	Peak Friction Angle (degree)	Peak Dilation Angle (degree)
5.399	10.24149	62.20	15.86
10.28	16.7196	58.41	14.18
20.4	30.12	55.89	14.15
30.14	42.6877	54.78	10.35

Table 118. No. 10 LSDS results—dry.

Normal Stress (psi)	Max Shear (psi)	Peak Friction Angle (degree)	Peak Dilation Angle (degree)
5.32	7.89	56.01	10.29
10.50	13.79	52.70	9.33
21.63	23.32	47.15	4.43
32.88	33.93	45.90	1.87

Table 119. No. 10 LSDS results—saturated.

Normal Stress (psi)	Max Shear (psi)	Peak Friction Angle (degree)	Peak Dilation Angle (degree)
5.29	7.41	54.48	7.59
10.61	10.97	45.94	0.77
20.98	18.96	42.10	0.58
34.27	29.17	40.40	0.00

Table 120. No. 10 LDTX results.

σ'_1 (psi)	σ'_3 (psi)	ϕ'_s (degree)	ψ_{max} (degree)
24.14	5.03	42.79	2.50
47.60	10.04	41.76	2.58
99.31	20.02	41.78	2.30
143.19	30.05	40.91	2.34

ACKNOWLEDGEMENTS

The authors thank Justice Maswoswe of the FHWA Resource Center and Khalid Mohamed of the FHWA Office of Bridges and Structures for their feedback and review of this study. The authors also recognize the contributions of Jan Li of ESC, INC., who performed many of the LSDS tests in this report. Tom Stabile of ESC, INC., and Phillip Ooi of the University of Hawaii at Manoa provided advice throughout the project; the authors gratefully acknowledge their insights.

REFERENCES

1. AASHTO. (2005). *M 43: Standard Specification for Sizes of Aggregate for Road and Bridge Construction,* American Association of State Highway and Transportation Officials, Washington, DC.

2. ASTM D448. (2012). "Standard Classification for Sizes of Aggregate for Road and Bridge Construction," *Annual Book of ASTM Standards,* ASTM International, West Conshohocken, PA.

3. Nicks, J.E. and Adams, M.T. (2013). *TechBrief: Friction Angles of Open-Graded Aggregates from Large-Scale Direct Shear Testing*, Publication No. FHWA-HRT-13-068, Federal Highway Administration, McLean, VA.

4. FHWA. (2003). *Standard Specifications for Construction of Roads and Bridges on Federal Highway Projects*, FP-03, Federal Highway Administration, McLean, VA.

5. HDOT. (2005). *Standard Specifications for Road and Bridge Construction*, Hawaii Department of Transportation.

6. ODOT. (2013). Construction and Material Specifications. Ohio Department of Transportation.

7. AKDOT. (2005). Standard Specifications for Highways. Alaska Department of Transportation, Juneau, AK.

8. Bowles, J.E. (1996). *Foundation Analysis and Design*, 5th Ed., The McGraw-Hill Companies, Inc., New York, NY.

9. Rowe, P.W. (1962). "The Stress Dilatancy Relation for Static Equilibrium of an Assembly of Particles in Contact," *Proceedings of the Royal Society*, A 269, pp. 500–527.

10. Terzaghi, K., Peck, R.B., and Mesri, G. (1996). *Soil Mechanics in Engineering Practice*, 3rd Ed., John Wiley and Sons, Inc., NY, 549 pp.

11. Lee, K.L. and Seed, H.B. (1967). "Drained Strength Characteristics of Sands," *Journal of the Soil Mechanics and Foundation Division, Proceedings of the American Society of Civil Engineers, 93,* No. SM6, pp. 117–141.

12. Alabdullah, J. (2010). *Testing Unsaturated Soil for Plane Strain Conditions: A New Double-Wall Biaxial Device*, PhD Thesis, Bauhaus-University Weimar, Homs, Syria.

13. Lee, K.L. (1970). "Comparison of Plane Strain and Trixial Tests on Sand," *Journal of the Soil Mechanics and Foundations Division,* 96:901–923.

14. Maccarini, M. (1993). “A Comparison of Direct Shear Box Tests with Triaxial Compression Tests for a Residual Soil,” *Geotechnical and Geological Engineering*, 11:69–80.

15. Evans, T.M. (2005). *Microscale Physical and Numerical Investigations of Shear Banding in Granular Soils*, PhD Thesis, Georgia Institute of Technology, Atlanta.

16. Wanatowski, D. (2005). *Strain Softening and Instability of Sand Under Plane-Strain Conditions*, PhD. Thesis, Nanyang Technological University, Singapore.

17. Peters, J., Lade, P., and Bro, A. (1988). “Shear Band Formation in Triaxial and Plane Stress Tests; Advanced Triaxial Testing of Soil and Rock,” *ASTM STP 977*, R. Donaghe, R. Chaney and M. Silver, Eds., ASTM, West Conshohocken, PA., 604–627.

18. Alshibli, K.A., Batiste, S., and Sture, S. (2003). “Strain Localization in Sand: Plane Strain Versus Triaxial Compression,” *J. Geotech. Geoenviron. Eng.*, 129:483–494.

19. Sadrekarimi, A. (2009). *Development of a New Ring Shear Apparatus for Investigating the Critical State of Sands*, PhD Thesis. University of Illinois at Urbana-Champaign, Urbana.

20. Desures, J., Chambon, R., Mokni, M., and Mozerolle, F. (1996). “Void Ratio Evolution Inside Shear Bands in Triaxial Sand Specimens Studied by Computed Tomography,” *Geotechnique*. 46:529–546.

21. Alshibli, K.A., Sture, S., Costes, N.C., Frank, M.L., Lankton, M.R., Batiste, S.N., and Swanson, R.A. (2000). “Assessment of Localized Deformations in Sand Using X-ray Computed Tomography,” *Geotechnical Testing Journal*, 23:274–299.

22. Sadrekarimi, A. and Olson, S.M. (2011). “Critical State Friction Angle of Sands,” *Geotechnique*, 61:771–783.

23. Sterpi, D. (2000). “Influence of the Kinematic Testing Conditions on the Mechanical Response of a Sand,” *Computers and Geotechnics*, 26:23–41.

24. Araei, A.A., Soroush, A., and Rayhani, M. (2010). “Large-Scale Triaxial Testing and Numerical Modeling of Rounded and Angular Rockfill Materials,” *Scientia Iranica, Transaction A, Civil Engineering*, *17*(3), 169–183.

25. Zeller, J., and Wullimann. R. (1957). “The Shear Strength of the Shell Materials for the Goschenenalp Dam, Switzerland,” *Proc., 4th Int. Conf. on Soil Mechanics and Foundation Engineering*. 2:399–404.

26. Lowe, J. (1964). “Shear Strength of Coarse Embankment Dam Materials,” *Proc., 8th Int. Congress on Large Dams*, 3:745–761.

27. Fumagalli, E. (1969). “Tests on Cohesionless Materials for Rockfill Dams,” *J. Soil Mech. And Found. Div.*, *95*(1): 313–332.

28. Frost, R.J. (1973). “Some Testing Experiences and Characteristics of Boulder-Gravel Fills in Earth Dams; Evaluation of Relative Density and Its Role in Geotechnical Projects Involving Cohesionless Soils (STP523),” *ASTM*, West Conshohocken, PA, 207–252.

29. Honkanadavar, N.P. and Sharma, K.G. (2013). “Testing and Modeling the Behavior of Riverbed and Blasted Quarried Rockfill Materials,” *Int. J. Geomech.*, 10.1061/(ASCE)GM. 1943-5622.0000378, 04014028.

30. Ramamurthy, T., and Gupta, K.K. (1986). “Response Papers to How Ought One to Determine Soil Parameters to Be Used in the Design of Earth and Rockfill Dams,” *Proc., Indian Geotechnical Conf., 2*, Indian Geotechnical Society, New Delhi, India, 15–19.

31. Varadarajan, A., Sharma, K.G., Venkatachalam, K., and Gupta, A.K. (2003). “Testing and Modeling Two Rockfill Materials,” *J. Geotech. Geoenviron. Eng.*, 10.1061/(ASCE)1090-0241(2003)129:3(206), 206–218.

32. Indraratna, B., Ionescu, D., and Christie, H.D. (1998). “Shear Behavior of Railway Ballast Based on Large-Scale Triaxial Tests,” *Journal of Geotechnical and Geoenvironmental Engineering*, *124*(5):439–449.

33. Lambe, T.W. (1964). “Methods of Estimating Settlement,” *Journal of the Soil Mechanics and Foundations Division, ASCE*, *90*, No. SM5, 47–74.

34. Das, B.M. 2010. *Principles of Geotechnical Engineering*, 7th Ed., Cengage Learning, Stamford, CT.

35. Charles, A., and Watts, K.S. (1980). “The Influence of Confining Pressure on the Shear Strength of Compacted Rockfill,” *Geotechnique*, *30*, 353–367.

36. Nusier, O.K., Almohd, I.M., and Jaradat, R.A. (2008). *Nonlinearity of Shear Strength and Stress-Strength Behavior and Induced Stress Predictions*, ICCBT 2008, June 16–20, Kuala Lumpar, Malaysia.

37. Ravi Sharma, M.S., Baxter C.D.P., Hoffmann, W., Moran, K., and Vaziri, H. (2010). “Characterization of Weakly Cemented Sands Using Nonlinear Failure Dnvelope, *Int. J. Rock Mech. Mining Sci*. doi:10.1016/j.ijrmms.2010.06.008.

38. Lade, P.V. (2010). “The Mechanics of Surficial Failure in Soil Slopes,” *Engineering Geology*. 114:57–64.

39. Hoek, E. & Brown, E.T. (1997). “Practical Estimates of Rock Mass Strength,” *International Journal of Rock Mechanics and Mining Sciences*, 34(8):1165–86.

40. Eberhardt, E. (2012). “The Hoek-Brown Failure Criterion,” *Rock Mech. Rock Eng*. 45:981–988.

41. Baker, R. (2004). “Nonlinear Mohr Envelopes Based on Triaxial Data,” *Journal of Geotechnical and Geoenvironmental Engineering*. 130:498–506.

42. Bolton, M.D. (1986). "The Strength and Dilatancy of Sands," *Géotechnique*, *36*(1), pp. 65–78.

43. Poulos, S.J. (1971). *The Stress-Strain Curves of Soils*, Geotechnical Engineers, Inc. Winchester, MA, pp. 1–80.

44. AASHTO. (2012). *LRFD Bridge Design Specifications*, 5th Ed., American Association of State Highway and Transportation Officials, Washington, DC.

45. Munfakh, G., A. Arman, J. G. Collin, J. C.-J. Hung, and R. P. Brouillette. (2001). *Shallow Foundations Reference Manual*, FHWA-NHI-01-023. Federal Highway Administration, U.S. Department of Transportation, Washington, DC.

46. AASHTO. (2010). *LRFD Bridge Construction Specifications*, 3rd Ed., American Association of State Highway and Transportation Officials, Washington, DC.

47. Berg, R., Christopher, B., and Samtani, N. (2009). *Design of Mechanically Stabilized Earth Walls and Reinforced Soil Slopes—Volume 1*, Report No. FHWA-NHI-10-024, National Highway Institute, Federal Highway Administration, Arlington, VA.

48. Bareither, C.A., Edil, T.B., Benson, C.H., Mickelson, D.M. 2008. "Geological and Physical Factors Affecting the Friction Angle of Compacted Sands," *Journal of Geotechnical and Geoenvironmental Engineering*. DOI: 10.1061/(ASCE)1090-0241(2008)134:10(1476).

49. Aksharadananda, T. and Wu, J.T.H. (2001). *Strength Parameters of Backfills for Design and Construction of Retaining Walls*, CDOT Report No. 2001-07, Colorado Department of Transportation Research Branch, Denver, CO.

50. Yamaguchi, Y., Satoh, H., Hayashi, N., Yoshinaga, H. (2009). *Strength Evaluation of Rockfill Materials Considering Confining Pressure Dependency*, 1st International Symposium on Rockfill Dams, 18–21 October 2009, Chengdu, China.

51. Fitsum, Y.E. (2011). *Shear Strength of Bremanger Sandstone Rockfill at Low Stress*, MSc Thesis, Delft University of Technology, The Netherlands.

52. Duncan, J.M., Brandon, T., Jian, W., Park, Y., Griffith, T., Corton, J., and Ryan, E. (2007). *Densities and Friction Angles of Granular Materials with Standard Gradations 21b and #57*, Report CPGR #45, Center for Geotechnical Practice and Research, Virginia Polytechnic Institute, Blacksburg, VA, 100 pp.

53. Rowe, P.W. (1969). "The Relation Between the Shear Strength of Sands in Triaxial Compression, Plane Strain and Direct Shear," *Geotechnique*, *19*, No. 1. pp. 75–86.

54. Cerato, A.B. (2005). *Scale Effects of Shallow Foundation Bearing Capacity on Granular Material*, PhD Dissertation, University of Massachusetts Amherst.

55. Pells, P.J.N., Maurenbrecher, P.M., and Elges, H.F.W.K. (1973). “Validity of Results from the Direct Shear Test,” *Proceedings of the 8th International Conference on Soil Mechanics and Foundation Engineering*, *1.2*, pp. 333–339.

56. Ladd, R.S. (1977). “Specimen Preparation and Cyclic Stability of Sands,” *ASCE Journal of the Geotechnical Engineering Division*, *103*, No. GT6, pp. 535–547.

57. Kulhawy, F.H. and Mayne, P.W. (1990). *Manual on Estimating Soil Properties for Foundation Design*, EL-6800, Electrical Power Research Institute (EPRI): Research Project 1493-6.

58. Allen, T.M. and Bathurst, R.J. (2003). *Prediction of Reinforcement Loads in Reinforced Soil Walls*, Report No. WA-RD 522.2, Washington State Department of Transportation, 363 pp.

59. Allen, T.M., Christopher, B.R., Elias, V., and DiMaggio, J.D. (2001). *Development of the Simplified Method for Internal Stability Design of Mechanically Stabilized Earth (MSE) Walls*, WSDOT Research Report WA-RD 513.1, 108 pp.

60. Hribar, J., Dougherty, M., Ventura, J., and Yavorskyu, P. (1986). “Large Scale Direct Tests on Surface Mine Spoil,” *Proceedings of the International Symposium on Geotechnical Stability in Surface Mining*, Calgary, AB, November 1986, pp. 295–303.

61. Matsuoka, H. and Liu, S.H. (1998). “Simplified Direct Box Shear Test on Granular Materials and Its Application to Rockfill Materials,” *Soils and Foundations*, *38*(4):275–284.

62. Fox, N.S. and Cowell, M.J. (1998). *Geopier Foundation and Soil Reinforcement Manual*, Geopier Foundation Company, Inc., Scottsdale, AZ.

63. Stewart, G.A. (1955). “Age Relations of the Middle Devonian Limestones in Ohio,” *Ohio Journal of Science*, *55*(3), pp. 147–181.

64. Toewe, E.C. (1966). *Geology of the Leesburg Quadrangle Virginia*, Report of Investigations 11, Virginia Division of Mineral Resources, Charlottesville, VA.

65. AASHTO. (2011). *T27: Standard Method of Test for Sieve Analysis of Fine and Course Aggregates*, American Association of State Highway and Transportation Officials, Washington, DC.

66. ACI. (1980). *ACI Manual of Concrete Practice, Part I*, American Concrete Institute, Detroit, MI.

67. ASTM C33. (2003). “Standard Specification for Concrete Aggregates,” *Annual Book of ASTM Standards*, ASTM International, West Conshohocken, PA.

68. ASTM D4254. (2006e1). “Standard Test Methods for Minimum Index Density and Unit Weight of Soils and Calculation of Relative Density,” *Annual Book of ASTM Standards*, ASTM International, West Conshohocken, PA.

69. ASTM D4253. (2006). “Standard Test Methods for Maximum Index Density and Unit Weight of Soils Using a Vibratory Table,” *Annual Book of ASTM Standards*, ASTM International, West Conshohocken, PA.

70. Adams, M., Nicks, J., Stabile, T., Wu, J., Schlatter, W., and Hartmann, J. 2011. *Geosynthetic Reinforced Soil Integrated Bridge System Interim Implementation Guide*, Report No. FHWA-HRT-11-026, Federal Highway Administration, McLean, VA.

71. Smith, D. R. (2007), “Construction of Bases for Permeable Interlocking Concrete Pavements- Part II,” Contractor Focus, *Interlocking Concrete Pavement Magazine*, November 2007.

72. Liu, J. and Zhou, J. (2008). “Numerical Study on Sandpile Formation of Granular Materials with Different Grain Size Distributions,” *Geotechnical Engineering for Disaster Mitigation and Rehabilitations, Proceedings of the 2nd International Conference GEDMAR08*, Nanjing, China.

73. Gates, L., Masad, E., Pyle, R. and Bushee, D. (2011). *Aggregate Imaging Measurement System 2 (AIMS2): Final Report*, Report No. FHWA-HIF-11-030, Federal Highway Administration, Washington, DC.

74. Masad. E.A. (2005). *Aggregate Imaging System (AIMS): Basics and Applications*, Report No. FHWA/TX-05-5-1707-01-1, Texas Transportation Institute, Texas Department of Transportation, Austin, TX.

75. ASTM D3080. (2004). “Standard Test Method for Direct Shear Test of Soils under Consolidated Drained Conditions,” *Annual Book of ASTM Standards*, ASTM International, West Conshohocken, PA.

76. Montoya, B.M. (2012). *Bio-Mediated Soil Improvement and the Effect of Cementation on the Behavior, Improvement, and Performance of Sand*, Doctoral Dissertation, University of California, Davis, pp. 238.

77. Olson, R.E. (2007). *Direct Shear Testing*, Lecture notes, Department of Civil, Architectural, and Environmental Engineering, University of Texas, Austin.

78. ASTM D5321. (2008). “Standard Test Method for Determining the Coefficient of Soil and Geosynthetic or Geosynthetic and Geosynthetic Friction by the Direct Shear Method,” *Annual Book of ASTM Standards*, ASTM International, West Conshohocken, PA.

79. Simoni, A. and Houlsby, G.T. (2006). “The Direct Shear Strength and Dilatancy of Sand-Gravel Mixtures,” *Journal of Geotechnical and Geological Engineering*, *24*, pp. 523–549.

80. ASTM D7181. (2011). “Method for Consolidated Drained Triaxial Compression Test for Soils,” *Annual Book of ASTM Standards*, ASTM International, West Conshohocken, PA.

81. Chakraborty, T. and Salgado, R. (2010). “Dilatancy and Shear Strength of Sand at Low Confining Pressure,” *Journal of Geotechnical and Geoenvironmental Engineering*, *136*(3):527–532.

82. Germaine, J.T. and Ladd, C.C. (1988). *State-of-the-Art: Triaxial Testing of Saturated Cohesive Soils; Advanced Triaxial Testing of Soil and Rock*, ASTM STP 977, Donaghe, R.T., Chaney, R.C., and Silver, M.L., Eds., American Society for Testing and Materials, Philadelphia, PA, pp. 421–459.

83. Triaxial User’s Manual. (2012). *Control and Report Software for Fully Automated Triaxial UU, CU, CD and Stress Path Soil Tests on LoadTrac-II/FlowTrac-II Systems Using Windows®XP/Vista/7*, Geocomp Corporation, Acton, MA.

84. Noor, M.J.M., Nyuin, J.D., and Derahman, A. (2012). “A Graphical Method for Membrane Penetration in Triaxial Tests on Granular Soils,” *The Institution of Engineers*, *73*(1):23–30, Malaysia.

85. Paikowsky, S.G. Canniff, M.C., Lesny, K., Kisse, A., Amatya, S. and Muganga, R. (2010). *LRFD Design and Construction of Shallow Foundations for Highway Bridges*, NCHRP Report 651, Transportation Research Board, Washington, DC.

86. NAVFAC. (1986). *Soil Mechanics Design Manual 7.01*, Naval Facilities Engineering Command, Alexandria, VA, p. 7.1–149.

87. Sadrekarimi, A. and Olson, S.M. (2011). “Critical State Friction Angle of Sands,” *Geotechnique, 61*, No. 9, pp. 771–783.

HRDI-40/06-15(WEB)E